Fermi National Accelerator Laboratory
FERMILAB-PUB-95-075-T

Complex Systems: Equilibrium Configurations of N Equal Charges on a Sphere ($2 \leq N \leq 112$)

T. Erber
Department of Physics and Department of Mathematics, Illinois Institute of Technology, Chicago, Illinois 60616

G.M. Hockney
Fermi National Accelerator Laboratory, P.O. Box 500, Batavia, Illinois 60510
(April 18, 1995)

Abstract

The emergence of complexity in many-body systems is illustrated by the progression of equilibrium states of N charges confined to the surface of a sphere. This is an electrostatic problem with spherically symmetric interactions and boundary conditions. For increasing values of N, the equilibrium solutions break this symmetry and differentiate into sets of complex figures. For instance, states with non-vanishing dipole moments appear when $N = 11, 13, 19$, etc.; the first enantiomeric or chiral state appears at $N = 15$; and robust metastable states are encountered with increasing freqency for $N = 16, 22, 32, 35, 37 \ldots$. Computer searches show that when $N \sim 100$, sets of 50-90 metastable states—separated by energy differences of about 0.001%—are the norm. The capture basins, or statistical weights, of some metastable states are larger than those of the ground state. For $N \geq 80$, the energy variations of individual charges *within* configurations exceed the energy differences *between* configurations by factors of 10-50. Angular comparisons show that energetically similar states generally have completely different configurations. Moreover, the geometrical patterns of the charge distributions tend to become increasingly irregular for larger values of N. Nevertheless, there is statistical order in the overall angular distributions, and isolated regular configurations appear at a series of N values extending up to $N = 112$. Since the dipole moments of all known equilibrium states (for $N \leq 112$) are bounded by 10^{-2}, whereas the average dipole moments of spherical random N-point distributions grow as $0.92\, N^{\frac{1}{2}}$, it is clear that the geometric irregularity of the Coulomb states coexists with complex order. Common features of the spherical Coulomb and Tammes problems, as well as other cooperative models such as Ewing arrays and vortex lattices, suggest several general conjectures concerning the behavior of complex systems.

Operated by Universities Research Association Inc. under contract with the United States Department of Energy

1. Introduction

Symmetry and stability criteria are useful for describing charge configurations in a great variety of situations ranging from J.J. Thomson's original plum pudding model of the atom to current investigations of carbon and indium fullerene cages [1-5]. In particular, the O(4) symmetry associated with the Coulomb interaction underlies both the standard Bohr-Pauli level structure of the elements as well the nested charge rings of the old plum pudding model [6-8]. This robust symmetry constraint enabled Thomson to establish the first quantitative connections between recurrences in the patterns of charge distributions and the periodicities of Mendeleyev's chemical table. The most striking recent success of symmetries in charge configurations is the discovery that C_{60} can exist in a stable form resembling a truncated icosahedron [9]. However, since this is the last but one of the 13 Archimedean polyhedra, there are no further regular structures of this kind that can serve as templates for more complex chemical cages. One method of extending the inventory of geometric figures is to use computers to search for the static equilibrium states of N equal point charges on the surface of a sphere. In contrast to the plum pudding or 'jellium' model, where Thomson and Föppl [10] started with the presumption that the equilibrium states would be a series of symmetric nested rings, locally stable solutions of the surface Coulomb problem can be obtained without imposing any *a priori* constraints of symmetry or other types of structural regularities. For small values of N, the results confirm the intuitive expectation that the charge configurations are symmetric and unique. They are also extremely robust because for the special values $N_L = 2 - 6, 12$, the equilibrium configurations remain invariant if the Coulomb law r^{-2} is replaced by the limiting form r^{-n}, $n \rightarrow \infty$ [11]. This 'ultra-repulsive' interaction is the basis of the biological *Tammes* problem of finding arrangements of

N points on the surface of a sphere with the largest possible minimum distance between any pair [12 - 15]. Since exact solutions of the Tammes problem are known for the set N_T^{ex} = 2 - 12, 24; this invariance also yields optimum configurations for the surface Coulomb problem for the particular values N_C^{ex} = 2 - 6, 12. Of course, these geometric solutions coincide with the computer generated patterns. If the mutual charge repulsions are described by logarithmic interactions rather than a power law, the corresponding equilibrium solutions for N = 2 - 6, 12, are again given by the Coulomb set N_C^{ex} [16]. Similar configurations --- except for a few changes in length scales --- appear in the jellium model [10]. All of these equivalences suggest that in cooperative systems with few degrees of freedom symmetry principles alone may be sufficient to determine the character of the equilibrium states. However, when N > 6, the sets of equilibrium configurations for these four different force laws lose their resemblance. These divergences illustrate the symmetry breaking effects associated with the emergence of new levels of complexity in larger systems.

In the range 50 ≤ N≤ 112, the surface Coulomb problem has at least 1945 locally stable solutions. These configurations may be classified with the help of several measures based on geometric and energy criteria. Specifically, for any particular value of N, there are a total of N(N-1)/2 angles between the $\vec{r}_i$ vectors that specify the locations of the charges on the surface of the sphere. A simple measure of the geometric regularity of a charge distribution is then given by the *angular diversity ratio* (%)

$$D_a(N) \equiv 100 \frac{number\ of\ distinct\ angles}{N\ (N\ -\ 1)/2} . \qquad (1.1)$$

Clearly, large values of D_a (percentages exceeding 96% occur frequently when N > 50) indicate irregular configurations that cannot be identified with any of the 123 standard types of convex polyhedra [17, 18]. This irregularity also implies that the vertices, or charge positions, of these Coulomb states cannot be interchanged by means of any of the usual rotational symmetry operations. Nevertheless, lack of congruence in vertex separations or edge lengths doesn't exclude the persistence of other kinds of order. A quantitative measure of the difference between random and geometrically irregular distributions of N points on the surface of a sphere is given by the dipole moment or center of charge [19, 20]; i.e.,

$$\vec{d}(N) = \sum_{i=1}^{N} \vec{r}_i . \qquad (1.2a)$$

In particular, for a unit sphere, where $|\vec{r}_i| = 1$, the average value of the dipole moment of a random configuration of N unit charges increases with N,

$$\langle |\vec{d}\ (N)| \rangle_{Ran} = \langle | \sum_{i=1}^{N} \vec{r}_i | \rangle_{Ran} = (\frac{8}{3\pi} N)^{1/2}. \qquad (1.2b)$$

On the other hand, the dipole moments of all the equilibrium Coulomb states, for $N \leq 112$, are bounded by 10^{-2}, and typically fall in the range $10^{-5} \lesssim |\vec{d}(N)| \lesssim 10^{-3}$. Obviously, this is an orders-of-magnitude reduction from the random values. The regularities of the Coulomb states are even more apparent in cases where the angular diversity ratios are small, say $D_a \leq 10\%$. The computer searches show that there are at least 23 geometrically ordered configurations of this kind for a series of N values between $24 \leq N \leq 112$. None of these patterns match the Archimedean polyhedra. For instance, there are four semi-regular Archimedean polyhedra with 24 vertices; and in fact one of them, the snub cube, resembles the ordered Coulomb state with 24 charges because both configurations have 38 faces, 60 edges, and occur in enantiomeric forms. However, all edges of the snub cube have equal length and subtend an angle of 43.68° at the center of the sphere, whereas the 60 edges of the Coulomb configuration are split into three sets with approximately equal lengths: 24 subtending an angle of 42.07°, 24 with an angle of 45.04°, and 12 with an angle of 45.71°. Additional comparisons for other sets of states show that this symmetry breaking is pervasive: there is a general trend away from strict geometric regularity in larger systems.

The emergence of complexity is also reflected in several physical effects. For example, the electrostatic interaction energy of N unit charges, E(N), can be represented as the sum of the partial energies associated with the individual charges, $\mathrm{E}_i\,(N)$; i.e.,

$$\mathrm{E}(N) = \sum_{i=1}^{N} \mathrm{E}_i\,(N); \qquad \mathrm{E}_i(N) = \frac{1}{2} \sum_{j \neq i}^{N} |\vec{r}_i - \vec{r}_j|^{-1}. \tag{1.3}$$

This energy sharing is completely symmetric for the equilibrium states of the surface Coulomb problem in small systems; that is, $E_i(N) = E(N)/N$ *for* $N < 5$. However, when N = 5, the equilibrium arrangement is a triangular bipyramid with three charges positioned at the vertices of an equilateral triangle around a great circle, e.g. the equator, and the other two charges at the north and south poles. Since the distances between pairs of equatorial charges exceed the distance from the equator to either pole, Eq. (1.3) implies that each of the two polar charges has a slightly greater partial energy than the equatorial charges. This energy splitting tends to increase for larger values of N; until at N = 59 the state with the greatest capture basin, or statistical weight, is so asymmetric that all of the charges have different partial energies. Beyond this point irregular states with angular diversities at the maximum value D_a =100%, *cf.*(1.1), and a complete splitting of all partial energies occur with increasing frequency.

The transition from symmetry to asymmetry also appears in a shift of the center of charge, Eq. (1.2a). For all N < 11, the equilibrium configurations of the surface Coulomb problem are sufficiently regular so that the center of charge coincides with the center of the sphere. This situation is analogous to the absence of permanent electric dipole moments in symmetric atomic and molecular charge distributions [21]. But parity arguments alone cannot exclude the existence of dipole moments in static situations. In the surface Coulomb problem this symmetry is broken at N = 11, where the equilibrium pattern consists of an irregular equatorial pentagon and two tilted isosceles triangles in the northern and southern hemispheres [22]. This state has a moment given by $|\vec{d}(11)| \cong 0.0132$; which implies the existence of an intrinsic pattern 'direction', as well as a non-vanishing electric field at the center of the sphere.

Another kind of dipole symmetry breaking appears when the charge interactions are varied. For instance, if the Coulomb law is replaced by an $|\vec{r}_i - \vec{r}_j|^{-1}$ force, the dipole moments of all of the corresponding equilibrium configurations vanish identically [16].

A common feature of all three spherical surface problems --- associated with the $|\vec{r}_i - \vec{r}_j|^{-n}$, n = 1, 2, and ∞ (Tammes) interactions --- is the occurrence of enantiomeric states beginning at N = 15. This division marks another threshold of structural complexity. For example, if computer searches for the equilibrium states of the surface Coulomb problem are started at 10^4 random initial positions of 15 points, the trials will lead with about 50% - 50% probability to two geometrically distinct terminal configurations, $\mathbb{C}_G^L$ (15) *and* $\mathbb{C}_G^R$ (15), having precisely the same energy. These pairs of states are labeled 'left' (L) and 'right' (R) because they can be transformed into each other by an improper isometry consisting of a rotation combined with a reflection in a plane perpendicular to the axis of rotation [13]. It is intuitively plausible that there should not be any statistical bias favoring either the 'L' or 'R' states if they are derived from a random mix of initial states by a symmetric process. But in computer simulations the 'L' and 'R' labels may be regarded as a deterministic binary code that can be incorporated into the pseudo-random number algorithms that specify the initial states; and this information can create a preference. Specifically, if $\mathbb{C}_{Ran}$ (15) denotes a computer generated initial state of 15 charges, and M is an energy minimizing algorithm, then it can be shown that the mappings M [$\mathbb{C}_{Ran}^{L,R}$ (15)] → $\mathbb{C}_G^{L,R}$ (15) induce a correspondence between the 'L' and 'R' enantiomers of the equilibrium configuration and two disjoint sets of initial states,

$\{\mathbb{C}^{L}_{Ran}\ (15)\}$ *and* $\{\mathbb{C}^{R}_{Ran}\ (15)\}$. These sets of initial states are also enantiomeric because they occur in 'L' and 'R' variants --- each pair related by an improper isometry, and degenerate in energy. In general, the points that make up the initial states are distributed uniformly over the surface of the sphere by sets of pseudo-random number generators. The chirality of the N = 15 states then implies that the initial angular coordinates of the charges --- and the corresponding sets of pseudo-random numbers --- can be labeled by a binary 'L' and 'R' alphabet. By choosing appropriate sequences of states it is therefore possible to construct any desired string or 'message' composed of L's and R's. This information, in turn, may be encoded in the pseudo-random number generators by algorithms that retrodict any given sequence [23]. The net effect is that either ground state, $\mathbb{C}^{L}_{G}\ (15)$ *or* $\mathbb{C}^{R}_{G}\ (15)$, can be generated by deterministic means although the initial charge configurations are a racemic mix of L and R enantiomers. This method of choice by-passes some of the controversial issues of biological stereochemistry [24, 25].

The equilibrium states of the surface Coulomb problem exhibit many other types of structural transitions. It almost seems as if the addition of every new charge leads to another level of complexity. Basically, this diversity is due to the long range of the Coulomb force: the stable N- body configurations are the result of all N(N-1)/2 charge interactions and not just nearest neighbor forces. Similarly, the domain structures and hysteresis of magnetic Ewing arrays arise from the long reach of multipole forces [26]. Finding the stationary states of these cooperative systems by analytical means is generally very difficult. 'Greedy' algorithms that search for global extremals by piecing together a series of local 'best' choices can go astray even in simpler packing and covering problems [27]. For instance, the arrangement of N congruent

spheres whose convex hull has the smallest volume is a straight line or sausage for all $N \leq 56$; but for larger aggregates of spheres the optimum packings have entirely different shapes [28]. In a similar vein, the Tammes problem is equivalent to finding the maximum density --- or fraction of covered area --- when N congruent spherical caps are packed on the surface of a sphere. Since any cap can touch at most five other caps, this appears to be a nearest neighbor problem with simple contact forces [29]. But the global constraint that all the caps must fit together on the surface of the sphere, in a not necessarily rigid packing, makes this a hard problem. The geometric methods used to construct exact solutions for the set N_T^{ex} =2 - 12, 24, cannot be extrapolated to algorithms valid for arbitrary N. The best results available for $N \leq 90$ have been obtained by computer searches that simulate the non-overlapping caps with an ultra-repulsive $|\vec{r}_i - \vec{r}_j|^{-n}$, n = 1, 310, 720 potential [30]. The surface Coulomb problem is still more complicated because both self-consistent boundary conditions and long range forces determine the extremals. Exact results for this situation are sparse: Topological lower bounds for the number of equilibrium states are known only for N < 4 [31]; and local stability has been verified for only a few symmetric ring patterns [32]. Computer studies of this problem are complicated by the existence of many metastable states separated by very small energy differences. In the range $N \leq 112$, this requires double precision computations, high statistics searches starting from many random initial configurations, and numerical stability checks. But even with these precautions some states may be missed; and for large N, roundoff errors affect the correspondence between analytical and numerical stability criteria. These ambiguities are also implicit in computer simulations of the formation of ionic

'crystals' in electromagnetic traps [33, 34], and the relation of protein structures to amino acid sequences [35-37].

Prior work on the surface Coulomb problem, and computer results extending to N = 65, are discussed in references [38] and [39]. The values of the ground state energies have meanwhile been confirmed by several independent calculations [40-42, 16]. The Coulomb configurations have a number of practical applications: these include problems in structural chemistry [43, 44], the design of multi-beam laser implosion drives, and the optimum placement of communication satellites. Comprehensive summaries of related packing and covering problems --- with applications to error-free data transmission --- are given in [45]. Some quantum mechanical extensions are discussed in [46-48].

A. Contents

In Section 2A we set up the surface Coulomb problem for N equal point charges, and derive a simple relation between the partial energies associated with the individual charges and the dipole moments of the equilibrium states. The computer algorithms and conventions for orienting the charge configurations are described in Section 2B. Tabulations of the results for the range $2 \leq N \leq 112$ are given in Appendix B. Trends in the number of locally stable states M, found by the computer searches, are summarized in Section 3A. The results indicate an exponential increase in the number of states, i.e., $M \sim \exp\{0.05\ N\}$, *for* $N \geq 50$. Energy relations for the random initial states, ground states, metastable states, and the partial energy distributions within states are discussed in Section 3B. The ground state energies can be represented by a semi-empirical expression of the form $E\ (N) \approx 0.5\ N^2 - 0.55\ N^{3/2}$ over the

entire range $6 < N \leq 112$. Geometric properties of the equilibrium configurations are considered in Section 4: These include the distributions of dipole moments and chiral states in Sections 4A and 4D. Measures of order, such as the angular diversity ratios, and comparisons with Tammes configurations and regular polyhedra are summarized in Section 4B, 4C, and 4E-1. Some general conjectures concerning locally stable states of complex systems are discussed in Section 5. The corresponding analytical and numerical stability criteria are reviewed in Appendix A.

2. The Surface Coulomb Problem

A. Analytic Formulation

The set of N unit vectors $\{\vec{r}_i,\ 1 \leq i \leq N\}$ describes the position of N point charges constrained to lie on the surface of a unit sphere. If all charges are equal the corresponding dimensionless Coulomb energy is

$$E(N) = \sum_{i=1}^{N} \sum_{j>i}^{N} |\vec{r}_i - \vec{r}_j|^{-1}. \tag{2.1}$$

The static equilibrium configurations of this system are specified by the requirement that the total force $\vec{F}_i$ acting on the i^{th} charge is parallel to $\vec{r}_i$. This condition implies

$$\vec{F}_i = \sum_{\substack{j=1 \\ j \neq i}}^{N} \frac{\vec{r}_i - \vec{r}_j}{|\vec{r}_i - \vec{r}_j|^3} = E_i(N)\vec{r}_i, \tag{2.2}$$

where $E_i(N)$ is the partial energy associated with the i^{th} charge, cf. (1.3). The equilibrium states of the surface Coulomb problem are special cases of the central configurations of the (non-relativistic) gravitational N-body problem [49-51]. Clearly, the total force on the sphere vanishes

$$\sum_{i=1}^{N} \vec{F}_i = \sum_{i=1}^{N} \sum_{\substack{j=1 \\ j \neq i}}^{N} \frac{\vec{r}_i - \vec{r}_j}{|\vec{r}_i - \vec{r}_j|^3} = \sum_{i=1}^{N} E_i(N)\, \vec{r}_i = 0 \tag{2.3}$$

because the double sum is odd under an interchange of indices. If all the partial energies are equal, i.e., $E_i(N) = E(N)/N$, Eq. (2.3) implies that the corresponding dipole moments also vanish, cf. (1.2a):

$$\vec{d}(N) = \sum_{i=1}^{N} \vec{r}_i = 0. \tag{2.4a}$$

But this is only a sufficient condition. There are many equilibrium configurations for which

$$\sum_{i=1}^{N} E_i(N)\, \vec{r}_i = \sum_{i=1}^{N} \vec{r}_i = 0, \tag{2.4b}$$

even though $E_i(N) \neq E_j(N)$ for at least one pair of indices. If the interaction energies of the charges are logarithmic, Eq. (2.2) is replaced by

$$\vec{F}_i = \sum_{\substack{j=1 \\ j \neq i}}^{N} \frac{\vec{r}_i - \vec{r}_j}{|\vec{r}_i - \vec{r}_j|^2} = \frac{1}{2}(N - 1)\,\vec{r}_i. \qquad (2.5)$$

This expression shows that all the equilibrium forces have the same magnitude and --- in analogy with (2.4b) --- the corresponding dipole moments vanish identically [16]. These constraints indicate that the equilibrium configurations of the surface logarithm problem generally tend to be more regular than the equilibrium states of the surface Coulomb problem. In both cases the equilibrium coordinates $\vec{r}_i$ satisfy sets of linear relations, such as (2.3) and (2.4b), which are vectorial generalizations of cryptographic knapsack problems: these are known to be computationally difficult, or NP - hard [52].

The locally stable equilibrium configurations of the surface Coulomb problem satisfy the additional constraint that the associated energies are local minima. Specifically, if the charge positions are described by spherical coordinates --- the co-latitudes $0 \leq \phi_i \leq \pi$, and longitudes $-\pi \leq \theta_i \leq \pi$ --- then the Coulomb energy (2.1) is $E(\phi_i, \theta_i)$, $1 \leq i \leq N$; and the equilibrium condition (2.2) is equivalent to

$$\frac{\partial E}{\partial \phi_i} = \frac{\partial E}{\partial \theta_i} = 0, \; 1 \leq i \leq N. \qquad (2.6a)$$

If Ω_κ, $1 \leq \kappa \leq 2N \leftrightarrow \phi_1 \ldots \phi_N, \theta_1 \ldots \theta_N,$, then a sufficient condition for the local stability of the solutions of (2.6) is that the associated Hessian matrix

$$\mathcal{H}(\Omega_\kappa, \Omega_\mu) = \frac{\partial^2 E}{\partial\Omega_\kappa\, \partial\Omega_\mu}, \quad 1 \leq \kappa, \mu \leq 2N \tag{2.6b}$$

is positive definite. See Appendix A. Physically, this simply means that tangential restoring forces, i.e. $\vec{F}_i^{rest} \cdot \vec{r}_i = 0$, counter small displacements from equilibrium. In potential theory these locally stable configurations are known as Fekete points, and some asymptotic estimates of the rate of approach to the limit of continuous charge distributions are available [55, 56]. In Section 3B these methods are used to construct an expression for the ground state energy E(N).

Both in the Coulomb and dipole problems analytic solutions of the equilibrium equations (2.6a) and evaluation of the associated Hessians (2.6b) becomes tedious for as few as four interacting objects [32, 57]. At present, the only practical way of surveying the locally stable states of the Coulomb systems for larger values of N is to use computers to find energy minima. However, since the number of minima appears to grow exponentially with N, the energy surface $E(\phi_1, \theta_1; \ldots; \phi_N, \theta_N)$ becomes progressively more convoluted, and for $N > O(10^2)$ has many small hills and valleys. This leads to fundamental difficulties in mapping out the topography of the energy surfaces: It is necessary to distinguish genuine physical features such as minute ridges or clefts arising from the competition among the N(N-1)/2 charge interactions from numerical artifacts such as corrugations due to roundoff or truncation errors. Furthermore, even high statistics computer searches can miss some minima with small capture basins or special symmetries. The net result is that computer trials can both over - and underestimate the actual number of locally stable states. Analytic and numerical stability criteria for multidimensional

energy surfaces are discussed in more detail in Appendix A.

B. Computer Algorithms

Most of the numerical work was carried out with the ACPMAPS supercomputer at Fermilab. This is a parallel processing machine utilizing 600 double precision nodes. The computer searches for the locally stable states of the surface Coulomb problem were started from sets of points randomly distributed over the surface of the sphere --- specifically, 10^4 random starts for every value of N in the range $2 \le N \le 64$; 2000 starts for each successive N in the interval $65 \le N \le 108, 111$; and 1000 starts for N = 109, 110, and 112. The initial charge configurations were described by sets of spherical coordinates $\vec{r}_i\ (\phi_i, \theta_i)$, where each angle is represented by a 24-bit, or 7 decimal, pseudo-random number normalized to yield a uniform spherical distribution [19, 20]. The equilibrium states were found by allowing the points to move in the direction of the forces acting on them subject to the constraint of remaining on the surface of the sphere. The steepest descent method of iterating the map $\vec{r}_i \rightarrow \vec{r}_i' = (\vec{r}_i + \gamma\ \vec{F}_i)/|\vec{r}_i + \gamma\ \vec{F}_i|$, with γ chosen to maximize convergence, was used for this problem by Claxton and Benson [43]. In the limit $\gamma \rightarrow \infty$, the update formula reduces to $\vec{r}_i \rightarrow \vec{r}_i' = \vec{F}_i\ /|\vec{F}_i|$, which is an over-relaxed update step with good convergence. If this step is so large that the $\{\vec{r}_i'\}$ configuration has a higher energy than the $\{\vec{r}_i\}$ state, γ is automatically adjusted downward for that step until the energy does decrease. The iterations are terminated when the energies stabilize within the machine precision of one part in 2^{-48} (~14.4 decimals).

Since these computations involve the cancellation of large forces it is essential to use at least 48-bit precision. Conjugate-gradient methods do not improve this technique because of the highly convoluted structure of the energy surface.

In order to compare the geometric properties of the equilibrium states it is useful to rotate the configurations into a standard set of orientations. According to (1.3) the N charges of a locally stable state may be labeled by their partial energies. Suppose that these are ordered in a non-decreasing sequence, i.e.

$$E_1(N) \leq E_2(N) \leq E_3(N) \leq \ldots\ldots \leq E_N(N). \tag{2.7}$$

As a first step in orienting, pick a charge with the lowest partial energy --- if $E_1(N) = E_2(N)$, etc., this won't be a unique choice! --- and rotate the configuration so that this charge is placed at the north pole, $\theta = \phi = 0$. Consider next the set of charges with the second lowest partial energies: for instance, E_3, E_4, E_5, if (2.7) has the special form

$$E_1 = E_2 < E_3 = E_4 = E_5 < E_6 \ldots\ldots \leq E_N. \tag{2.8}$$

Find the (not necessarily unique) charge in this set closest to the north pole, and rotate the entire configuration so that this second charge is at zero longitude, $\theta = 0$. If the second charge happens to be at the south pole, repeat the process with another charge from the set with the third lowest partial energies. This scheme is adequate because the orientations are unique for

irregular configurations, and the ambiguities are irrelevant for comparing symmetric configurations.

The numerical reproducibility of the computations can be checked by comparing the results obtained from minimizing runs starting at different random initial configurations. For instance, for N = 84, the reproducibilities of some of the typical values that describe the characteristics of the configurations --- e.g., the chiral states with the largest capture basin --- are:

total energy	Eq. (1.3)	3103. 478 717 096	13 digits	(2.9a)
lowest partial energy	Eq. (1.3)	36. 885 477	8 digits	(2.9b)
typical angular coordinates (rad.)	θ	0. 039 852 25	7 digits	(2.9c)
	ϕ	0. 010 146 18	7 digits	

The disparity in significant digits between the total and partial energies is not due to statistical fluctuations or roundoff errors. Rather, it indicates that the computer runs end in a multiplicity of shallow stability valleys that merge into the local energy minima. The relation of these 'eigenmodes' to the Hessian stability criterion, Eq. (2.6b), is discussed in Appendix A. The basic numerical consequence is that the slight variations of the individual charge positions and energies compensate in such a way that the total energies of the equilibrium configurations are reproducible with a gain of five additional significant digits.

3. Locally Stable States of the Surface Coulomb Problem

A. Variation of the Number of States with the Particle Number N

The computer trials show that when there are only a few interacting charges --- that is

N is in the range $2 \leq N \leq 14$ --- the energy minimizing algorithm leads to a unique terminal energy E(N) for every value of N. If the associated charge configurations are rotated into a standard orientation by means of the conventions established in Section 2B, then the resulting geometrical patterns $\mathbf{C}(N)$ are also unique. A new level of complexity appears at N = 15. In this case all the computer searches still converge to a unique final energy value E(15) = 80. 670 244 11; but the associated charge configurations are split into a pair of enantiomeric states: Out of a total of 10^4 randomized initial configurations 4958, or 50%, of the energy minimizing sequences terminate in a charge pattern $\mathbf{C}^L(15)$, which is the chiral transform of another pattern $\mathbf{C}^R(15)$ reached in the other 5042 energy minimizations.

Three distinct terminal configurations appear when N = 16. As indicated in Table VIII in Appendix B, 75.7% of the 10^4 minimizing runs end at an energy of E_1 (16) = 92. 911 655 30. The frequency of occurrence of this state, or 'capture basin', is in turn almost evenly divided (37.7% and 38.0%) between two enantiomeric configurations $\mathbf{C}_1^L(16)$ and $\mathbf{C}_1^R(16)$. The remaining 24.3% of the computer searches end at a locally stable state with a slightly higher energy, $E_2(16)$ = 92. 920 353 96. The associated charge configuration $\mathbf{C}_2(16)$ is a symmetric set of four rings outlining a series of four relatively rotated squares with a charge at every corner. Figures 1(a) - 1(d) show these configurations in detail.

A summary of the multiplicities of the states M(N) for all N in the range $2 \leq N \leq 112$ is given in Table I. As indicated in column two of the Table, M(15) = 2 and M (16) = 3 because every chiral configuration is counted as a separate state. Columns 3, 6, 9 and 11 also list the cumulative number of states

$$M_C(N) = \sum_{j=2}^{N} M(j). \tag{3.1}$$

The graph in Figure 2 shows that M_c (N) increases at an exponential rate with N. In particular, if we assume that

$$M(N) = Ae^{\nu N} \tag{3.2a}$$

then (3.1) implies

$$M_C(N) = A(e^{\nu N} - e^{\nu})/(1 - e^{-\nu}). \tag{3.2b}$$

A Newton-Raphson optimization shows that for $70 \leq N \leq 112$, *Eq.* (3.2*b*) provides an excellent fit of the data with

$$A \simeq 0.382 \quad \text{and} \quad \nu \simeq 0.0497. \tag{3.2c}$$

An exponential growth of the multiplicities of states is also observed in two-dimensional arrays of pivoted magnets. Extensive experiments with $n \times n$, $2 \leq n \leq 6$ systems, initially stirred by fluctuating magnetic fields, and then allowed to settle into locally stable configurations, show that the number of distinct patterns $M^m(N)$ is of the order of

$$M^m(N) \simeq 1.3\, e^{0.19N}, \tag{3.3}$$

where $N = n \times n$ is the number of magnets [57, 58]. Figure 2 shows that the multiplicity of the magnetic states grows much more rapidly than the multiplicity of the surface Coulomb states. This trend is plausible because the magnets are coupled by a vector interaction that generates complex domain structures.

Table I

Variation of the Number of States M(N) with the Particle Number N

N	M(N)	$M_c(N)$[a]	N	M(N)	$M_c(N)$	N	M(N)	$M_c(N)$	N	M(N)	$M_c(N)$
2	1		29	2		57	9		85	19	505
3	1		30	3	43	58	18		86	46	
4	1		31	1		59	9		87	39	
5	1		32	2		60	11	200	88	32	
6	1		33	1		61	13		89	37	
7	1		34	2		62	6		90	44	703
8	1		35	5	54	63	4		91	37	
9	1		36	2		64	10		92	49	
10	1	9	37	3		65	6	239	93	41	
11	1		38	2		66	4		94	55	
12	1		39	4		67	2		95	35	920
13	1		40	6	71	68	9		96	41	
14	1		41	3		69	9		97	21	
15	2	15	42	7		70	13	276	98	37	
16	3		43	1		71	7		99	24	
17	1		44	1		72	10		100	52	1095
18	1		45	3	86	73	10		101	82	
19	1		46	8		74	22		102	87	
20	1	22	47	10		75	6	331	103	52	
21	2		48	3		76	12		104	56	
22	2		49	2		77	9		105	70	1442
23	2		50	1[b]	110	78	7		106	93	
24	2		51	3		79	7		107	86	
25	1	31	52	8		80	10	376	108	75	
26	2		53	3		81	19		109	86	
27	3		54	10		82	30		110	93	1875
28	2		55	11	145	83	31		111	88	
			56	8		84	30		112	91	2054

[a] Cumulative number of states, Eq. (3.1).
[b] $M(N) > 1$ for $N > 50$.

There are several other N-body systems that exhibit an exponential growth of M(N) with $\nu \sim 0.07$ and 0.16, [59]. In these statistical models the index ν is identified with a 'maximum configurational entropy', i.e.

$$\nu = \lim_{N\to\infty} \frac{1}{N} \ln [M(N)]. \tag{3.4}$$

If these results are combined with the trends of the surface Coulomb problem and the magnetic arrays, it is plausible to conjecture that in general the number of locally stable states of N-body cooperative systems increases exponentially with N. This conjecture has several practical consequences: If the exponential growth in the number of metastable states of the surface Coulomb problem continues to increase at the rates indicated in (3.2a) and (3.2c), then the numerical simulation of large systems $N > O(10^3)$ involves severe problems. For instance, the energy manifold describing the Coulomb interaction of 2000 charges constrained to the surface of a sphere would have about 5×10^{42} locally stable minima. Implementing numerical optimization or search algorithms and testing for stability on such an intricately corrugated energy landscape would strain current computing resources beyond their limits.

B. Energy Distributions

The electrostatic energy of the N- particle surface Coulomb problem, Eq. (2.1), is given by explicitly by

$$E(\phi_1,\theta_1;\ldots;\phi_N,\theta_N) = \frac{1}{2}\sum_{i=1}^{N}\sum_{j>i}^{N}\{\sin\phi_i \sin\phi_j \sin^2[\frac{1}{2}(\theta_i - \theta_j)] + \sin^2[\frac{1}{2}(\phi_i - \phi_j)]\}^{-1/2}, \quad (3.5)$$

where $\phi_i \in [O, \pi]$ and $\theta_i \in [-\pi, \pi]$ are the spherical coordinates of the i^{th} charge.

Geometrically, $E(\phi_1 \ldots \theta_N)$ corresponds to a surface in a 2N + 1 dimensional space. The highest peaks on this energy 'landscape' are generated by configurations where some of the charges are close together. The median range of heights is associated with randomly distributed sets of coordinates --- such as those used as the starting configurations for the computer searches. The lowest points of the valleys and craters correspond to locally stable configurations of the surface Coulomb problem. As indicated by (3.2a) and (3.2c), the number of these local minima increases at an exponential rate with N. Geometrical comparisons show that for a given value of $N > 1$, the charge configurations associated with these minima all tend to be quite different. Nevertheless, the relative energy variations between the lowest and highest local minima are less than 0.006% even for the largest multiplicities of states, i.e. $M(112) \propto 0.382\ e^{5.56} \propto 100$.

B-1. Energies of Random Initial Configurations. Let $E_j^{Ran}(N)$, $1 \le j \le p$, denote the energies of a set of random distributions of N charges on the surface of a unit sphere, where a total of $p > 1$ configurations are generated. Then ergodic arguments and rigorous results of potential theory [56] both show that the average energy of the set of random states is given by

$$\langle E^{Ran}(N)\rangle = \lim_{p\to\infty} \frac{1}{p} \sum_{j=1}^{P} E_j^{Ran}(N) = \frac{N^2}{2}, \tag{3.6}$$

where $N^2/2$ is the Coulomb energy of a continuous uniform spherical surface charge distribution with total charge N. Figure 3 and Table II show some of the results obtained from computer simulations with $p = 10^5$, and N varying throughout the range $6 \le N \le 100$. The overall agreement is good although the computer generated averages $\langle E^{Ran}(N)\rangle$ tend to exceed the theoretical values $N^2/2$ by about 6%. This bias is also evident in the asymmetric distribution of the maximum and minimum energy values about the mean displayed in columns 3,4 and 5 of Table II. The underlying reason is that random selections of angular coordinates include charge clusters [60], and these configurations boost the energy values in (3.5).

The computer simulations of the random charge configurations can also be checked by calculating their dipole moments, Eq. (1.2a). In an independent series of trials the 'random walk' result $\langle|\vec{d}(N)|\rangle_{Ran} \approx 0.9213\ N^{1/2}$, cited in (1.2b), was verified by generating 100 random configurations for every value of N in the range $3 \le N \le 64$. Finally, by combining (1.2b) and (3.6) in the invariant ratio

$$R \equiv \frac{\langle|\vec{d}(N)|\rangle_{Ran}}{\langle E^{Ran}(N)\rangle^{1/4}} = \left[\frac{2^{7/2}}{3\pi}\right]^{1/2} = 1.095\ 637, \tag{3.7}$$

it is possible to cross-check the consistency of the energy and dipole moment simulations. The numbers listed in the last column of Table II yield an average ratio of R = 1.110, which is within 1.3% of the theoretical value.

B-2. Minimum Energy States. Let $E_1(N)$ denote the lowest energy states of the N-body surface Coulomb problem found by computer searches. A complete set of values, ranging from $E_1(3) = 3^{1/2} \approx 1.732..$, to $E_1(112) = 5618.044882\,33$, is listed in column 4 of Table VIII in Appendix B. In the absence of rigorous analytical bounds we cannot exclude the existence of other configurations with even lower energies. The sequence of crosses in Fig. 3 shows the variation of E_1 with N in graphical form. On this coarse energy scale $E_1(N)$ is a smooth monotonic function: The simple expression

$$E_{1F}(N) = 0.5N^2 - 0.5513\ N^{3/2} \tag{3.8}$$

fits the data with error bounds of 0.1% at N = 20 and 0.01% at N = 112. Using $E_{1F}(N)$ as a smooth baseline, it is possible to construct scatterplots of the energy differences $E_{1F}(N) - E_1(N)$ on an enlarged scale. However, searches for systematic deviations resembling the energy peaks associated with atomic clusters [61] or analogues of Thomas-Fermi oscillations [62] have not led to any conclusive results [16, 40].

The functional form of $E_{1F}(N)$ has two physical interpretations [30]: (*i*) $N^2/2$ is the electrostatic energy of a uniform surface charge density — with total charge N — on a unit

Table II

Electrostatic Energies and Dipole Moments of Random Spherical Charge Distributions

N	$N^2/2^a$	$\langle E^{Ran}(N)\rangle^a$	σ^b	$Max\ \{E^{Ran}(N)\}$	$Min\ \{E^{Ran}(N)\}$	R^c
10	50	47.30	7.76	99.11	34.35	1.116
20	200	197.85	13.32	270.65	164.82	1.092
30	450	457.74	78.76	2594	395.85	1.107
40	800	835.63	198.4	3716	721.6	1.204
50	1250	1317.2	288.9	4416	1143	1.092
64	2048	2182.0	446.5	6229	1920	1.050
80	3200	3428.9	630.3	7824	3047	-
100	5000	5392.4	864.1	10 886	4851	-

[a] Eq. (3.6)
[b] standard deviation
[c] Eq. (3.7)

sphere. In order to recover the energy of a distribution of N point charges it is necessary to subtract the self-energies of a set of N uniformly charged spherical caps centered on these points. For $N > 1$, it is plausible to approximate the caps by disks. Since the energy of an infinitely thin disk of charge with radius a is $E_D = 2\pi^2\sigma^2a^3\ \{0.4244\}$, where σ is the charge density [63, 64]; the total self-energy correction is of the order of NE_D where $\sigma = (\pi a^2)^{-1}$. For simplicity, suppose that all the disks have the same radius. Then the crudest measure of

the total area covered by the N disks is the surface area of a unit sphere, i.e., $N\pi a^2 = 4\pi$. Consequently, the self-energy correction is approximately given by

$$NE_D \simeq 0.4244\ N^{3/2}; \tag{3.9}$$

which accounts for the second term in (3.8). More elaborate estimates that improve the agreement with the empirical coefficient 0.5513 are outlined in reference [40]. (ii) Equation (3.6) shows directly that $N^2/2$ can also be identified with the average energy of a set of N unit charges randomly distributed over the surface of a unit sphere. In this case, the $O(-N^{3/2})$ term represents the correlation energies of the ordered Coulomb equilibrium states.

B-3. Energies of Metastable States. The most striking feature of the metastable states is that their energies are closely bunched just above the minimum energy states. This trend begins with the first metastable state at N = 16: As indicated in column 4 of Table VIII in Appendix B, the energy difference ΔE (16) between the two states is

$$\begin{aligned} \Delta E(16) &= E_2\ (16)\ -\ E_1\ (16) \\ &= 92.920\,353\,96\ -\ 92.911\,655\,30, \\ &= 0.008\,698\,66; \end{aligned} \tag{3.10}$$

and this implies $\Delta E\ (16)/E_1(16) \simeq 9.36 \times 10^{-5}$. Figures 1 (a) and 1 (c) show that this small relative energy difference is not reflected in any geometric similarities between these

two states. At the other extreme, for N = 112, the computer searches lead to 60 locally stable states with distinct energy values --- 31 of these states occur in enantiomorphic pairs. In this case it is convenient to describe the level spacings by the average energy difference $\langle \Delta E\ (112) \rangle$, i.e.,

$$\begin{aligned} \langle \Delta E(112) \rangle &= [E_{60}\ (112) - E_1\ (112)]/59, \\ &= [5618.419\ 481\ 31 - 5618.\ 044\ 882\ 23]/59, \\ &= .006\ 349\ 14; \end{aligned} \tag{3.11}$$

which indicates that the relative spacings are of the order

$\langle \Delta E(112) \rangle / E_1(112) \simeq 1.13 \times 10^{-6}$.

In general, $\langle \Delta E(N) \rangle = [E_n\ (N) - E_1\ (N)]/(n-1)$, for N charges, where n (> 1) denotes the number of distinct energy levels. Table III shows the trends in level spacings for

Table III

Variation of the Average Energy Level Spacing $\langle \Delta E(N) \rangle$ with the Number of Charges N

N	16	21	22	27	30	32
n	2	2	2	2	2	2
$\langle \Delta E(N) \rangle$	.008 70	.000 29	.020 42	.006 99	.000 45	.207 12
N	55	56	57	58	59	60
n	6	4	5	10	5	6
$\langle \Delta E(N) \rangle$	.005 49	.051 22	.022 16	.013 08	.004 36	.030 07
N	107	108	109	110	111	112
n	52	47	56	59	52	60
$\langle \Delta E(N) \rangle$	.007 38	.007 37	.004 94	.004 01	.007 16	.006 35

18 values of N ranging from 'small' to 'large'. Since $\langle \Delta E(N) \rangle / E_1(N) \sim 10^{-6}$ for $N > 100$, computer searches for the lowest energy states in complex systems of this type require high precision. In fact this energy scale is so fine that neither the empirical fit (3.8), nor its graph on Fig. 3, can discriminate between the ground and metastable states.

It is also interesting to display the distribution of the density of states. Table VIII shows that for N = 112 there are 60 states with energies spread between 5618.044 and 5618.419. If these states were distributed uniformly there would be about 8 states per bin for bins of width 0.05. With this particular choice of bin width, the first bin covers the energy interval 5618.044 to 5618.094, but according to Table VIII contains only two states. The second bin extends from 5618.094 to 5618.144, and contains no states; etc. Similarly, for N = 111, the first bin of width 0.05 spans the interval 5515.293 to 5515.343, and contains only the ground state; etc. The histogram in Fig. 4 shows the combined statistics for N = 111 and 112 --- a total of 112 states. Clearly the level distribution is not uniform. There is a dip, or 'level-repulsion', in the energy bin just above the ground state; a pronounced maximum in the middle of the range; and an eventual decrease in the density of the highest levels. This density profile formally resembles the Wigner distribution of the energy level spacings of large 'random' Hamiltonian systems [65].

Figure 5 shows a semi-log plot of the density of states weighted by the probability of occurrence. It is a straightforward matter to include this additional information. Specifically, for N = 112, Table VIII shows that the two states falling into the first energy bin between 5618.044 and 5618.094 appeared 620 times in 1000 computer searches starting from different random configurations. On average, therefore, their relative probability of

occurrence is 62%. Similarly, for N = 111, the state in the first energy bin occurred in 48% of the computer trials. The combined average for these three states therefore is 55%; and this is the value indicated for the first bin in Fig. 5. The rest of the histogram can be obtained by similar means.

The most conspicuous difference between the two histograms in Figs. 4 and 5 is that the maximum of the probability density occurs near the minimum energy states. In general, this implies that for values of $N \gtrsim 100$ there is about a 95% probability that a computer search will end at an energy level within 0.003% of the ground state. But it is difficult to improve this precision. In the range $100 \leq N \leq 112$, the average probability that a computer minimization will actually reach the minimum energy state is only 35%. Of course, this result depends on the choice of minimizing algorithm. Nevertheless, similar statistical behavior occurs in the distribution of patterns in magnetic cooperative arrays [58]. All of these systems display the same basic trend: as the number of interacting objects increases, the statistical weight of the ground state decreases.

The survey of metastable states summarized in Table VIII is based on a total of about 7×10^5 computer trials. Rare states, with probabilities of occurrence as low as 0.01% are found for N = 21, 30, 42, 48, 58, and 61. Possibly there are additional states with still smaller capture basins. Certainly it is plausible that for N = 112 some states on the high energy tail of the histogram in Fig. 4 have been missed due to limited statistics (only 1000 energy minimizing searches). But the essential observation is that none of the numerical trials — for any value of N — has yet turned up any trace of isolated energy levels; that is, single levels separated by large 'band gaps' ($>> \langle \Delta E(N) \rangle$) from the cluster of states above the ground state. It remains

to be seen whether this trend continues for still larger values of N.

B-4. Energies of Individual Charges. The total electrostatic energy of a locally stable state of N charges can be represented as the sum of the partial energies associated with the individual charges. These partial energies have two interesting properties: (1) The variation of the individual charge energies *within* a configuration is generally much larger than the variation of the total energy *between* configurations. And (2), since the energy apportioned to a charge is simply the sum of the inverse distances to all the other charges, the variation of the individual energies is a measure of the geometric regularity of the configurations. Fig. 6 illustrates some of these energy relations. Specifically, let E_m (N) denote the total energy of the m^{th} state of N charges. Then a slight extension of (1.3) shows that

$$E_m(N) = \sum_{i=1}^{N} E_{m,i}(N); \qquad E_{m,i}(N) = \frac{1}{2} \sum_{j \neq i}^{N} |\vec{r}_i - \vec{r}_j|^{-1}, \tag{3.12}$$

where $E_{m,i}$ (N) is the partial energy of the i^{th} charge in the m^{th} state of N objects. The scatter plot in Fig. 6 begins at N = 16. This entry corresponds to the following array of total and partial energies, cf. (3.10):

N = 16; ground state	N = 16; metastable state
Fig. 1(c) and Fig. 1(d)	Fig. 1(a) and Fig. 1(b)
E_1 (16) = 92.911 655 30	E_2 (16) = 92.920 353 96
$E_{1,1}$ (16) = 5.762 143 2	$E_{2,1}$ (16) = 5.793 787 0
↓	↓
$E_{1,4}$ (16) = 5.762 143 2	$E_{2,8}$ (16) = 5.793 787 0
$E_{1,5}$ (16) = 5.821 923 5	$E_{2,9}$ (16) = 5.821 257 1
↓	↓
$E_{1,16}$ (16) = 5.821 923 5	$E_{2,16}$ (16) = 5.821 257 1

(3.13)

The spread of partial energies in the ground state is $E_{1,16}$ (16) - $E_{1,1}$ (16) = 0.059 780 3; and in the metastable state $E_{2,16}$ (16) - $E_{2,1}$ (16) = 0.027 470 1. Consequently, the average maximum energy variation *within* these configurations is 0.043 625, whereas the total energy difference *between* the configurations is only E_2 (16) - E_1 (16) = 0.008 698 66 --- smaller by a factor of 5. This disparity is also reflected in the individual charge energies: Twelve charges in the ground state, $E_{1,5}$ (16), ..., $E_{1,16}$ (16), have greater energies than any of the charges in the metastable state!

In the general case, when there are n distinct energy levels associated with N charges, the average maximum variation of partial energies within the configurations $\langle \Delta E_{part}(N) \rangle$ is given by

$$\langle \Delta E_{part}(N) \rangle = \frac{1}{n} \sum_{m=1}^{n} \{E_{m,N}(N) - E_{m,1}(N)\}. \qquad (3.14)$$

Table IV

Variation of the Partial Energy Differences $\langle \Delta E_{part}(N) \rangle$ Within Configurations

N	16	21	22	32	55	60	111	112
$\langle \Delta E_{part}(N) \rangle^a$	.043	.055	.030	.054	.117	.098	.211	.208
R(N)[b]	5.01	189	1.44	0.26	21.3	3.19	29.5	32.7

[a] Eq. (3.14)
[b] Eq. (3.15)

Table IV shows that this energy spread is a slowly increasing function of N. The differences in partial and total energies can be combined in the ratio

$$R(N) = \frac{\langle \Delta E_{part}(N) \rangle}{\langle \Delta E(N) \rangle} \sim \frac{\text{Energy Differences Within Configurations}}{\text{Energy Differences Between Configurations}} \qquad (3.15)$$

which is the ordinate of the scatter plot in Fig. 6. Some representative values are also listed in Table IV. Clearly most of the points in Fig. 6 fall into the band between $5 < R(N) < 50$. This demonstrates that the scale of total energy differences between successive metastable states

is much finer than the variation of the individual charge energies. A complementary pattern is exhibited by the stabilities: Eqs. (2.9a) and (2.9b) show that the numerical reproducibilities of the total energies of the configurations generally exceed the reproducibilities of the partial energies by five orders of magnitude.

The contrast between individual and collective energies is also illustrated by the following example: Suppose that the partial energy of a charge has the value 36.935 241. Then it is easy to verify from the computer results that this charge cannot be a constituent of any locally stable state with either $N \leq 83$ or $N \geq 85$; it must belong to one of the 30 configurations with $N = 84$. However, there is no finer scale of energy rankings to help in locating this charge. Everyone of the 30 states is comprised of sets of 84 partial energies that straddle the value 36. 935 241. Consequently all of these states have to be examined in detail before it can be established that 36.935 241 corresponds to $E_{10,37}$ (84) — the partial energy of the 37th charge in the 10th equilibrium state of 84 objects. This assignment is unique because all 84 partial energies in the 10th state are different, and $E_{10,37}$ (84) $\neq E_{m,i}$ (84) for all $1 \leq i \leq 84$ and $m \neq 10$. The only remaining ambiguity is geometric: as indicated in Table VIII, E_{10} (84) has two enantiomeric configurations.

Equation (3.12) shows that the partial energy of a charge is proportional to the sum of its inverse distances to all the other charges. This implies that highly symmetric equilibrium configurations that 'look alike' from every charge or vertex have unique partial energies, i.e., $E_{m,i}(N) = E_m(N)/N$ for all $1 \leq i \leq N$. Indeed, this is the case for three of the Platonic solids, the tetrahedron, octahedron (dipyramid), and icosahedron, whose vertices are the equilibrium positions of the surface Coulomb problem for $N = 4$, 6, and 12 respectively. The partial

energies are also unique for N =8 and 24, even though these configurations are not included among the standard semi-regular (Archimedean) polyhedra. Clearly, less symmetric charge distributions will have a greater variety of reciprocal distances, and this dispersion can be used as a measure of geometric irregularity analogous to the angular diversity ratio (1.1): If n_e (N, m) denotes the number of distinct partial charge energies that occur in the m^{th} state of N objects, then the corresponding *energy diversity ratio* (%) is given by

$$D_e(N,m) = 100 \frac{n_e(N,m)}{N}. \tag{3.16}$$

In the range $2 \leq N \leq 112$, the computer trials yield 1248 equilibrium states with distinct energies; 806 of these states occur in enantiomorphic pairs, cf. Table I. The associated energy diversity ratios are listed in column 9 of Table VIII in Appendix B, and displayed graphically in Fig. 7. Two trends are evident: (i) D_e(N, m) is a slowly increasing function of N. The first configuration that is so irregular that all of its partial charge energies are different occurs at N = 35; i.e., $D_e(35,4) = 100\%$. By the time N reaches 102, 34 out of a total of 54 locally stable states have energy diversity ratios in excess of 95%. This is another confirmation of the basic trend that increasing complexity is correlated with greater geometric irregularity. (ii) Figure 7 also shows that the energy diversity ratios tend to cluster in a series of bands near 17%, 24%, 50%, 75%, and 100%. It is plausible that this regularity is connected with a deeper symmetry of the surface Coulomb problem.

4. Geometric Properties of the Surface Coulomb States

The locally stable solutions of the N-charge surface Coulomb problem are constrained solely by spherical boundary conditions and the O(4) symmetry of the Coulomb interaction. The exponential growth of the multiplicity of solutions --- M(N) ~ $e^{0.05N}$, Eq. (3.2a) --- shows that these restrictions are compatible with a great variety of geometric structures. Only in the simplest systems is there an overlap with the criteria of strict regularity that underlie the classical theories of polygons and polyhedra [13]. For instance, the Coulomb solution for N = 3 corresponds to an equilateral triangle inscribed in a great circle: this is the simplest example of a *regular polygon*, i.e., a plane polygon with equal interior angles and equal sides. Similarly, *regular polyhedra* are bounded by congruent regular polygons and have congruent vertices. Only the solutions for N = 4 (tetrahedron), N = 6 (dipyramid), and N = 12 (icosahedron) share this high degree of symmetry. The other Platonic solids, the cube with 8 vertices, and the dodecahedron with 20 vertices, do not correspond to solutions of either the surface Coulomb or Tammes problems. The *semi-regular polyhedra* are also bounded by regular polygons with congruent vertices and edges, but the polygons do not all have to be congruent to each other. This class of objects includes the thirteen Archimedean polyhedra as well as infinite sets of semi-regular prisms and anti-prisms. None of the surface Coulomb configurations match any of these semi-regular polyhedra. In particular, the well known 'bucky ball', or truncated icosahedron, associated with C_{60} is not a solution of either the Tammes or surface Coulomb problems for N = 60.

Every Archimedean polyhedron has a dual formed by joining a point that is above the center of each face of the polyhedron to equivalent points above all the neighboring faces. The

lines connecting these points are constrained to intersect the edges of the original polyhedron. The resulting *duals of the semi-regular polyhedra* have congruent faces but none of these faces are regular polygons. These duals are also less symmetric than the Archimedean figures because not all of their vertices lie on a single sphere; consequently none of the dual polyhedra coincide with any of the solutions of the surface Coulomb problem [66, 67, 68]. However, there is an interesting 'near miss' for N = 32. The *pentakis dodecahedron* is a convex polyhedron with 32 vertices, 90 edges, and 60 faces composed of congruent isosceles triangles: This object is the dual of the truncated icosahedron which has 60 vertices and 32 faces. The two types of edges of the pentakis dodecahedron intercept angles of

$$\sin^{-1}\left(\frac{2}{3}\right) = 0.729\ 727\ 656 \qquad (4.1)$$

and

$$\frac{1}{2}\left[\pi - \sin^{-1}\left(\frac{2}{3}\right) - \tan^{-1}(2)\right] = 0.652\ 358\ 139$$

as seen from the center of symmetry, i.e., the origin of the inter-sphere [67, 68]. These values agree to within six significant figures with the corresponding angles of the minimum energy Coulomb configuration for N = 32 (see the entries on lines 13 and 14 of Table V). A pictorial comparison of the pentakis polyhedron and the Coulomb configuration would show that they are essentially identical. But pentakis breaks strict spherical symmetry because its 32 vertices are distributed over two concentric spheres whose diameters differ by 2.58%. Consequently, the ratio of the two edge lengths of the pentakis dodecahedron, 1.127 322, deviates by 0.77% from the corresponding edge ratio, 1.118 600, of the Coulomb solution. In this instance, the surface Coulomb problem actually leads to a more symmetric 'dual' partner of an Archimedean

polyhedron than the original construction of pentakis by Catalan in 1862 [69]. Moreover, the minimum energy solution for N = 32 is not only geometrically regular, but it is also robust: in the range $12 < N \leq 65$, it is the only equilibrium configuration common to both the Coulomb and logarithmic interactions [16].

In addition to the 5 Platonic solids and 26 Archimedean polyhedra and their duals, there are only 92 other convex polyhedra whose faces are entirely composed of regular polygons --- generally not all of the same kind [17, 18]. These objects are geometrically irregular or *non-uniform* in the sense that there are no symmetry operations that transform a particular vertex into each of the other vertices in turn. Twenty-four of these non-uniform polyhedra may be inscribed in a sphere [68]. By comparing the corresponding numbers of vertices and faces it is easy to verify that none of these 24 objects match any of the surface Coulomb equilibrium configurations. In summary, therefore, out of a total of 2054 surface Coulomb states and 123 convex polyhedra derived from classical geometry, there are only three configurations common to both sets. This number is also an upper bound because further extensions of the Coulomb problem to larger systems with $N > 112$ cannot yield any additional matches. These results show that the locally stable states of complex cooperative systems of this kind tend to have symmetries that differ from those that characterize the regular polyhedral configurations of classical geometry.

A. Dipole Moments. The distribution of the dipole moments of the surface Coulomb states can be used to answer two basic questions: (1) Are the configurations for large values of N so irregular that they are approximately equivalent to random networks of points on a sphere? And furthermore, (2) do these networks approach some kind of universal asymptotic statistical

distribution that is independent of the laws of repulsion that act between the individual charges? To settle these issues, it is convenient to recall from Eq. (1.2b) that the average value of the dipole moment of a random configuration of N unit changes on a sphere is an increasing function of N, i.e., $\langle |\vec{d}\ (N)| \rangle_{Ran} \sim N^{1/2}$. As indicated in connection with Eq. (3.7), the applicability of this 'random walk' result to the Coulomb problem can be confirmed by computer trials. In particular then for N = 100, the expectation value of the dipole moment of a random distribution is quite large, $\langle |\vec{d}\ (100)\ | \rangle_{Ran} \approx 9.2$; whereas the entries in column 5 of Table VIII show that $0 \leq |\vec{d}\ (100)| \leq 0.0037$ for all 52 of the Coulomb states found by computer searches. This upper bound indicates that the metastable state with the highest energy and nearly maximal angular diversity (see below) for N = 100 has a dipole moment that is about 4×10^{-4} smaller than that expected for a random configuration. Figure 8 shows that this trend of small dipole moments prevails for all the Coulomb configurations in the range $N \leq 112$. The logarithmic ordinate scale of the graph extends down to 10^{-6}, which is near the limit of numerical accuracy for large systems, $N \sim O(100)$. Table VIII shows that states with vanishing dipole moments are quite common for small values of N, but tend to become less frequent as N approaches 100. Nevertheless, they don't disappear entirely: the ground state with the largest capture basin for N = 112 apparently has a vanishing moment. These results clearly show that the charge distributions of the surface Coulomb configurations have intrinsic regularities that persist despite the lack of the congruences or symmetries associated with the polyhedra of classical geometry.

There are systematic variations of the dipole moments that depend on the strength of the

force acting between the charges. According to Eq. (2.5), if the interaction is logarithmic, or 'soft', all locally stable configurations have vanishing dipole moments [16]. At the other extreme, the 'hard' Tammes potential, $|\vec{r}_i - \vec{r}_j|^{-n}$, $n \to \infty$, leads to states with sizable moments. Spot checks of some of the Tammes configurations found by Kottwitz's computer searches [30] yield moments larger than unity. All the available information can be summarized as follows:

Force Law	*Size of Dipole Moment*	*Source of Result*
$\|\vec{r}_i - \vec{r}_j\|^{-1}$	0	analytical identity, Eq. (2.5)
$\|\vec{r} - \vec{r}_j\|^{-2}$	$0 - 10^{-2}$	computer trials ($N \leq 112$)
$\|\vec{r}_i - \vec{r}_j\|^{-n}$, $n>1$	$O(1)$	computer trials ($N \leq 90$)
random	$(8N/3\pi)^{1/2}$	combinatorial lemma, Eq. (1.2b)

(4.2)

Obviously, in the range $2 \leq N < O(100)$, there is no tendency for a convergence of the dipole moments associated with the logarithmic, Coulomb, or Tammes interactions. This diversity suggests the conjecture that for large values of N different force laws lead to distinct asymptotic distributions of spherical charge networks. Comparisons of trends in the Tammes and Coulomb angles (see Section 4E-1) also support this surmise.

B. Distributions of Angles. Another measure of the regularity of the surface Coulomb configurations is the *angular diversity ratio* introduced in Eq. (1.1). This has a simple basis: If $\vec{r}_i$ *and* $\vec{r}_j$ specify the locations of two charges on the surface of a sphere with unit radius, then the set of N(N-1)/2 angles, $\psi_{ij} = \cos^{-1}(\vec{r}_i \cdot \vec{r}_j)$, where $\psi_{ij} \leq 180°$, $1 \leq i,j \leq N$, $i \neq j$,

describes the geometry of the charge distribution. The degeneracy of this set is a measure of the symmetry of the configuration. For instance, if 5 points are distributed arbitrarily over the surface of a sphere, there will generally be $5 \times 4/2 = 10$ distinct angles between pairs of points. However, in the case of the surface Coulomb problem, the unique equilibrium arrangement of 5 charges is a triangular dipyramid --- one charge at the north pole, another at the south pole, and the remaining three charges equally spaced around the equator. Obviously only three distinct angles appear between any pair of charges in this highly symmetric configuration: 180° occurs once, 120° occurs three times, and 90° occurs six times. The corresponding angular diversity ratio therefore has the low value of

$$D_a(N) = 100 \frac{\text{number of distinct angles}}{N(N-1)/2} \rightarrow 100 \frac{3}{10} = 30\% \qquad (4.3)$$

Similarly, the clustering of the irregular N = 11 and 13 configurations around the highly symmetric icosahedron at N = 12 is immediately apparent from the D_a fluctuations, without the need for any graphical comparisons; viz.

N	$D_a(N)$	$D_e(N)$	$\lvert\vec{d}(N)\rvert$
11	36.4%	45.5%	0.0132
12	4.5%	8.3%	0
13	37.2%	46.2%	0.0088

(4.4)

This array shows that all three indices of regularity --- the angular diversity ratio D_a, the energy diversity ratio D_e [Eq. (3.16)], and the dipole moment $|\vec{d}|$ --- yield consistent results. These correlations also appear in the detailed list of values in columns 5, 9, and 10 of Table VIII in Appendix B, as well as in the graphical summaries in Fig. 9 and Fig. 10. In particular, the parallel increase of both the angular and energy diversity ratios confirms once again the general conjecture that increasing complexity tends to be associated with decreasing symmetry. For instance, the first configuration that is so irregular that all of its vertices are inequivalent (D_e = 100%), and most of its edges have different lengths (D_a = 99.2%) occurs at N = 35. Fig. 9 shows the development of this trend in graphical form. At N = 102, 30 out of a total of 54 locally stable states have energy and angular diversity ratios in excess of 95%. These irregularities are pervasive for $N \sim O(100)$.

The distribution of values in the sets of angles ψ_{ij} is also useful for comparing the structures of different charge configurations belonging to the same value of N. Since the data in Section 3B-3 show that the energies of all of these locally stable states are very nearly the same --- within 0.007% for N = 102 --- it is possible that some of these states also have geometrical resemblances. Well known examples of sets of complex configurations with common 'backbones' and minor 'peripheral' variations include the tautomers and conformers of structural chemistry. However, everyone of the surface Coulomb states with non-identical energies appears to have a distinct structure. For instance, at N = 102, there are 87 configurations (cf. Table I) each of which is described by a ψ_{ij} - set with 5151 angles.

Comparisons show that there are 33 sets that occur twice: each matching pair has the same energy and is geometrically related by an improper isometry --- evidently these are just the enantiomeric configurations. Apart from these degeneracies, there are then a total of 87- 66/2 = 54 different states. Further comparisons of the associated angular sets, ψ_{ij}^{k}, $1 \le k \le 54$, show that the *maximum* fraction of coincidences among any pair of these sets is bounded by 9%. Computer surveys for all N in the range $50 < N \le 112$, where multiple states become more frequent, indicate that this overlap estimate is actually a general result; i.e., if V(N) denotes the fraction of common angles, then

$$V(N) = \frac{\#(\psi_{ij}^{k} \bigcap \psi_{ij}^{l})}{N(N-1)/2} \le 0.09, \tag{4.5}$$

where $k \ne l$, and the set intersections exclude enantiomeric pairs. The low value of this overlap ratio shows that it is implausible that configurations with non-identical energies share any major structural features such as common 'backbones'.

The overlap bound in (4.5) is based on very conservative angle matching criteria. When $N \gtrsim 100$, the precision of the angular coordinates of the individual charges in rare states can decrease to about one part in 10^5. This is degraded further by the computation of the inter-particle angle sets ψ_{ij}. Finally, the coarseness of the matching may be relaxed even more to ensure that all the enantiomeric states are correctly paired up. Consequently, the actual values of the overlap ratios V(N) may be significantly smaller than the bound shown in (4.5). For

example, at $N = 84$, all 16 states with distinct energies are sufficiently irregular so that the positioning conventions of Section 2B yield unique orientations. Under these circumstances, the charge coordinates of all of these states --- which are known to 7 figures, (2.9c) --- can be compared directly. Extensive spot checks have failed to turn up even one matching charge position, apart from the common fixed point at the north pole. It seems, therefore, that the exponential increase in the number of states for larger values of $N(> 50)$ is accompanied by a tremendous proliferation of geometric structures.

C. **Coulomb Polyhedra: Regular Configurations.** The coexistence of order and disorder in the geometric structure of the surface Coulomb states is illustrated in Fig. 11. This diagram shows the equilibrium configuration of 19 charges on the surface of a sphere. The apparent symmetry of this arrangement is highlighted by the auxiliary polyhedron whose vertices coincide with the charge positions. The faces and edges of this polyhedron can be constructed with the help of some computer graphics: Given N (>3) points on the surface of the sphere, the set of all combinations of 3 points determines a maximum of $N(N-1)(N-2)/6$ planes. Associated with each plane and triple of points --- located by the unit vectors $\vec{r}_j$, $j = \alpha, \beta, \gamma$ --- is another vector $\vec{r}_c$ extending from the center of the sphere to the plane and perpendicular to it. Since the plane and sphere intersect in a circle ($C_{\alpha\beta\gamma}$) all the scalar products $\vec{r}_c \cdot \vec{r}_j$ are equal. Suppose now that $\vec{r}_k$ ranges over the positions of all the charges *not* included in the $\vec{r}_j$ triplet --- i.e., the set $\{\vec{r}_\ell\}_1^N \backslash \vec{r}_\alpha, \vec{r}_\beta, \vec{r}_\gamma$ --- and furthermore that $\vec{r}_k \cdot \hat{r}_c \leq \vec{r}_j \cdot \vec{r}_c$; then the plane containing the charges α, β, γ is a face of the polyhedron. Geometrically, this inequality simply means that

the spherical cap bounded by $C_{\alpha\beta\gamma}$ contains no other charges. In cases where two or more charge triplets determine coincident planes, the associated polyhedron face is bounded by four or more vertices. Figure 11 includes an example of this situation. The end result of this construction is that the Coulomb polyhedron for N = 19 has a total of 33 faces. The corresponding number of edges (e) then follows from Euler's formula

$$N + f - 2 = e,$$

or (4.6)

$$19 + 33 - 2 = 50.$$

Column 11 of Table VIII in Appendix B lists the number of faces (f) of the Coulomb polyhedra for all configurations in the range $4 \leq N \leq 112$.

The symmetries of the Coulomb polyhedron in Fig. 11 are reflected in the low values of the energy diversity, $D_e = 7/19 \approx 36.8\%$ [Eq. (3.16)], and the angular diversity, $D_a = 52/171 \approx 30.4\%$ [Eq. (4.3)]. In particular — apart from the charge at the north pole with the least partial energy — all the other 18 charges occur in pairs: each partner with the same partial energy and longitude, but the two charges differing by 180° in latitude. This symmetric pattern has a small but non-vanishing dipole moment, $|\vec{d}(19)| = 0.000\ 135$, pointing towards the north pole. The contrasting irregular features of this polyhedron arise from a lack of congruence among the edge lengths. No more than four edges have equal lengths. In fact, the 50 edges are composed of 10 groups of 4 congruent edges and 5 groups of 2 congruent edges. Consequently the polygonal faces in Fig. 11 are too irregular to fit into the standard set of non-uniform polyhedra [17,18].

A useful measure of the degree of congruence in the Coulomb polyhedra is the ratio of the number of distinct edge lengths to the total number of edges. Since the edge lengths are determined by the central angles between the corresponding vertices, this congruence measure is equivalent to a *nearest neighbor angular diversity ratio* analogous to (4.3), viz.

$$D_a^{nn}(N) = 100 \frac{\textit{number of distinct edge lengths } (\ell)}{\textit{total number of edges } (e)} \tag{4.7}$$

Whereas the angular diversity D_a is a global index of the variety of all possible angles between charges, D_a^{nn} is a strictly local measure that takes into account only the diversity of angles between adjacent charges. In the case of the N = 19 polyhedron, both the local and global measures of regularity yield nearly the same result

$$D_a^{nn}(19) = 100 \times \frac{15}{50} = 30.0\% \leftrightarrow 30.4\% \approx 100 \times \frac{52}{171} = D_a(19). \tag{4.8}$$

Computer surveys of all the other Coulomb polyhedra with N vertices in the range $4 < N \leq 112$ show a similar equivalence. If this trend extends beyond $N \sim 112$, it would simplify the identification of regular charge patterns: estimates of $D_a^{nn}(N)$ *for* $N > 1$ require at most the comparison of 3N nearest neighbor angles.

Although the dominant geometric trend of the Coulomb states is one of increasing irregularity for larger values of N, the sporadic appearance of small percentages among the

diversity ratios listed in columns 9 and 10 of Table VIII shows that some ordered patterns persist up to the limits of the computer explorations. The distribution of these special states is indicated graphically by the set of points in the 0 - 20% bands in Fig. 7 and Fig. 9. Quantitative information concerning the most regular configurations is summarized in Table V. For reference, the entries in the first line recapitulate the data for the icosahedron (N = 12) --- the largest Platonic solid whose vertices coincide with the solutions of the logarithmic, Coulomb, and Tammes problems. Comparisons with the indices for N = 16, 24, 32, and 72 show that these new polyhedra are also highly symmetric. The two N = 16 configurations are depicted in Figs. 1(a) - 1(d): they illustrate the interesting point that the lowest energy state is not necessarily the most symmetric. Table VIII shows that this situation recurs at several other values of N; e.g., the most symmetric N = 82 pattern is ranked eighth in order of increasing energy, and has an extremely low probability of occurrence. The N = 24 Coulomb polyhedron resembles the snub cube, one of the semi-regular Archimedean solids. However, the Coulomb interactions distort the symmetry of the classical polyhedron: Whereas the snub cube has 32 triangular and 6 square faces, all with equal edges, the faces of the Coulomb polyhedron include 24 scalene triangles [41]. The N = 32 situation corresponds to the 'near miss' of the pentakis dodecahedron discussed previously in connection with Eq. (4.1). In this case the Coulomb polyhedron is slightly more symmetric than its classical counterpart. The lowest energy Coulomb state for N = 72 is also conspicuously symmetric. All faces of this polyhedron are triangular. There is no resemblance to the aspherical N = 72 'fullerene' cage containing 12 pentagons and 26 hexagons [70].

Table V

Regular Coulomb Polyhedra

N[a]	E[b]	f[c]	e/ℓ[d]	n_e[e]	$D_a^{nn}(\%)$[f]	Nearest neighbor angles (degrees)	Multiplicity[g]
12	49.165	20	30/1	1	3.3	63. 4349[i]	30
16*[h]	92.911	28	42/4	2	9.5	48.9362	6
						52.5452	12
						54.6580	12
						61.8004	12
16	92.920	26	40/4	2	10.0	50.1269	8
						52.0044	8
						54.2578	16
						63.0252	8
24*	223.347	38	60/3	1	5.0	42.0653	24
						45.0400	24
						45.7102	12
32	412.261	60	90/2	2	2.2	37.3773	60
						41.8103	30
72*	2255.001	140	210/4	2	1.9	24.4917	60
						24.9262	30
						25.4334	60
						28.2068	60

[a]Number of charges or vertices.
[b]Coulomb energy, Eq. (3.5).
[c]Number of faces, Eq. (4.6).
[d]Number of edges/distinct edge lengths, Eq. (4.7).
[e]Number of distinct partial energies, Eq. (3.16).
[f]Diversity ratio, Eq. (4.7).
[g]Number of times this angle appears.
[h]Enantiomeric states.
[i] $2 \sin^{-1} [\frac{1}{2} (2 - 2/5^{1/2})^{1/2}]$.

The entries in Table V do not continue beyond N = 72 because the more complex symmetric polyhedra contain at least 11 different nearest neighbor angles. Nevertheless, the ordered patterns stand out clearly among the increasing variety of irregular polyhedra. For example, at N = 112, there are at least 60 locally stable states with distinct energies. The first, second, and tenth levels are clearly different because their nearest neighbor ratios D_a^{nn} [Eq. (4.7)] are 10.5%, 8.2%, and 24.1% respectively; all the other states have angular diversities exceeding 45%. The marked regularity of the second level is also apparent from the small number of partial charge energies --- equivalent to 10 types of polyhedron vertices --- and the symmetric grouping of the 330 nearest neighbor angles: these occur in 26 sets of 12 equal angles, and a residual set of 18 angles, also all alike. Unraveling the complex order of these large polyhedra is a challenging problem in 'physical' geometry.

D. Enantiomorphic Configurations. A set of points on the sphere may be transformed by *isometries* or *congruence mappings* that preserve the distances between all pairs of points. All isometries, in turn, can be built up from three basic types of transformations [71]: (i) rotations about an axis; (ii) mirror reflections in a plane; and (iii) parallel displacements of all points. If the mappings are restricted to a fixed sphere, parallel displacements play no role, and the congruence transformations reduce to *proper isometries* or (rigid body) rotations, and *rotatory reflections* composed of a reflection and a rotation whose axis is perpendicular to the mirror [13, 72]. *Central inversions*, in which the coordinates of all points are reflected in the origin of the sphere, i.e., $\vec{r} \rightarrow -\vec{r}$, are special cases of rotatory reflections in which the rotation is a half-turn.

If a pattern $\mathbb{C}_i$ of identical charges on the surface of a sphere is sufficiently irregular --- though not necessarily random --- then the only isometric mapping, I: $\mathbb{C}_i \rightarrow \mathbb{C}_f$, that yields a final configuration $\mathbb{C}_f$ indistinguishable from the initial state is the identity transformation. In contrast, highly symmetric configurations such as the icosahedron are invariant under a great variety of isometric transformations, e.g. the composite group $A_5 \times C_i$ [14]. The set of solutions of the surface Coulomb, logarithmic, and Tammes problems interpolates between these two extremes: In all three cases larger values of N are associated with less symmetric point groups [16, 30, 41, 42]. However, as emphasized in connection with the dipole moments in Section 4A, even Coulomb states whose only isometric symmetry is the identity transformation have ordered structures.

When $N > 50$, the surface Coulomb states tend to cluster in pairs, each with the same sequence of partial energies, equal total energy, and nearly equal probability of occurrence. Suppose that $\mathbb{C}^L(N)$ *and* $\mathbb{C}^R(N)$ denote such a pair of states. Since the orientation conventions established in Section 2B automatically include rotational degeneracies, it remains to check whether these states are related by an improper isometry. In practise, this mirror symmetry can be verified by picking a state, say $\mathbb{C}^L(N)$, and reflecting it in an arbitrary plane through the center of the sphere. The resulting configuration is then rotated so that the charge with the lowest partial energy is positioned at the north pole, $\theta = \phi = 0$, and the charge with the next lowest partial energy is at zero longitude, $\theta = 0$. If all the partial energies are different, this orientation is unique, and the final configuration will coincide with $\mathbb{C}^R(N)$. In case there is a

degeneracy in the partial energies, some auxiliary comparisons may be required.

The distinctions between proper and improper isometries can be illustrated with two simple examples: Figure 1(b) is a plan view of the symmetric four-ring structure of the N = 16 metastable Coulomb solution, C_2 (16). Obviously this pattern is invariant under 90° rotations and reflections --- if the rings are copied on a transparency, and the transparency is flipped over, the reversed image will coincide with the original pattern. This symmetry is broken by the greater complexity of the two N = 16 ground states. If Fig. 1(d) is copied, the image on the flipped transparency cannot be rotated into coincidence with the original pattern, but it will match the other ground state configuration. In general, any configuration that cannot be brought into coincidence with its mirror image by rotations is *chiral* or *enantiomorphic*. Hence the familiar example of right (R) and left (L) handedness suggests the notation C_1^R (16) *and* C_1^L (16) for the two N = 16 chiral ground states. But for arbitrary patterns --- in fact, even the simple perspective view in Fig. 1 (c) --- there are no obvious pictorial cues of handedness, or a 'screw-sense', and chirality has to be checked by other means such as exhaustive computer comparisons [73].

The asterisks in column 3 of Table VIII mark the enantiomeric states of the surface Coulomb problem. Comparisons show that N = 15 is the common threshold for the appearance of chiral configurations in the surface Coulomb, logarithmic, and Tammes problems [14, 16, 39]. Furthermore, in the range $15 \le N \le 65$, the ground states of the logarithmic potential are chiral if and only if the ground states of the associated surface Coulomb problem are chiral [16]. However, the results for N = 15, 16, 19, 21, etc., show that there is no such one-to-one

correspondence between the ground states of the surface Coulomb and Tammes problems [30].

There are interesting connections between chirality, 'chaos', symmetry breaking, and cryptography in the surface Coulomb problem. Let $M[\mathbb{C}^R_{Ran}\ (15)] \rightarrow \mathbb{C}^R_1\ (15)$ represent the mapping of a randomly chosen initial state of 15 charges, $\mathbb{C}^R_{Ran}\ (15)$, to one of the pair of chiral ground states, $\mathbb{C}^R_1\ (15)$ by means of an energy minimizing algorithm M. Suppose further that the initial configuration is sufficiently irregular so that it can be verified that $\mathbb{C}^R_{Ran}\ (15)$ is indeed a chiral state with a mirror image $\mathbb{C}^L_{Ran}\ (15)$. Then it can be shown that the minimizing algorithm of Section 2B, as implemented on a computer, preserves chirality. (An analytic analogue is discussed in [74].) This leads to an array of parallel mappings that can be extended to include many initial states:

	strings of (pseudo) random numbers		
	↓	↓	
sets of (pseudo) random initial states	$\{\mathbb{C}^R_{Ran}\ (15)\}$	$\{\mathbb{C}^L_{Ran}\ (15)\}$	
	↓	↓	(4.9)
locally stable energy minima: terminal states	$\mathbb{C}^R_1\ (15)$	$\mathbb{C}^L_1\ (15)$	

This diagram shows that the net effect of the chirality preserving map M is to transfer the 'L' and 'R' labels from the ground states up to the level of the random initial states, and to split these into two corresponding sub-sets $\{\mathbb{C}^R_{Ran}(15)\}$ *and* $\{\mathbb{C}^L_{ran}\ (15)\}$. Since the initial configurations

are distributed uniformly over the surface of the sphere, slight changes in the angular coordinates of the charges in any particular state $\mathbb{C}^{R}_{Ran}$ (15) can transform it into a $\mathbb{C}^{L}_{Ran}$ (15) state, and *vice versa*. Consequently the end result of an energy minimization can be sensitively affected by slight perturbations of the initial conditions: This mix of randomized states and unstable evolution is a basic characteristic of 'chaotic' dynamics [75].

Chiral symmetry breaking can occur in a variety of ways. For instance, varying the index n in the power law $|\vec{r}_i - \vec{r}_j|^{-n}$ can induce transitions between chiral and non-chiral states. The simplest illustration is provided by N = 16. In this case the ultra-repulsive Tammes potential $|\vec{r}_i - \vec{r}_j|^{-n}$, $n \rightarrow \infty$, can be approximated by choosing n = 1 310 720 [15, 30]. Both geometrical arguments [76] and computer trials then show that the N = 16 Tammes solution is a symmetric four-ring structure closely resembling the pattern in Figs. 1(a) and 1(b). (The latitudes of the rings are $\pm$ 13.632° *and* $\pm$ 51.490° in the Tammes case, and $\pm$ 11.342° *and* $\pm$ 51.684° in the Coulomb case.) But the lowest energy solution for the surface Coulomb problem is quite different: It is split into a pair of chiral states one of which is shown in Figs. 1(c) and 1(d). Evidently then, as the potential index n decreases from 1 310 720 to 1, there must be at least one threshold where chiral states appear.

The chiral 'L' and 'R' indices are equivalent to a binary alphabet. In principle, therefore, it is possible to construct any desired string or 'message' with an appropriate series of $\mathbb{C}^{R}_{1}$ (15) *and* $\mathbb{C}^{L}_{1}$ (15) configurations. But as (4.9) shows, each ground state configuration can be enciphered in an enormous number of ways by the mappings M [$\{\mathbb{C}^{R,L}_{Ran}$ (15)$\}$] $\rightarrow$ $\mathbb{C}^{R,L}_{1}$ (15).

For instance, on a double precision computer, the number of initial states with a particular chirality can easily exceed 10^{10}. The element of ambiguity or concealment then lies in the assignment of a specific 'L' or 'R' label to any one of these random initial states. Although it is easy to verify that a particular state is chiral, the spatial arrangement of charges is usually too complex to exhibit an obvious 'handedness' --- it is necessary to go through an explicit energy minimizing sequence leading to either $\mathbb{C}_1^R$ (15) *or* $\mathbb{C}_1^L$ (15) in order to identify whether an initial state is 'L' or 'R'.

The strings of random numbers in the top line of (4.9) refer to the angular positions of the charges in the initial configurations. In particular, if the latitudes and longitudes of the charges are specified to an accuracy of 12 decimals, then the configurations $\mathbb{C}_{Ran}^{R,L}$ (15) can be represented by strings of 15 × 2 × 12 nominally random digits, $\{d_j\}_1^{360}$, d_j = 0, 1, .., 9. The security of this 'chiral-energy' encipherment therefore relies both on the algorithmic complexity of the mapping M and the tremendous redundancy of the correspondence

$$\mathbb{C}_{Ran}^{R,L}\ (15) \leftrightarrow \{d_j\}_1^{360} \rightarrow R \text{ or } L. \tag{4.10}$$

In analogy with other schemes involving 'trap-door' or 'one-way' functions [77], eq. (4.10) is hard to invert because the reversion is a *set-valued* function that associates an entire set with a particular input [78].

In practice, the charge coordinates of the initial configurations are derived from deterministic pseudo-random number generators. The complete sequence of the chiral-energy

encipherment is therefore a combination of (4.9) and (4.10), i.e.,

$$\begin{matrix}\text{pseudo-random} \\ \text{number generator}\end{matrix} \rightarrow \{d_j\}_1^{360} \leftrightarrow \mathbb{C}_{Ran}^{R,L}(15)\text{: } M[\mathbb{C}_{Ran}^{R,L}(15)] \rightarrow \mathbb{C}_1^{R,L}(15) \rightarrow R \text{ or } L. \qquad (4.11)$$

Since the number generators can be programmed to produce any sequence, Eq. (4.11) is a slow but feasible means of encipherment.

The concealed propagation of order through pseudo-random numbers and geometric complexity also adds a novel twist to the problem of chiral bias. This concerns the observation that naturally occurring proteins are almost exclusively composed of chiral amino acids of the 'L' variety [24, 25]. Although these compounds are far more complex than the surface Coulomb states, the basic production mechanisms are presumed to be similar in both cases: The underlying idealization is that a uniform statistical mix of initial states evolves towards equilibrium in a symmetric pair of potential wells whose minima correspond to states of opposite chirality. Since processes of this kind always lead to a racemic mix of final states, the observed 'handedness' of the biosphere is usually attributed to a critical fluctuation ('spontaneous' symmetry breaking), or a fundamental chiral force (*e.g.*, β - *decay*) that introduces an asymmetry in the potential wells [24, 25]. Equation (4.11) indicates still another possibility: that the final chirality is actually predetermined by a set of algorithmic instructions at a non-geometric level. It is certainly feasible to generate long strings of pseudo-random numbers that will consistently produce 'L'- handed initial configurations [23]. The appearance of a racemic or unbiased mix of initial states is therefore an illusion --- the 'L' - die has already been cast

before the game begins.

The binary code of chirality disappears when (4.11) is rewritten for 14 charges. The essential difference in this case is that the ground state is not enantiomorphic even though the pseudo-random initial configurations may be chiral, i.e.,

$$\begin{matrix}\text{pseudo-random} \\ \text{number generator}\end{matrix} \rightarrow \{d_j\}_1^{336} \leftrightarrow \mathbb{C}_{Ran}^{R,L}(14): M[\mathbb{C}_{Ran}^{R,L}(14)] \rightarrow \mathbb{C}_1(14). \qquad (4.12)$$

The transition from (4.12) to (4.11) illustrates another threshold of structural complexity. When there are 15 charges represented by 30 blocks of 12 digit numbers --- as in Eq. (4.10) --- each string of 360 digits specifies a unique dichotomic variable, an 'L' or an 'R'. However, if the strings are parsed differently --- as in Eq. (4.12) --- they are too simple to generate the chiral alphabet. By this means the threshold of a geometric property is expressed as a minimum complexity requirement for a coding algorithm.

E-1. Coulomb Angles and Tammes Angles. The Tammes problem is equivalent to finding the largest angular diameter $\Theta_T(N)$ of N congruent caps that can be packed on the surface of a sphere without overlapping [12-14]. Column 7 of Table VIII lists the optimum values of $\Theta_T(N)$ obtained by Kottwitz [30] and Tarnai [79] for $3 \leq N \leq 100$. Clearly, $\Theta_T(N)$ is a (not strictly) decreasing function of N, with an asymptotic dependence $\Theta_T(N) \propto (8\pi/3^{1/2}N)^{1/2}$, *for* $N > 1$. There is an analogous angle for the surface Coulomb problem $\Theta_c(N)$ determined by the minimum angular separation between neighboring charges in

a locally stable configuration [39]. Several examples are contained in column 7 of Table V: $\Theta_c(16) = 48.9362°$, $\Theta_c(24) = 42.0653°$, $\Theta_c(32) = 37.3773°$, etc. A comprehensive survey is given in column 6 of Table VIII. Since the optimization in the surface Coulomb problem is carried out with respect to total energy rather than nearest neighbor separations, the two sets of angles are related by $\Theta_T(N) > \Theta_c(N)$ *when* $N > 6$, $N \neq 12$. $\Theta_c(N)$ is a non-monotonic but generally decreasing function of N with an asymptotic estimate resembling the Tammes result; $\Theta_c(N) \sim (4\pi/N)^{1/2}$, *for* $N > 1$. If this estimate were accurate to leading order in N, then the relative difference between the two sets of angles would approach a constant value for large N,

$$[\Theta_T(N) - \Theta_c(N)]/\Theta_T(N) \rightarrow 1 - 3^{1/4}/2^{1/2} \sim 0.07, \; N > 1. \qquad (4.13)$$

Figure 12 shows this relative difference in graphical form when $\Theta_c(N)$ is averaged over all locally stable states belonging to a given value of N. Despite the prominent fluctuations, the overall trend is roughly consistent with (4.13).

The basic purpose of these comparisons is to see whether the configurations of points have some kind of asymptotic regularity for large values of N that is insensitive to the precise nature of the underlying interactions. If the trends in Fig. 12 can be extrapolated beyond $N \sim 112$, then it would be an indication that the local equilibrium states of the Coulomb law $|\vec{r}_i - \vec{r}_j|^{-2}$ and the Tammes interaction $|\vec{r}_i - \vec{r}_j|^{-1\,310\,720}$ retain a distinct character even for arbitrarily large values of N.

E-2. The Largest 'Hole' Angle. A useful complement to the Coulomb angle $\Theta_C(N)$, which measures the minimum separation between charges, is the hole angle $\Theta_H(N)$, which is the angular diameter of the largest spherical cap containing *no* charges in its interior. The set of these empty regions was obtained previously in Section 4C as an aid in the construction of the Coulomb polyhedra. Column 8 of Table VIII lists values of the hole angle $\Theta_H(N)$ for all surface Coulomb configurations in the range $4 \le N \le 112$. As expected, for regular configurations such as the icosahedron the ratio of the hole and Coulomb angles is close to one — $\Theta_H(12)/\Theta_C(12) \approx 1.18$ — but shows a larger disparity for irregular states — $\Theta_H(13)/\Theta_C(13) \approx 1.34$. For larger values of N, the minimum ratio (1.10) occurs at N = 44, and the maximum ratio (1.32) at N = 92. There is no evidence for conspicuous empty regions which may be analogues of the interstices in complex molecules.

In the Tammes problem, the densest packing of congruent caps on a sphere doesn't necessarily lead to rigid configurations. In fact, Kottwitz's solutions show a slowly increasing trend in the number of caps free to 'rattle' for larger values of N [30]. These partially empty regions can also be characterized by a set of hole angles. Specifically, if a Tammes configuration is represented by the center points of a set of caps, the corresponding *minimum* hole angle $\psi_H(N)$ is the angular diameter of the *smallest* circular region that does not contain any of these points in its interior. It is easy to show that

$$\Psi_H(N) = 2 \sin^{-1} \left(\frac{2}{3^{1/2}} \sin \left[\frac{\Theta_T(N)}{2}\right]\right), \tag{4.14}$$

where $\Theta_T(N)$ is the standard Tammes angles (Section E-1). Numerical comparisons of the Coulomb and Tammes hole angles for the respective ground states lead to the inequality $\Theta_H(N) > \Psi_H(N)$ *for* $12 < N \leq 90$. If this relation were valid for all $N > 12$, it would indicate still another optimum property of the Tammes configurations.

E-3. Edges and Faces of Coulomb Polyhedra. The conjecture that the surface Coulomb and Tammes configurations remain distinct for large values of N is also supported by the statistical behavior of the number of faces and edges of the associated polyhedra. As in Section 4C, let e and f denote the total number of edges and faces of a convex polyhedron whose N vertices coincide with the charge positions. Then if $\langle \eta(N) \rangle$ is the average number of edges that meet at a vertex, Euler's theorem (4.6) shows that

$$\langle \eta(N) \rangle \equiv \frac{2e}{N} = 2\left(1 - \frac{2}{N} + \frac{f}{N}\right). \tag{4.15}$$

In the special case that all the faces of a polyhedron are triangular, 3f = 2e, and (4.6) implies

$$f = 2(N - 2) \text{ and } e = 3(N - 2). \tag{4.16a}$$

These relations yield the sharper constraint

$$\langle \eta (N) \rangle_{tri} = 6 - \frac{12}{N}. \qquad (4.16b)$$

Table VI displays the trends in the numerical values of the 'edge/vertex' ratio $\langle \eta (N) \rangle$ for the ground states of the surface Coulomb and Tammes problems. The middle row of the Table lists the corresponding values for polyhedra whose faces consist solely of triangles.

Table VI

Values of the Edge/Vertex Ratio $\langle \eta (N) \rangle$ for the Coulomb and Tammes Polyhedra

N	12	32	71	72	109	112
Surface Coulomb[a]	5	5.625	5.775	5.833	5.853	5.893
Triangular tessellation[b]	5	5.625	5.831	5.833	5.890	5.893
Tammes[c]	5	4.125	3.887	4.083	-	$\leq$ 4.9988[d]

[a]Eq. (4.15) and Table VIII.

[b]Eq. (4.16b)

[c]Reference [30]

[d]Eq. (4.17)

Obviously, for large values of N, most of the Coulomb polyhedra have triangular faces. However, the 'hard' Tammes potential ($\sim |\vec{r}_i - \vec{r}_j|^{-1310720}$) can generate more complex

polyhedra because of inherent geometric constraints. Specifically, since in any packing of congruent caps on the surface of a sphere any cap can have at most 5 neighbors, (4.16b) and Table VI show that the icosahedron is the only figure with a triangular covering whose associated caps have the maximum possible mutual contact [29]. For $N > 12$, the edge/vertex ratios of the Coulomb polyhedra tend towards the triangular limit (4.16b), i.e., $\langle \eta \rangle_{tri} \rightarrow 6$; whereas the Tammes ratios cannot exceed 5. In fact a rigorous sharper bound is available:

Theorem [80]. There is an $r_o > 0$ such that for any packing of congruent caps of radius $r \leq r_o$ on the sphere of unit radius, the average number of neighbors of the caps in the packing is at most

$$\frac{4204}{841} = 4.99881 \ldots \geq \langle \eta(N > [2/r_o]^2) \rangle \qquad (4.17)$$

Further trials suggest that for any congruent cap packing on the sphere --- not necessarily the densest packing --- the maximum possible value of $\langle \eta(N \rightarrow \infty) \rangle$ is 4.4 [80].

E-4. Minimal Properties of Coulomb Energies. The computer results for N = 112 illustrate three general trends in the distributions of the Coulomb States: (i) For every $N > 1$ there are many locally stable states --- at least 60 for N = 112. (ii) These states are nearly degenerate in energy --- for N = 112, Eq. (3.11) shows that the relative energy spacings are ~ 10^{-6}. (iii) And, finally, angular comparisons indicate that the geometrical configurations of all of these states are quite different. These features impose interesting constraints on the energy 'landscapes' of the Coulomb states. The data in Table II and Fig. 3 show that the average value

of the energy E for arbitrary choices of the angles ϕ_1, ..., ϕ_N; θ_1, ... θ_N in Eq. (3.5) is ~ $N^2/2$. In other words, most of the energy surface lies in the highlands. Furthermore, it is obvious, since the number of arbitrary (initial) states is far larger than the number of terminal equilibrium states, that these highlands surround a few valleys whose lowest points lie at a depth ~ 0.55 $N^{3/2}$ below the average height of the landscape, cf., Eq. (3.8). What is not at all obvious is that according to (ii) all of the valley bottoms are situated at nearly the same depth, even though (iii) indicates that these minima are widely dispersed over the landscape. The essential implication is that the energy surface is bounded form below by a *single* plane that is effectively tangent to *every* local minimum. This plane is also tangent to every rigid Tammes configuration in the range $2 \leq N \leq 87$. Specifically, if $\mathbb{C}_T$ (N) denotes the optimum Tammes solution for N points; and each point is assigned a unit charge, Eq. (2.1) and Eq. (3.5) can be used to compute a Coulomb energy E_{CT} (N) for this configuration. Table VII shows some representative comparisons of the ground state Coulomb energies E_1 (N) and Coulomb-Tammes energies E_{CT} (N) for various values of N.

Since the Coulomb problem yields the minimum energy for the $|\vec{r}_i - \vec{r}_i|^{-1}$ potential whereas the Tammes problem optimizes inter-particle distances, it is evident that E_{CT} $(N) > E_1$ (N), except for N = 2 - 6, 12. But there is no *a priori* reason for the pervasive near equality E_{CT} $(N) \approx E_1$ (N) displayed in Table VII. In fact, significant differences might be expected to arise from the tremendous disparity between the effective Tammes potential,

Table VII

Comparisons of Ground State Coulomb Energies E_1 (N) and Coulomb-Tammes Energies E_{CT} (N)

N	E_1 (N)	E_{CT} (N)	$[E_1 - E_{CT}]/E_{CT}$
2 - 6	-	-	0
7	14. 452 977	14. 461 864	6.15×10^{-4}
8	19. 675 288	19. 725 173	2.53×10^{-3}
12	49. 165 253	-	0
13	58. 853 231	58. 909 592	9.57×10^{-4}
16	92. 911 655	92. 951 183	4.25×10^{-4}
32	412. 261 274	412. 376 77[a]	2.80×10^{-4}
78	2662. 046 474	2662. 677	2.37×10^{-4}
79	2733. 248 357	2734. 540	4.72×10^{-4}
80	2805. 355 876	2805. 908	1.97×10^{-4}
84	3103.465 124	3104. 142	2.18×10^{-4}
87	3337. 000 750	3337. 978	2.93×10^{-4}

[a] Values for $N \geq 32$ from [30].

$|\vec{r}_i - \vec{r}_j|^{-1\,310\,720}$, and the Coulomb law, as well as the general lack of resemblance of the Tammes and Coulomb equilibrium configurations. For instance, in the simplest case N = 7, the surface Coulomb distribution consists of 5 points spaced equally around the equator, with the remaining two points at the poles (pentagonal dipyramid), while the points of the Tammes solution are given by the vertices of an equilateral triangle at 43. 476 677° south latitude, another equilateral triangle, rotated by 60° , at 12. 130 450° north latitude, and the remaining point at the north pole. Computer trials also confirm that if the N = 7 Tammes solution is chosen as the initial configuration of a surface Coulomb minimization, the algorithm of Section 2B will eventually converge to the pentagonal dipyramid solution. Despite these qualitative distinctions,

the Coulomb energies associated with these two configurations differ by less than 0.062%.

Although these insensitive energy variations may be accidental, they are certainly not isolated accidents. Extensive numerical evidence from the analysis of magnetic cooperative systems [57, 58], and computer simulations of vortex arrays [81] also yield examples of complex systems with a variety of metastable states all of which are very nearly degenerate in energy. The most prominent example of this type is the electrostatic interaction energy of ionic crystals. Madelung, in his initial computations [82], already emphasized the severe requirements of accuracy necessary for discriminating between different kinds of lattices. A canonical example is the 0.857% difference in Madelung constants between the sodium chloride and cesium chloride structures [83]. After a long series of evolutionary developments, a useful description of these structures is finally available; but this requires a quantum mechanical density functional formalism and implementation on 'super-computers' [84, 85]. Even these sophisticated methods haven't resolved the inverse problem: Given a complex gradient system, what are the characteristics of the configurations that are nearly degenerate in energy with the ground state? Or, more informally, why is it that the energy surfaces of some complex gradient systems have multiple valley bottoms with very little height variation?

5. Conjectures Concerning the Stable Equilibrium Configurations of Complex Gradient Systems

The locally stable equilibrium states of the surface Coulomb problem share many of the characteristics of planar magnetic dipole configurations [57, 58]. Similar trends are exhibited by other systems such as arrays of vortex patterns [81,86]; the 'jellium' model, or its equivalent,

the three-dimensional spherical Coulomb problem [10]; and sets of floating magnets interacting with an external magnetic field [87]. These common features suggest several general conjectures concerning the locally stable states of complex gradient systems [88].

In the simplest cases, when there are only a few identical interacting objects, general arguments of balance and symmetry show that the equilibrium configurations are regular polygons or polyhedra whose form is essentially independent of the detailed nature of the forces [11]. The underlying assumption is that the potential energy of these systems can be derived from the superposition of identical pair-wise interactions. Although these results agree with observations, the steps from arguments or conjectures to rigorous assertions are incomplete even for the smallest gradient systems consisting of only 3-6 objects. Analytical methods involve tedious computations [10, 32, 57, 89, 90], and topological estimates of the number of critical points, including stable equilibria, are just being developed [91].

For the spherical charge systems, the influence of the force laws becomes dominant in the transition from 6 to 7 objects. Specifically, when $N \leq 6$, all of the force laws, ranging from the 'soft' logarithmic interaction to the 'hard' Tammes potential, generate identical equilibrium patterns; whereas for $N \geq 7$ ($\neq 12, 32$), all of the ground states appear to be markedly different [43]. This sensitivity to the form of the interactions also appears in magnetic arrays: As the number of interacting objects increases, the organization of the domain structures shifts from the control of the strong dipole interactions to the weaker octupole forces [26]. It is plausible to conjecture that this sensitivity is a general attribute of cooperative gradient systems when all of the N (N - 1)/2 interparticle forces are taken into account. A more complicated analogue is the folding of protein molecules under the influence of nominally weak secondary and tertiary forces

[35, 36, 92].

The diminishing importance of strict geometric symmetry as an organizing principle in complex systems is also illustrated in a different but related problem concerning the positions of N points in a unit square arranged so that the minimum distance d_N between any pair is as large as possible. Evidently, this is a two-dimensional version of the Tammes problem in which a set of N congruent circles with diameter d_N is packed into a square with side $1 + d_N$. The successive panels in Fig. 13, taken from [28], show that beginning at N = 10, the optimum configurations in this problem also tend to be asymmetric. Clearly this trend parallels the evolution of the surface Coulomb states, where for increasing values of N, computer graphics and other indices such as the dipole moments (1.2a), and energy and angular diversity ratios (3.16), (4.3), (4.7), show that the equilibrium configurations became more irregular. When N > 12, there is no overlap with any of the 123 convex regular polyhedra [17, 18], and indeed many states are so disordered that their only invariant isometry is the identity transformation. Since this progression from 'broken' symmetries to 'fragmented' symmetries appears in other N-body problems, it may be a general attribute of many complex systems. Nevertheless, it still remains unclear what characteristics distinguish force laws that lead to complicated equilibrium states from those that generate extended regular lattices.

As emphasized in reference [92], *diversity* is a prerequisite for complexity: In general, complex systems should exhibit many significantly different states. A typical chemical illustration of the proliferation due to simple combinatorics is the estimate that "$C_{167}\ H_{336}$ is the smallest alkane with more realizable isomers than the observed universe has 'particles' ~ 10^{80}" [93]. Similar arguments can be applied to sets of coupled non-linear oscillators to determine

their maximum configurational entropy (3.4). The results support the general surmise that the number of local minima of the energy landscapes of N-body cooperative systems increases at an exponential rate with N [59, 94]. Direct confirmation of these trends is displayed in Fig. 2. The magnetic data are derived from extensive experimental observations of the stable configurations of planar dipole arrays [58]: The graph showing the increase in the number of surface Coulomb states is based on the summary of computer results given in Tables I and VIII. In the currently accessible ranges of N, the evidence for exponential growth is consistent and convincing.

Angular comparisons among the sets of surface Coulomb configurations for fixed values of N (> 1), show very little overlap (4.5). This is a counter - example to the presumption that the structural properties associated with different local minima are fairly similar [36]; but is in accord with the general diversity conjecture which asserts that complex systems should appear in many *significantly different* states. This diversity is also connected with the irregularity of configurations and their sensitive dependence on the nature of the underlying interactions. If, for instance, contrary to the observations, the surface Coulomb configurations were all in the form of regular polyhedra, then there could not be any more than 123 different equilibrium states [17]. Analogous constraints of symmetry limit the total number of possible crystallographic space groups to 230 distinct types [13]. In this obvious sense, significant diversity is not compatible with symmetry.

For large values of N, it is possible that the trend towards increasing diversity eventually merges into a statistically regular sequence of patterns that is effectively insensitive to the details of the interparticle forces. However, all the available evidence from the spherical charge systems

points in the opposite direction. The stable configurations can be characterized by their dipole moments, or centers of charge [cf. (1.2a) and Fig. 8]; the nearest neighbor angles (4.7); and the average number of edges that meet at the vertices of the associated polyhedra (4.15). Comparisons of these indices for the 'soft' logarithmic interaction, the Coulomb law, and the 'hard' Tammes repulsion, given in Eq. (4.2), Fig. 12, and Table VI, show that they are all different. Moreover, in the range $N < O(100)$, there is no indication of any trend towards confluence. Of course, it remains an open question whether there are any qualitative changes for still larger values of N.

Planar magnetic dipole arrays exhibit a different type of structural stability. Experimental observations and computer checks show that the domain patterns generated by pivoted dipoles are *insensitive* to variations of the individual magnetic moments and perturbations of the underlying lattices. The net result is that the domain structures are robust under changes of scale, but vulnerable to qualitative shifts in the strength of multipolarities [26]. These examples indicate that various levels of structural stability and instability can coexist in complex systems.

This duality also appears in the mingling of order and disorder in complex systems. For instance, most of the surface Coulomb configurations seem to be highly irregular, but their small dipole moments (4.2), and the band structures in Figs. 7 and 9, clearly show that the charge distributions are far from random. The most striking element of order is the uniformity of the energies displayed in Table III. These correlations imply that the corresponding Coulomb energy landscapes are bounded from below by a single plane that is effectively tangent to every local minimum (cf. 4E-4 and [95]). Table VII shows that this *same* 'flat bottom' underlies the Tammes landscapes when the energy minima of the $|\vec{r}_i - \vec{r}_j|^{-1\,310\,720}$ interactions are rescaled

to the Coulomb values. Furthermore, the occurrence of 'rattlers' --- or, non-rigid configurations --- in more complex Tammes solutions indicates that the associated minima actually lie in flat valley bottoms that are tangent to this bounding plane [30]. Similar uniformities of the energy minima occur in magnetic arrays even though the corresponding domain patterns are quite distinct. All of these observations run counter to the expectation that the energy landscapes of complex systems have a random --- possibly Gaussian --- distribution of local minima as a function of 'altitude' [92]. But this does not necessarily imply a contradiction. Combinatorial arguments can lead both to narrow as well as widely scattered distributions of pseudo-random variables. The near-degeneracy of the local energy minima in many cooperative systems may be connected with the sharply peaked distribution of the zeros of random polynomials [96].

Another basic characteristic of complex systems is "*contingency*", or more precisely, the history dependence of their evolution [92]. In the special case of gradient systems, all continuous quasi-static changes can be described in terms of trajectories on the corresponding energy landscapes. The situation that is most frequently considered is the transition from some arbitrarily chosen set of initial states, scattered throughout the 'highlands' of the landscape, down to the local energy minima in the valley bottoms. Since these steepest descents are not equilibrium processes, and the energy minima are often nearly degenerate, Boltzmann statistics cannot be used to infer the occupation probabilities of the terminal states. An obvious alternative is to assume that the occupation probabilities are proportional to the size of the drainage or capture basins that surround each local minimum. Experiments and computer trials show that this size is determined by the lowest neighboring mountain passes in the 'slow cooling' limit, and by the mountain crest lines or watershed basins, in the 'fast quench' limit [57]. In either case,

the topography of the energy landscapes controls the occupation probabilities of the various minima.

All the available evidence indicates that in many cooperative systems the occupation probabilities are highly non-uniform even if there are many local minima that are nearly degenerate in energy. A typical example is shown in Fig. 5. In first approximation, the decrease from the peak follows a steep power law, which then trails off into a plateau. This type of empirical Pareto or Zipf distribution has long been familiar in demographics (ranking of cities by population) and economics (apportionment of wealth) [97]. Occupation probabilities that are concentrated in a small number of states are also connected with search problems such as the Levinthal paradox [35, 92]: Namely, how does a protein find a global optimum without an unreasonably long global search? In the case of the gradient systems, the explanation is simply that a few states are favored because they are fed by the largest drainage basins on the energy landscapes. Although this picture is consistent with computer simulations, it has to be interpreted with caution because minimizing algorithms --- such as the procedure described in Section 2B --- do not necessarily correspond to physical processes. This is illustrated by the discussions in references [98-100] which show that discrepancies can arise from differences in the computing schemes without any import on the basic physics.

Acknowledgments

We are grateful to many colleagues and students for information and assistance. We would particularly like to thank Prof. B. Bernstein, J. Cheevers, Prof. R. Filler, Prof. A. Florian, Prof. M. J. Frank, Dr. D. R. Gavelek, Prof. N. W. Johnson, Dr. D Lazić, Prof. P.

Lykos, Prof. S. Miller, Prof. E. T. Olsen, Prof. A. Sklar, Prof. T. Tarnai, and R. K. Bernett-Zasadzinski. This work was supported in part by the Research Corporation and AFOSR. Fermilab is operated by Universities Research Association Inc. under contract DE-AC02-76CHO3000 with the U.S. Department of Energy.

Appendix A: Minima of Complex Energy Landscapes

The Surface Coulomb problem is a special type of gradient system with constraints [88]. Its extremals are determined by the simultaneous solutions of

$$\frac{\partial E}{\partial \phi_i} = 0, \quad \frac{\partial E}{\partial \theta_j} = 0, \ \forall\ i,j \tag{A-1}$$

where E is the energy given in (3.5). There are also infinite energy maxima at cusps due to coincident charges. The extremals are often referred to as critical, stationary, or equilibrium points. The simplest locally stable minima are a subset of extremal points $p(\phi_i, \theta_j)$ whose associated Hessian matrices $\mathcal{H}\ [p(\phi_i, \theta_j)]$ are positive definite [53, 54]. Since these Hessians are arrays of all second order partial derivatives of the energy --- including terms such as $\frac{\partial^2 E}{\partial \phi_i \partial \phi_j}$, $\frac{\partial^2 E}{\partial \phi_i \partial \theta_j}$, *and* $\frac{\partial^2 E}{\partial \theta_i \partial \theta_j}$ --- it is convenient to introduce a single symbol Ω_κ, $1 \le \kappa \le 2N$, that ranges over all the angles $\phi_1, \ldots, \phi_N, \theta_1, \ldots, \theta_N$. The Hessian at p then is

$$\mathcal{H}\ [p] = \frac{\partial^2 E}{\partial \Omega_\kappa\ \partial \Omega_\mu}\Big|_p \quad 1 \le \kappa, \mu \le 2N. \tag{A-2}$$

A necessary and sufficient condition for a real symmetric matrix such as $\mathcal{H}$ [p] to be positive definite is that all of its eigenvalues are positive.

Figure 14(a) is a plan view of part of an energy landscape containing three locally stable minima at E_m, E_{m+1}, *and* E_{m-1}. For N charges, this landscape is actually a surface in a 2N + 1 dimensional space spanned by Ω_1, ..., Ω_{2N}, *and* E. Figure 14(b) is an elevation showing the altitude or energy variations along a steepest descent path (path 1) connecting E_m *and* E_{m+1}. As indicated in Fig. 14(a) there may be several mountain pass routes between adjacent valleys. The saddle points at $SP^{(1)}$, ..., $SP^{(5)}$, etc. are of course also extremals satisfying (A-1). These points are distinguished by the property that the associated Hessians $\mathcal{H}$ [SP] have at least one negative eigenvalue: specifically, if λ denotes the number of negative eigenvalues, then $0 < \lambda < 2N$.

Figure 14(a) illustrates some of the technical problems that can occur in mapping complex energy landscapes by means of computers. For instance, the convolutions of path 3 indicate that some minima may be difficult to reach from random initial points located in the energy 'highlands'. The large iteration values listed in column 2 of Table VIII for $N = 7, 13, 19, 36$, *etc*. are probably due to such labyrinthine obstacles. But these results have to be interpreted with caution because the 'convolution of paths' has a dual significance: (1) *Analytically* it refers to steepest descent paths constrained to wind through highly corrugated landscapes; and (2) *numerically* it corresponds to complicated patterns of steps generated by computer algorithms seeking lower ground on rugged terrain. Path 4 illustrates these distinctions

in a complementary setting. Suppose for the moment that E_m were *not* a strict minimum because --- as shown in Figs. 14(a) and (b) --- there is another winding narrow defile leading from E_m to a lower energy minimum at E_{m-1}. If this track passes through the mountains via a flume rather than a saddle point, the energy can decrease monotonically between E_m *and* E_{m-1}. In principle, the existence of such a narrow exit from E_m presents no difficulties for an analytical description. It simply means that the associated Hessian would show that E_m is a shallow saddle point with respect to one direction. But numerically it would be very difficult to detect the existence of this escape route if the scale of topographic variations of the energy surface were comparable to the roundoff errors of the search routines. Similar computational problems can occur for minima with small capture basins. If we revert to the assumption that $\mathcal{H}[E_m]$ is positive definite, standard Morse theory shows that E_m is an isolated minimum [101, 102]. This means that E_m is located in the interior of an open neighborhood all of whose points have energies exceeding E_m. But this theorem is of little practical use in cases where the neighborhood is so small that it falls below the threshold of resolution of numerical surveys.

All the surface Coulomb states listed in Table VIII were screened for numerical robustness with respect to roundoff. Generally, N-charge equilibrium configurations are described by 2N angular coordinates with a resolution of 10 decimal digits. Every coordinate was successively truncated to 6, and then to 3 decimal digits. All of these sets of truncated coordinates were taken as the starting configurations of new energy minimizing searches.

Numerical stability was then verified in every instance by checking that these minimizations led back to the original equilibrium configurations. Nevertheless, despite these precautions, numerical methods can both under and overestimate the actual number of minima. As indicated previously, states may be missed because they are concealed by tortuous approaches or have minute capture basins. And states may be counted as locally stable minima because narrow escape routes such as path 4 on Fig. 14(a) can be overlooked by numerical surveys.

The correspondences between the analytical and numerical descriptions of multi-variable gradient systems tend to be even more complicated in situations where the Hessian matrices are singular at critical points. Figures 14(c) and (d) indicate some of the topographic complexities that can appear on the energy landscapes. In particular, the rippled stalagmite in Fig. 14(c) is a schematic representation of the cumulation of critical points around a non-isolated singularity. Typical one-dimensional potentials illustrating such a clustering of sequences of maxima and minima around the origin are $U(q) = e^{-1/q^2} \cos(1/q)$, *and* $e^{-1/q^2} \sin^2(1/q)$ [101, 103, 104]. Although the surface Coulomb potential (3.5) clearly does not contain any terms resembling $\sin(1/q)$, etc., the exponential increase of extremals (3.2a) on a 2N + 1 dimensional surface is bound to produce a crowding that is numerically equivalent to a clustering. Fig. 14(d) shows two extremal *lines* in the form of intersecting valley bottoms. If the crossing point is taken as the origin of a set of local coordinates, say α, β, ..., then potential expressions such as $U \sim \alpha^2 \beta^2$ will generate this kind of topography. Generally, the lower the rank r of the Hessian, i.e. $r < 2N$, or equivalently, the larger the dimensionality of the *nullity* (= 2N - r), the 'flatter' will be the associated valley bottom on the energy surface [101]. The rattling or

labile states found by Kottwitz [30] at N = 19, 20, etc., for the extremely repulsive Tammes potential $|\vec{r}_i - \vec{r}_j|^{-1\,310\,720}$ are examples of such extended minima. Similar trends appear in the surface Coulomb problem. For instance, the 13 - digit reproducibility of the total energy in Eq. (2.9a) represents the sharply defined level of a valley bottom on the energy landscape --- i.e. *lim inf* E [$\mathbb{C}_2$ (84)] = 3103.478 .... But the much lower precision of the individual charge coordinates (2.9 b,c) reflects the influence of shallow grooves (or eigenmodes) surrounding the minimum. This quasi-degenerate behavior is also connected with the poor performance of conjugate-gradient methods in the Coulomb problem.

It is plausible that for increasing values of N, the energy landscapes of the surface Coulomb problem include a greater proportion of complex features such as those shown in Figs. 14(c) and (d). Analytically, this incidence of singular Hessians means that more of the critical point behavior falls outside the scope of Morse theory [102]. The corresponding numerical description of singular or close-to-singular $2N \times 2N$ matrices with $N > 100$, then also requires greater computational effort [105, 106]: First, it is necessary to evaluate all of the N (2N + 1) independent matrix elements in (A-2) at the relevant critical points. And then, since roundoff errors make it impractical to check directly whether det | $\mathcal{H}$ [p]| vanishes, the proximity of singularities has to be detected by sensitivity analyses. One criterion of this type is the condition number of a matrix; which is also proportional to the inverse 'distance' to a singularity [105]. Standard software packages are available for implementing these diagnostics, but it remains to be seen whether they will be of any significant help in extending the surface Coulomb analysis to more complex systems.

Appendix B: Summary of Results

Table VIII contains a survey of the numerically robust states of the surface Coulomb problem extending up to 112 charges. The first column lists the number of charges N. The next column shows the *average* number of iterations required to reach an equilibrium state. (Note that every charge is simultaneously moved at each iterative step.) The frequency of occurrence, or 'capture basin' of each state is indicated in the third column. The asterisks mark enantiomeric states. Column 4 lists the dimensionless energy (1.3) of each state. The center of charge, or magnitude of the dipole moment (1.2a) of every configuration is given in column 5. Column 6 shows the minimum angular separation (radians) between pairs of points of the surface Coulomb states. A corresponding set of values for the Tammes problem is listed in column 7. The hole angles, given in column 8, denote the angular diameters of the largest spherical caps containing *no* charges in their interior, cf. Section 4E-2. Columns 9 and 10 list the energy and angular diversity ratios defined in (3.1) and (1.1) respectively. Finally, column 11 indicates the number of faces of the polyhedra associated with each configuration, cf. Section 4C.

Table VIII: Equilibrium configurations for the surface Coulomb problem

N	Average iterations	Frequency %	Coulomb energy	Dipole moment	Coulomb angle	Tammes angle	Hole angle	% Energy diversity	% Angular diversity	Faces N_f
3	14	100.00	1.73205081	0	2.094395	2.094395	3.1416	33.3	33.3	
4	16	100.00	3.67423461	0	1.910633	1.910633	2.4619	25.0	16.7	4
5	78	100.00	6.47469149	0	1.570796	1.570796	2.2143	40.0	30.0	6
6	42	100.00	9.98528137	0	1.570796	1.570796	1.9106	16.7	13.3	8
7	2160	100.00	14.45297741	0	1.256637	1.359080	1.7812	28.6	19.0	10
8	182	100.00	19.67528786	0	1.251299	1.306527	1.6161	12.5	14.3	10
9	280	100.00	25.75998653	0	1.207589	1.230959	1.4835	22.2	16.7	14
10	442	100.00	32.71694946	0	1.134387	1.154480	1.4666	20.0	15.6	16
11	499	100.00	40.59645051	0.013220	1.021708	1.107149	1.3455	45.5	36.4	18
12	76	100.00	49.16525306	0	1.107149	1.107149	1.3047	8.3	4.5	20
13	1280	100.00	58.85323061	0.008820	0.913103	0.997224	1.2268	46.2	37.2	22
14	255	100.00	69.30636330	0	0.922687	0.971635	1.2060	14.3	9.9	24
15	437	100.00*	80.67024411	0	0.859136	0.936506	1.1307	20.0	20.0	26
16	293	75.66*	92.91165530	0	0.854098	0.911837	1.0730	12.5	10.0	28
	394	24.34	92.92035396	0	0.874880		1.0938	12.5	10.8	26
17	677	100.00	106.05040483	0	0.874550	0.891694	1.0637	17.6	10.3	30
18	502	100.00	120.08446745	0	0.829632	0.864927	1.0517	16.7	11.8	32
19	9109	100.00	135.08946756	0.000135	0.783822	0.832381	0.9934	36.8	30.4	33
20	662	100.00	150.88156833	0	0.804480	0.827828	0.9716	20.0	13.7	36
21	3976	99.99	167.64162240	0.001406	0.773536	0.796101	0.9348	42.9	32.9	38
	847	0.01	167.64183186	0.001425	0.767113		0.9334	38.1	48.1	36
22	541	97.30	185.28753615	0	0.755763	0.780863	0.9350	13.6	7.4	40
	1442	2.70	185.30795160	0	0.746305		0.9498	13.6	10.8	40
23	442	100.00*	203.93019066	0	0.723982	0.762883	0.9213	21.7	19.0	42
24	440	100.00*	223.34707405	0	0.734178	0.762548	0.9018	4.2	5.8	38
25	7560	100.00	243.81276030	0.001021	0.691333	0.726658	0.8593	56.0	53.3	45
26	2292	100.00*	265.13332632	0.001919	0.677923	0.716242	0.8531	50.0	70.8	48
27	662	99.97	287.30261503	0	0.697089	0.709958	0.8397	14.8	8.5	50
	402	0.03*	287.30961176	0	0.680734		0.8422	18.5	27.6	50
28	529	100.00*	310.49154236	0	0.660149	0.686877	0.8309	10.7	9.3	52
29	3133	100.00*	334.63443992	0	0.635147	0.675681	0.8073	17.2	30.3	54
30	2470	99.99*	359.60394590	0	0.644763	0.673647	0.7921	26.7	40.9	56
	1290	0.01	359.60439833	0.000004	0.637774		0.7886	36.7	43.9	54
31	390	100.00	385.53083806	0.003205	0.634831	0.658161	0.7744	29.0	20.0	58
32	239	97.93	412.26127465	0	0.652358	0.654066	0.7920	6.2	2.2	60
	673	2.07	412.46839720	0	0.621525		0.7699	12.5	8.9	58
33	7818	100.00	440.20405745	0.004356	0.588174	0.632761	0.7621	60.6	52.7	61
34	1591	100.00*	468.90485328	0	0.580730	0.624964	0.7448	26.5	34.0	64
35	3873	81.76*	498.56987249	0.000419	0.577711	0.616423	0.7290	51.4	51.1	66
	961	0.02	498.56991740	0.000480	0.576922		0.7288	42.9	49.2	64
	5649	18.20	498.57345404	0.001266	0.581227		0.7257	60.0	52.8	66
	988	0.02	498.57346232	0.001202	0.581086		0.7250	100.0	99.2	66
36	19168	100.00*	529.12240842	0.000048	0.579503	0.614177	0.7203	50.0	51.1	68
37	1846	19.91	560.61888773	0	0.564307	0.600784	0.7294	13.5	7.8	70
	3543	80.09*	560.62797306	0.000925	0.558252		0.7033	56.8	84.8	70
38	640	43.87	593.03850357	0.000001	0.580086	0.597787	0.6967	10.5	6.5	72
	1119	56.13	593.04894354	0.001687	0.563323		0.6999	34.2	30.3	72
39	472	65.27	626.38900902	0	0.559429	0.584494	0.6991	15.4	10.7	74
	5256	30.18*	626.44095841	0.000399	0.547982		0.6869	51.3	51.3	74
	4013	4.55	626.44096635	0.000371	0.547924		0.6866	38.5	45.3	72
40	753	66.94	660.67527883	0	0.557045	0.578722	0.6905	10.0	5.9	76
	7442	23.54*	660.72530410	0.000004	0.551384		0.6812	35.0	48.8	76
	959	0.14*	660.72530735	0.000282	0.550872		0.6810	50.0	51.2	76
	743	9.38	660.74121431	0.001465	0.545251		0.6826	35.0	28.3	76
41	476	93.51	695.91674434	0	0.550264	0.571230	0.6802	17.1	10.9	78
	1466	6.49*	695.97869944	0	0.545295		0.6778	19.5	25.2	78
42	488	98.08	732.07810754	0	0.545324	0.567343	0.6760	11.9	7.3	80
	1953	0.96*	732.15182672	0	0.540498		0.6650	16.7	32.4	80

N	Average iterations	Frequency %	Coulomb energy	Dipole moment	Coulomb angle	Tammes angle	Hole angle	% Energy diversity	% Angular diversity	Faces N_f
	4625	0.92*	732.19816736	0.003638	0.529379		0.6624	40.5	47.2	78
	255	0.03	732.25624103	0	0.553574		0.6754	4.8	1.6	80
	761	0.01	732.45155921	0	0.515500		0.6713	14.3	11.3	80
43	7239	100.00	769.19084646	0.000400	0.538723	0.559980	0.6600	53.5	49.2	82
44	3606	100.00	807.17426309	0.000060	0.545548	0.558216	0.6486	6.8	5.6	78
45	6635	99.89*	846.18840106	0	0.527214	0.546691	0.6419	24.4	43.2	86
	908	0.11	846.18864878	0.000147	0.527383		0.6382	35.6	43.4	86
46	729	11.24*	886.16711364	0	0.519938	0.540339	0.6408	10.9	8.8	88
	1358	44.66	886.17021602	0.001066	0.504669		0.6341	34.8	27.8	86
	1821	26.25*	886.17143242	0.001395	0.509081		0.6336	50.0	50.7	88
	1561	17.23*	886.17710517	0.001838	0.509578		0.6336	60.9	56.2	88
	10912	0.62	886.25028042	0	0.500098		0.6415	30.4	38.6	88
47	1443	55.74*	927.05927068	0.002483	0.502432	0.537244	0.6250	57.4	59.6	89
	4315	31.32*	927.06226967	0.002536	0.487302		0.6272	68.1	86.8	89
	12603	8.81	927.07222457	0.004938	0.505445		0.6233	36.2	32.3	90
	1816	0.10	927.07227174	0.000921	0.505369		0.6245	46.8	52.2	88
	2067	3.69*	927.08823351	0.000803	0.505048		0.6280	51.1	75.9	90
	1942	0.34*	927.14108835	0.001525	0.491380		0.6325	48.9	72.6	90
48	1061	99.99*	968.71345534	0	0.518182	0.536912	0.6282	4.2	5.7	86
	538	0.01	968.71550891	0	0.517172		0.6258	10.4	8.0	90
49	1112	100.00*	1011.55718265	0.001529	0.495439	0.522265	0.6184	34.7	33.3	94
50	827	100.00	1055.18231473	0	0.501108	0.519287	0.6084	10.0	6.1	96
51	1502	98.56*	1099.81929032	0	0.491578	0.512456	0.5977	17.6	22.6	98
	1521	1.44	1099.94023114	0.002506	0.474308		0.5988	35.3	28.1	96
52	661	53.50*	1145.41896432	0.000457	0.482931	0.509545	0.5940	34.6	33.3	100
	1208	29.81*	1145.42198063	0	0.485412		0.6015	25.0	28.1	100
	1436	9.84*	1145.43570898	0.000720	0.484667		0.5978	50.0	59.0	100
	3641	6.85*	1145.43759698	0.002189	0.480104		0.5944	100.0	98.8	100
53	7869	69.19	1191.92229042	0.000279	0.473629	0.502897	0.5881	32.1	27.2	99
	1028	30.81*	1191.93158471	0.000293	0.471423		0.5868	50.9	50.6	102
54	1846	80.27*	1239.36147473	0.000138	0.471755	0.501205	0.5856	50.0	60.3	104
	2205	4.08*	1239.36525530	0	0.475519		0.5864	16.7	25.6	104
	3846	7.26*	1239.37119227	0.000371	0.474284		0.5871	72.2	88.3	104
	1033	0.02*	1239.37125018	0.000405	0.472860		0.5868	98.1	98.7	103
	1355	8.37*	1239.37320071	0	0.478224		0.5850	25.9	32.6	104
55	1080	26.82*	1287.77272078	0.000392	0.464521	0.493279	0.5777	50.9	50.8	106
	1657	19.71*	1287.77702746	0.000114	0.461470		0.5780	50.9	50.8	106
	2337	16.37	1287.77726081	0.000118	0.470319		0.5826	32.7	27.1	104
	2953	14.65*	1287.78870934	0.000025	0.466465		0.5762	56.4	80.5	106
	1476	21.03*	1287.78905724	0.000191	0.464988		0.5806	96.4	99.1	106
	3478	1.42*	1287.80015929	0.000551	0.467767		0.5767	58.2	84.6	106
56	2231	10.82*	1337.09494528	0	0.465704	0.491276	0.5757	25.0	26.4	108
	2502	49.91*	1337.09534827	0.000174	0.464412		0.5770	50.0	50.6	108
	2674	39.17*	1337.09872742	0.000275	0.465148		0.5744	96.4	98.7	108
	4680	0.08*	1337.24862285	0.000149	0.457559		0.5749	75.0	90.1	108
57	1886	90.37*	1387.38322925	0	0.466045	0.485667	0.5719	17.5	18.6	110
	2511	3.05	1387.42008235	0.000753	0.453763		0.5682	66.7	79.6	110
	4016	1.84*	1387.43037248	0.000285	0.453468		0.5700	63.2	89.4	110
	2107	4.28*	1387.43113006	0.000273	0.452877		0.5713	50.9	70.0	110
	1494	0.46*	1387.47189278	0.000870	0.452564		0.5678	49.1	62.1	110
58	1941	23.51*	1438.61825064	0	0.456495	0.480923	0.5680	25.9	29.4	112
	2656	17.69*	1438.62550858	0.000058	0.455362		0.5630	50.0	50.6	112
	2362	5.43*	1438.62628995	0	0.454155		0.5633	25.9	37.6	112
	2260	25.42*	1438.62722515	0.000308	0.456654		0.5598	53.4	74.6	112
	5281	4.71*	1438.63370800	0.000002	0.454605		0.5638	50.0	52.9	110
	3329	0.01	1438.63374161	0.000009	0.454111		0.5640	91.4	94.7	111
	1550	22.64*	1438.63810500	0.000198	0.452373		0.5643	100.0	98.7	112
	2411	0.39*	1438.64735982	0.001029	0.453854		0.5648	36.2	59.3	112
	1839	0.11*	1438.67209913	0	0.464794		0.5593	25.9	38.1	112
	1345	0.04	1438.73596329	0.000388	0.449459		0.5648	100.0	97.6	112
59	2127	27.53*	1490.77333528	0.000154	0.456757	0.478133	0.5593	55.9	73.9	114
	2747	61.39*	1490.77438608	0.000623	0.456849		0.5570	100.0	98.7	114
	7687	3.58*	1490.78475584	0.000245	0.457361		0.5604	76.3	91.4	114
	898	0.01	1490.78478568	0.000301	0.456913		0.5601	100.0	98.5	114
	1646	7.49*	1490.79077309	0.000608	0.453876		0.5581	50.8	50.4	114
60	893	26.04*	1543.83040098	0	0.453046	0.474604	0.5566	16.7	17.5	116
	883	69.38*	1543.83509960	0.000130	0.452967		0.5562	50.0	50.6	116
	1946	3.71*	1543.84153514	0.000177	0.452851		0.5544	36.7	58.0	116

N	Average iterations	Frequency %	Coulomb energy	Dipole moment	Coulomb angle	Tammes angle	Hole angle	% Energy diversity	% Angular diversity	Faces N_f
	1189	0.36	1543.86465762	0.000017	0.447471		0.5556	6.7	6.4	116
	6212	0.40*	1543.96947231	0	0.451689		0.5608	20.0	25.3	114
	1561	0.11*	1543.98073384	0.000005	0.447795		0.5526	18.3	17.5	116
61	1907	62.11*	1597.94183020	0.001091	0.443169	0.469011	0.5507	98.4	98.7	118
	1174	11.83*	1597.95155534	0.000648	0.442474		0.5530	49.2	53.0	118
	7882	13.29*	1597.95512785	0.001364	0.444069		0.5483	100.0	98.1	117
	1516	0.03*	1597.95514972	0.001289	0.445279		0.5504	50.8	53.7	118
	2744	10.45*	1597.97036059	0.000634	0.445656		0.5503	100.0	98.5	118
	9463	0.03*	1597.97266027	0.000330	0.449018		0.5530	91.8	96.4	118
	4070	2.26*	1597.98080362	0.001003	0.437864		0.5492	100.0	98.7	117
62	2785	26.00*	1652.90940990	0	0.451689	0.465714	0.5517	11.3	10.8	120
	2546	61.95*	1652.92859368	0.001117	0.444933		0.5483	50.0	64.9	120
	1477	12.05*	1652.94201427	0.000513	0.446840		0.5481	51.6	50.6	120
63	1922	99.71*	1708.87968150	0	0.440812	0.462284	0.5457	15.9	25.5	122
	946	0.29*	1709.00838502	0	0.434248		0.5429	17.5	17.4	122
64	1695	85.57*	1765.80257793	0	0.434936	0.457888	0.5388	25.0	26.7	124
	2255	3.24	1765.81619775	0	0.435611		0.5371	15.6	20.3	120
	2552	8.02*	1765.82032129	0.000253	0.430896		0.5371	50.0	50.4	124
	1100	1.05	1765.87533511	0	0.434467		0.5443	10.9	7.6	122
	2022	1.19*	1765.89790410	0.000152	0.427295		0.5380	50.0	50.4	124
	1520	0.93*	1765.91167428	0	0.439880		0.5380	26.6	30.2	124
65	5625	92.95*	1823.66796026	0.000400	0.428072	0.455004	0.5335	60.0	81.0	126
	6714	1.50*	1823.69459614	0	0.434582		0.5358	32.3	48.9	120
	2478	5.55*	1823.71802820	0.001283	0.423836		0.5321	100.0	98.8	126
66	12273	32.40*	1882.44152535	0.000776	0.432235	0.452868	0.5312	50.0	50.5	128
	2446	20.05*	1882.44209276	0	0.434503		0.5293	16.7	29.0	128
67	1017	100.00*	1942.12270041	0	0.431572	0.448270	0.5294	11.9	10.8	130
68	2004	70.25*	2002.87470175	0	0.426435	0.444372	0.5221	23.5	28.1	132
	2244	16.05*	2002.88294764	0.000014	0.422194		0.5246	17.6	23.8	132
	8889	13.40	2002.89000272	0.000688	0.418399		0.5199	57.4	51.1	131
	3192	0.20*	2002.98206733	0.001807	0.413769		0.5236	50.0	50.3	132
	2505	0.10*	2003.06105788	0.003608	0.406507		0.5100	97.1	98.3	132
69	1114	5.55*	2064.53348323	0	0.421261	0.442131	0.5215	17.4	17.6	134
	8757	32.35*	2064.53606623	0	0.425080		0.5202	27.5	39.9	134
	1891	53.25*	2064.53944940	0.000688	0.419259		0.5187	97.1	98.7	134
	3182	8.00	2064.55491294	0.000685	0.420971		0.5161	33.3	33.6	133
	5525	0.85*	2064.60448326	0.000643	0.414273		0.5186	100.0	98.1	134
70	2604	61.15	2127.10090155	0	0.423952	0.439315	0.5142	15.7	21.7	132
	3377	9.55*	2127.11628069	0.000268	0.415831		0.5129	34.3	33.1	136
	2768	13.05*	2127.11814054	0.001250	0.416111		0.5138	34.3	33.1	136
	4194	8.65*	2127.12667460	0.000393	0.421508		0.5146	55.7	81.6	136
	4200	5.05*	2127.13628990	0.000474	0.422922		0.5129	57.1	75.7	136
	1733	2.40*	2127.21103001	0.000442	0.418839		0.5121	50.0	50.8	136
	4131	0.15*	2127.30372335	0.002756	0.398821		0.5072	64.3	81.0	134
71	4140	95.50*	2190.64990643	0.001257	0.415434	0.436121	0.5115	50.7	50.3	136
	3787	3.05*	2190.69381272	0.003693	0.410524		0.5026	98.6	97.9	138
	1874	1.40*	2190.76494784	0.001128	0.405700		0.5096	100.0	98.2	138
	8180	0.05	2190.88650071	0.000984	0.402219		0.5042	50.7	50.1	138
72	852	82.95*	2255.00119098	0	0.427461	0.435049	0.5140	2.8	2.0	140
	3747	7.45*	2255.13111676	0	0.423770		0.5082	4.2	10.1	134
	3986	5.45	2255.26271483	0.000678	0.404687		0.5073	58.3	70.3	137
	2762	3.30*	2255.29359234	0.001255	0.399868		0.5053	100.0	98.4	140
	12174	0.80*	2255.31431104	0.001425	0.403415		0.5038	100.0	98.1	140
	1842	0.05	2255.39323492	0.000681	0.397730		0.5035	98.6	97.7	140
73	3432	90.35*	2320.63388375	0.001573	0.398115	0.428544	0.5076	56.2	77.6	142
	4995	8.90*	2320.67535341	0.000383	0.405192		0.5059	98.6	98.0	142
	1384	0.35*	2320.79425065	0.000160	0.399849		0.5016	50.7	54.1	142
	8113	0.20*	2320.79742109	0.002966	0.403042		0.5019	84.9	95.4	142
	2687	0.20*	2320.82910544	0.002754	0.398270		0.4931	97.3	98.7	142
74	3039	28.60*	2387.07298184	0.000642	0.400828	0.426225	0.5006	52.7	70.9	144
	15994	20.05*	2387.07516717	0.000177	0.401819		0.4999	48.6	50.4	144
	2482	24.05*	2387.07993444	0.001345	0.402612		0.4980	97.3	97.8	144
	5762	20.50*	2387.08728748	0.000559	0.403742		0.5015	100.0	97.9	143
	7775	0.60*	2387.09418960	0.000834	0.399111		0.5009	52.7	62.5	144
	2728	0.55*	2387.10121441	0	0.400112		0.5000	50.0	49.6	144
	7289	0.30*	2387.10460931	0.000002	0.405705		0.5005	45.9	47.2	144
	4049	3.40*	2387.10711171	0.000295	0.402163		0.4994	50.0	50.3	144
	3038	0.40*	2387.11556802	0.003553	0.391427		0.5006	52.7	69.8	144
	5016	0.50*	2387.11557541	0.003445	0.389949		0.4999	83.8	88.7	144

N	Average iterations	Frequency %	Coulomb energy	Dipole moment	Coulomb angle	Tammes angle	Hole angle	% Energy diversity	% Angular diversity	Faces N_f
	3594	1.00*	2387.12809098	0.000074	0.400626		0.4994	66.2	83.9	144
75	5316	97.15*	2454.36968904	0	0.396826	0.424145	0.4999	17.3	17.3	146
	5583	0.65*	2454.47518023	0.001730	0.397887		0.4961	96.0	98.1	146
	3823	2.20*	2454.48282529	0.000221	0.399361		0.4942	48.0	50.0	146
76	2160	72.65*	2522.67487184	0.000943	0.399431	0.420968	0.4932	50.0	57.9	148
	7668	3.85	2522.70043604	0.001113	0.395642		0.4932	63.2	80.9	148
	5015	18.40*	2522.71740900	0.001136	0.397212		0.4910	98.7	97.4	146
	3483	3.00*	2522.73513045	0	0.400992		0.4954	28.9	39.3	148
	1999	0.70*	2522.79463635	0.001703	0.400674		0.4927	50.0	61.8	148
	6714	1.20	2522.79646997	0.002723	0.396414		0.4921	76.3	89.2	146
	2258	0.15	2522.83098418	0	0.400978		0.4913	17.1	16.7	148
	18057	0.05	2522.91577137	0.000209	0.396677		0.4931	46.1	49.4	148
77	1272	96.30*	2591.85015235	0	0.406420	0.418807	0.4947	11.7	10.8	150
	10481	0.30*	2592.01257632	0.003137	0.386295		0.4874	83.1	92.6	149
	4061	2.30	2592.01416288	0.001999	0.402892		0.4913	23.4	22.7	145
	1733	0.95*	2592.06613681	0.000433	0.392480		0.4886	98.7	97.7	150
	2255	0.10	2592.15817266	0	0.392444		0.4920	18.2	29.2	150
	9326	0.05	2592.16547594	0.000385	0.392832		0.4912	33.8	27.1	149
78	1192	0.80	2662.04647457	0	0.408867	0.417675	0.4876	6.4	4.6	152
	1944	93.90*	2662.04721329	0	0.404565		0.4877	16.7	17.3	152
	4909	3.05	2662.12291358	0.000584	0.397320		0.4857	33.3	37.0	151
	3831	1.45	2662.22689315	0.000615	0.394945		0.4863	30.8	26.6	149
	3430	0.80*	2662.27142693	0.000723	0.388632		0.4835	98.7	98.1	151
79	2625	92.60	2733.24835748	0.000703	0.395073	0.412316	0.4856	62.0	67.1	153
	3171	6.70	2733.27367184	0.001057	0.392687		0.4839	34.2	40.6	154
	4669	0.05	2733.43501631	0.001652	0.390014		0.4810	67.1	83.6	154
	3123	0.45	2733.44491374	0.000395	0.390023		0.4838	32.9	37.9	152
	5193	0.10	2733.45513921	0.002295	0.384218		0.4842	89.9	95.4	154
	2334	0.10*	2733.47618113	0.001284	0.390059		0.4815	50.6	50.1	154
80	2287	74.25	2805.35587598	0	0.397557	0.410912	0.4851	10.0	8.7	154
	6104	15.85*	2805.43731924	0.000424	0.390855		0.4820	66.3	84.0	156
	3538	4.05	2805.47175377	0	0.389448		0.4875	16.3	13.5	154
	6259	3.40	2805.47441738	0	0.385954		0.4840	25.0	25.1	152
	6135	1.75*	2805.52242977	0.001283	0.382592		0.4803	100.0	97.6	156
	2302	0.55*	2805.53769852	0.001393	0.385740		0.4814	50.0	50.1	156
	4869	0.15	2805.67140367	0.000801	0.385097		0.4786	58.8	65.0	156
81	5873	48.70*	2878.52282967	0.000194	0.382079	0.407493	0.4769	70.4	86.4	158
	8035	27.50*	2878.52853268	0.000381	0.379170		0.4779	97.5	97.5	158
	3140	7.35*	2878.54384730	0.000234	0.377999		0.4801	55.6	78.6	158
	7977	10.20*	2878.58533588	0.000788	0.374717		0.4776	100.0	97.7	157
	2963	0.80*	2878.59244543	0.001113	0.381752		0.4758	55.6	68.9	158
	8548	1.80*	2878.59516266	0.001047	0.382537		0.4793	98.8	98.0	158
	3832	0.75*	2878.59851237	0.000990	0.380933		0.4757	97.5	98.0	158
	3642	2.70*	2878.61621814	0.002079	0.380754		0.4755	97.5	97.5	158
	1584	0.05	2878.65259291	0.001830	0.379521		0.4768	33.3	32.9	158
	3544	0.15*	2878.70501519	0.001470	0.379058		0.4745	100.0	98.1	158
82	4515	27.75*	2952.56967529	0	0.387567	0.404787	0.4784	25.6	32.7	160
	5593	13.05*	2952.57368611	0	0.384226		0.4762	39.0	44.2	160
	3318	16.45*	2952.57478472	0.000107	0.375075		0.4746	48.8	49.9	160
	4092	15.45*	2952.58504951	0.000366	0.376074		0.4734	100.0	97.2	160
	3511	9.95*	2952.59404559	0.000869	0.378304		0.4757	98.8	97.9	159
	3995	7.40*	2952.59952750	0.001395	0.380152		0.4719	100.0	97.4	160
	2468	0.90*	2952.60156975	0.000424	0.382119		0.4771	50.0	70.9	160
	1581	0.10*	2952.60827268	0	0.382946		0.4784	11.0	16.7	160
	7724	3.70*	2952.61233304	0.000451	0.372213		0.4732	98.8	97.9	160
	9095	1.90	2952.61405693	0.000530	0.375110		0.4762	65.9	81.2	158
	6667	1.85*	2952.62580274	0.002129	0.376405		0.4762	100.0	97.6	160
	4510	0.60	2952.62681055	0.000549	0.381781		0.4729	74.4	86.3	160
	3051	0.10*	2952.64690930	0.001319	0.378503		0.4746	53.7	80.1	160
	2492	0.25*	2952.68656376	0.000516	0.377377		0.4738	50.0	50.3	160
	2569	0.40*	2952.70171196	0.000055	0.376233		0.4717	50.0	50.0	160
	4097	0.15*	2952.73357764	0.003106	0.374029		0.4697	100.0	97.7	160
83	5438	24.20*	3027.52848893	0.000340	0.377795	0.402874	0.4758	73.5	85.4	162
	2968	17.85*	3027.54137715	0.000128	0.377682		0.4734	50.6	50.0	162
	9602	19.80*	3027.55862902	0.000875	0.376526		0.4723	90.4	92.3	160
	3747	9.00*	3027.59245704	0.000099	0.379116		0.4705	54.2	73.1	162
	2898	9.10*	3027.59319407	0	0.383514		0.4716	18.1	22.4	162
	4424	5.25*	3027.59924209	0.000530	0.376939		0.4713	96.4	97.9	162
	2679	3.30*	3027.60050001	0.000521	0.374436		0.4729	50.6	50.2	162
	6300	2.10	3027.61937175	0.000291	0.376050		0.4712	78.3	87.7	158
	7075	1.50	3027.62808194	0.000669	0.380499		0.4677	57.8	67.3	162

N	Average iterations	Frequency %	Coulomb energy	Dipole moment	Coulomb angle	Tammes angle	Hole angle	% Energy diversity	% Angular diversity	Faces N_f
	4879	1.95*	3027.63179386	0.001527	0.373643		0.4724	97.6	97.9	162
	4567	1.35*	3027.63256198	0.000883	0.377717		0.4733	98.8	97.8	162
	4299	3.20*	3027.63425680	0.000991	0.375605		0.4709	100.0	98.0	162
	3594	0.75*	3027.64213174	0.001039	0.375153		0.4684	98.8	97.8	162
	10202	0.25*	3027.66414535	0.001978	0.378210		0.4710	98.8	97.5	162
	5174	0.25*	3027.66441132	0.000407	0.376792		0.4723	59.0	82.0	162
	3453	0.05	3027.68231381	0.001979	0.376238		0.4708	100.0	98.1	162
	6021	0.10*	3027.71099742	0.002902	0.373357		0.4653	97.6	97.4	162
84	8308	11.45*	3103.46512444	0.000407	0.375467	0.402329	0.4708	58.3	77.8	164
	2243	34.10*	3103.47871710	0	0.385740		0.4708	16.7	17.3	164
	2843	8.10*	3103.48273357	0	0.379225		0.4708	25.0	26.0	164
	5600	14.35*	3103.49243447	0.000587	0.375862		0.4676	98.8	97.4	164
	4610	4.95*	3103.49295073	0.000480	0.377327		0.4682	97.6	97.4	164
	5784	0.55	3103.49438022	0	0.383778		0.4705	27.4	28.5	164
	3960	3.25*	3103.50450535	0.000226	0.375240		0.4708	61.9	80.9	164
	2724	1.95*	3103.50942982	0.000373	0.376401		0.4690	50.0	49.8	164
	2598	8.65	3103.51025966	0.000479	0.375186		0.4702	58.3	69.6	164
	5379	6.85*	3103.51055938	0.000569	0.376813		0.4668	97.6	97.6	163
	5520	3.15*	3103.51244522	0.000544	0.378262		0.4697	50.0	50.1	164
	5423	1.00*	3103.54674529	0	0.379786		0.4686	39.3	45.4	164
	6238	0.45*	3103.55004326	0.000317	0.376672		0.4667	78.6	87.9	164
	3600	0.30*	3103.56428084	0.000369	0.374846		0.4679	57.1	79.9	164
	2897	0.45*	3103.59823623	0.002032	0.373768		0.4648	98.8	97.8	164
	4248	0.45*	3103.63951517	0.002169	0.363683		0.4642	97.6	97.8	163
85	3124	18.70*	3180.36144294	0.000417	0.375204	0.397563	0.4671	50.6	50.1	166
	6119	12.10*	3180.37847263	0.001008	0.374286		0.4665	50.6	49.9	166
	5850	13.00*	3180.38006415	0.001031	0.371294		0.4671	97.6	97.4	166
	3822	23.45*	3180.38254415	0.000826	0.372080		0.4650	98.8	97.9	166
	4525	7.25*	3180.38926265	0.001080	0.379221		0.4660	49.4	54.6	166
	10567	9.90*	3180.38946622	0.000324	0.376140		0.4670	49.4	69.8	166
	4834	7.40*	3180.39289716	0.000731	0.368077		0.4653	100.0	97.4	166
	5573	4.20*	3180.41240577	0.000241	0.373119		0.4642	100.0	97.4	165
	5820	2.40*	3180.42055571	0.001020	0.378541		0.4631	100.0	97.5	166
	2271	0.35	3180.49260922	0.001515	0.371106		0.4640	54.1	54.9	166
86	2290	15.25*	3258.21160571	0.001379	0.375622	0.395742	0.4631	50.0	56.3	168
	2897	5.05*	3258.21366308	0.000013	0.377280		0.4660	17.4	21.2	168
	7523	7.80*	3258.21995934	0.000165	0.368917		0.4612	48.8	50.0	168
	8512	6.90*	3258.22282967	0.000124	0.371239		0.4626	47.7	49.9	168
	3746	18.25*	3258.22413239	0.000179	0.371405		0.4624	54.7	77.2	168
	6651	3.75*	3258.22424493	0	0.374381		0.4651	39.5	45.6	168
	2182	13.40*	3258.23636072	0.000842	0.373502		0.4596	96.5	97.2	168
	2683	2.90*	3258.24051336	0.001038	0.372867		0.4616	59.3	73.1	168
	2495	7.60*	3258.24155989	0.001298	0.372814		0.4631	97.7	97.6	168
	3846	1.80*	3258.24178774	0.000004	0.372126		0.4624	48.8	49.8	168
	3935	2.90*	3258.25311944	0.000726	0.370914		0.4596	53.5	74.2	168
	2552	0.30*	3258.26358795	0	0.379686		0.4657	25.6	25.9	168
	5394	3.40*	3258.26882630	0.000727	0.370793		0.4584	98.8	98.0	168
	3750	1.70*	3258.27038695	0.000655	0.367979		0.4594	100.0	97.6	168
	4339	1.50*	3258.27058422	0.000564	0.367010		0.4597	96.5	97.7	168
	5915	1.05*	3258.27683885	0.000745	0.372503		0.4593	98.8	97.0	167
	3497	0.40*	3258.28163525	0.000569	0.372030		0.4629	64.0	83.2	168
	5225	0.20*	3258.28558850	0.000690	0.374568		0.4596	62.8	78.9	168
	9177	1.05*	3258.28614166	0.000563	0.369638		0.4603	98.8	97.8	166
	2981	2.30*	3258.28694076	0.000500	0.372375		0.4637	97.7	97.9	168
	3000	1.25*	3258.30567932	0.000833	0.369457		0.4617	98.8	97.3	168
	4136	0.65*	3258.32740180	0.000280	0.373141		0.4601	62.8	78.2	168
	8679	0.15*	3258.33606379	0.000876	0.365530		0.4608	98.8	97.3	168
87	1836	10.50*	3337.00075002	0.000755	0.374486	0.393513	0.4585	49.4	49.9	170
	3117	37.75*	3337.00264299	0.000858	0.370122		0.4576	97.7	97.6	170
	2725	14.85*	3337.01479783	0.000957	0.370999		0.4576	98.9	96.9	170
	2033	9.85*	3337.02117824	0.001104	0.371262		0.4624	49.4	50.0	170
	3487	2.80	3337.02362435	0.000711	0.371217		0.4562	55.2	51.2	166
	3393	5.95*	3337.02502927	0.000768	0.369781		0.4603	62.1	77.2	168
	2965	0.80*	3337.03446331	0.000075	0.375119		0.4602	57.5	74.9	170
	4297	5.50*	3337.04552047	0.000594	0.371494		0.4607	50.6	49.9	170
	1772	0.15	3337.05086065	0	0.375040		0.4614	17.2	21.6	170
	2351	0.80*	3337.05185933	0.000857	0.371193		0.4594	50.6	61.9	170
	3236	3.55*	3337.05440265	0.000767	0.371009		0.4583	97.7	97.5	170
	3587	1.75*	3337.06733548	0.000644	0.367472		0.4579	97.7	97.2	169
	3510	3.10*	3337.07025805	0.000394	0.368212		0.4596	98.9	97.5	170
	2789	0.90	3337.07431278	0.001329	0.376930		0.4605	33.3	34.8	168
	20000	0.15*	3337.08185385	0.000014	0.374393		0.4580	49.4	48.8	170
	18681	0.35*	3337.08619885	0.000651	0.367931		0.4554	94.3	96.6	170

N	Average iterations	Frequency %	Coulomb energy	Dipole moment	Coulomb angle	Tammes angle	Hole angle	% Energy diversity	% Angular diversity	Faces N_f
	6771	0.10*	3337.08860953	0	0.372228		0.4586	17.2	17.2	170
	2499	0.35*	3337.12378055	0.000641	0.368926		0.4627	50.6	49.9	170
	5071	0.35*	3337.13487826	0.000496	0.367306		0.4591	72.4	85.6	168
	9751	0.10	3337.14268447	0.000316	0.366066		0.4590	56.3	56.2	168
	4413	0.05	3337.18362893	0.003243	0.356901		0.4547	82.8	86.2	167
	7587	0.15*	3337.19679142	0.001123	0.368213		0.4536	74.7	88.1	170
88	1490	30.65*	3416.72019676	0	0.374994	0.392138	0.4607	25.0	27.6	172
	2017	15.35*	3416.73289041	0.000020	0.371882		0.4581	48.9	53.0	172
	1842	5.10*	3416.73291048	0.000144	0.373766		0.4573	34.1	33.2	172
	1679	1.05*	3416.73691630	0	0.376714		0.4565	9.1	9.5	172
	2637	3.25*	3416.74783597	0.000051	0.372089		0.4574	34.1	32.9	172
	4292	11.40*	3416.77258601	0.000771	0.370835		0.4578	100.0	97.0	172
	4805	13.95*	3416.77625791	0.000889	0.370321		0.4564	100.0	97.4	172
	6811	9.10*	3416.77838595	0.000001	0.372959		0.4565	38.6	62.4	168
	5142	7.15*	3416.78202265	0.000900	0.367094		0.4572	98.9	97.1	172
	2957	0.40*	3416.81629359	0.000686	0.367167		0.4552	51.1	65.4	172
	3871	1.15*	3416.82016056	0.000867	0.366852		0.4557	97.7	97.4	172
	7510	0.50*	3416.82931948	0.001497	0.366057		0.4552	96.6	97.7	172
	3374	0.55*	3416.84374846	0.000239	0.368103		0.4593	50.0	50.0	172
	2082	0.20*	3416.86252342	0.000195	0.368193		0.4587	47.7	60.5	172
	2861	0.05	3416.91071105	0.002782	0.357957		0.4540	98.9	97.4	172
	9667	0.05	3416.93710995	0.001651	0.364377		0.4481	98.9	97.3	172
	2792	0.05	3416.94511277	0.002845	0.362872		0.4533	100.0	97.6	172
	4248	0.05	3416.96926530	0.001848	0.362298		0.4548	95.5	97.5	172
89	4297	40.30*	3497.43901863	0.000071	0.369698	0.389498	0.4563	50.6	49.8	174
	3948	20.10*	3497.45922155	0.000444	0.369944		0.4531	98.9	97.1	174
	5382	0.95*	3497.48136472	0.000246	0.369170		0.4540	48.3	49.8	174
	2481	4.45*	3497.48778781	0.000712	0.370412		0.4555	52.8	65.0	174
	7108	9.05*	3497.49123325	0.000647	0.365935		0.4536	97.8	97.3	173
	2363	0.05	3497.49124830	0.000668	0.365652		0.4537	97.8	97.3	172
	4174	3.65*	3497.49643601	0.000644	0.372884		0.4546	57.3	77.1	174
	4072	10.20*	3497.49781554	0.000599	0.364690		0.4544	100.0	97.0	174
	4161	1.75*	3497.49806433	0.001277	0.368111		0.4525	62.9	76.0	174
	2991	2.40*	3497.50964066	0.000835	0.365823		0.4557	50.6	58.9	174
	3473	1.45*	3497.51520013	0.000788	0.366995		0.4519	97.8	97.4	174
	4100	0.05	3497.52108788	0.001096	0.372382		0.4553	59.6	75.2	174
	3082	1.05*	3497.52321530	0.000495	0.367655		0.4546	49.4	62.4	174
	3566	0.90*	3497.55221987	0.000726	0.365735		0.4536	50.6	49.7	174
	3138	2.10*	3497.55978555	0.000533	0.365594		0.4527	97.8	97.1	174
	4114	0.25*	3497.56016553	0.000631	0.367741		0.4533	64.0	74.4	174
	1704	0.10	3497.56437230	0.000599	0.370195		0.4558	57.3	50.9	174
	3126	0.45*	3497.58896492	0.001931	0.362087		0.4555	98.9	97.3	174
	7504	0.25*	3497.60394456	0.001580	0.357530		0.4557	97.8	97.0	174
	8698	0.50*	3497.61268734	0.001836	0.358466		0.4471	98.9	97.3	173
90	1776	24.90*	3579.09122272	0	0.370538	0.386661	0.4557	16.7	19.3	176
	11403	18.45*	3579.12767705	0.000074	0.365325		0.4518	85.6	94.0	172
	2338	12.25*	3579.12846222	0.000048	0.367046		0.4532	50.0	50.0	176
	11803	1.50*	3579.17005864	0.000623	0.365565		0.4535	87.8	94.1	174
	4637	11.00*	3579.17029217	0.000974	0.363114		0.4515	95.6	97.2	176
	3823	5.75*	3579.17065197	0.000939	0.365783		0.4503	98.9	97.2	176
	4174	1.75*	3579.17673789	0	0.366697		0.4524	26.7	39.3	176
	19207	6.20*	3579.18145257	0.000033	0.365676		0.4506	94.4	96.6	176
	4266	0.85	3579.18243002	0.001140	0.369312		0.4529	72.2	81.3	176
	4477	3.40*	3579.19150205	0.001428	0.364526		0.4529	98.9	97.5	176
	3473	0.60	3579.19355887	0.001843	0.357642		0.4458	57.8	56.9	174
	1978	2.00*	3579.19477433	0.000826	0.363556		0.4531	50.0	58.4	176
	3027	2.00*	3579.19786368	0.000662	0.362691		0.4499	97.8	97.6	176
	3343	1.15*	3579.19863938	0.001108	0.367189		0.4512	98.9	97.6	176
	8549	0.50	3579.19907772	0.001254	0.368101		0.4536	62.2	77.7	174
	4497	2.15*	3579.19964436	0.000946	0.362293		0.4525	100.0	97.2	176
	4882	1.20*	3579.20381518	0.000667	0.359699		0.4516	98.9	97.5	175
	7147	0.15*	3579.20634325	0.000822	0.361884		0.4516	98.9	97.1	176
	2276	1.45*	3579.21087514	0.000841	0.359267		0.4520	100.0	96.8	176
	1822	0.25	3579.22252725	0.000739	0.363807		0.4560	32.2	33.2	176
	5565	0.60*	3579.22894703	0.001375	0.356951		0.4518	98.9	97.2	175
	2469	0.10*	3579.22985701	0	0.367525		0.4542	25.6	42.2	176
	3014	0.10	3579.24035346	0.000663	0.358755		0.4489	50.0	65.5	176
	3825	0.05	3579.24117875	0.001173	0.361032		0.4523	100.0	97.8	176
	3552	1.55*	3579.24720647	0.001563	0.360988		0.4516	97.8	97.4	175
	4372	0.10	3579.31345102	0.000960	0.359610		0.4551	55.6	50.9	176
91	1813	51.60*	3661.71369932	0.000033	0.368345	0.381338	0.4517	50.5	60.5	178
	3471	14.75*	3661.73060424	0.000070	0.365807		0.4498	61.5	78.0	178
	2577	10.75*	3661.74414545	0.000223	0.365919		0.4499	50.5	66.3	178

N	Average iterations	Frequency %	Coulomb energy	Dipole moment	Coulomb angle	Tammes angle	Hole angle	% Energy diversity	% Angular diversity	Faces N_f
	2363	9.05*	3661.79159223	0.000942	0.363419		0.4496	97.8	97.3	178
	6112	3.15*	3661.79263713	0.001204	0.362612		0.4503	50.5	49.9	178
	3103	2.25*	3661.80392012	0.000980	0.363667		0.4527	52.7	68.4	178
	2633	2.35	3661.80949650	0.000972	0.362586		0.4513	54.9	51.1	178
	2082	0.60*	3661.81797984	0.000267	0.368668		0.4513	50.5	56.4	178
	5209	1.75*	3661.82455480	0.000941	0.364284		0.4471	97.8	97.6	178
	2479	0.55	3661.83475823	0.000815	0.363118		0.4500	56.0	57.7	178
	4778	0.45*	3661.84030385	0.001125	0.354871		0.4489	100.0	97.7	177
	5567	0.25*	3661.85032596	0.000715	0.361957		0.4509	70.3	84.7	178
	8358	1.30*	3661.86007289	0.001042	0.358145		0.4491	98.9	97.6	178
	14052	0.30*	3661.88538438	0.002588	0.354657		0.4450	95.6	97.5	178
	1236	0.05	3661.88539500	0.002570	0.355246		0.4449	97.8	97.1	178
	13450	0.20*	3661.89681239	0.001013	0.355467		0.4486	98.9	97.2	177
	4817	0.05	3661.90331648	0.001947	0.355836		0.4452	96.7	97.3	178
	3194	0.15*	3661.90669487	0.001062	0.359267		0.4494	96.7	97.4	178
	20000	0.20*	3661.90686604	0.001758	0.358115		0.4429	98.9	97.1	175
	4433	0.20*	3661.94247551	0.002006	0.355772		0.4492	97.8	97.1	176
	3379	0.05	3662.00817185	0.000034	0.358704		0.4476	35.2	62.9	178
92	2256	28.10*	3745.29163624	0	0.366970	0.380107	0.4512	25.0	25.7	180
	1946	13.60*	3745.32218334	0.000023	0.365232		0.4504	48.9	50.0	180
	1968	9.40*	3745.32555284	0.000227	0.363114		0.4490	48.9	60.5	180
	1949	6.90*	3745.33860835	0.000466	0.363444		0.4485	50.0	50.1	180
	3287	6.70*	3745.36351634	0.001062	0.360649		0.4486	97.8	97.0	180
	2576	0.15	3745.36772048	0	0.369486		0.4487	10.9	15.0	180
	7273	6.05*	3745.38100894	0.001837	0.353498		0.4411	97.8	97.2	180
	4231	7.80*	3745.38177221	0.001112	0.354172		0.4443	94.6	96.9	180
	2949	2.30*	3745.38212626	0.000809	0.361606		0.4477	50.0	49.9	180
	4784	0.95*	3745.38297242	0.000764	0.362623		0.4479	98.9	97.6	180
	9572	0.70*	3745.38713069	0	0.370293		0.4483	21.7	33.3	180
	8056	4.55*	3745.38930840	0.001010	0.355401		0.4435	98.9	96.8	180
	3404	3.10*	3745.38943470	0.000940	0.362068		0.4468	97.8	96.8	180
	2972	2.65*	3745.39152813	0.000684	0.363450		0.4477	52.2	69.5	180
	3519	4.05*	3745.39598792	0.000796	0.359341		0.4484	97.8	97.4	180
	3955	0.35*	3745.40796449	0.000293	0.358002		0.4496	51.1	73.1	180
	3589	0.60	3745.40999059	0.000263	0.365047		0.4488	57.6	50.8	180
	5133	0.25*	3745.41663889	0.000909	0.362572		0.4472	67.4	79.9	178
	4972	0.15	3745.42597609	0.000464	0.357381		0.4482	78.3	88.6	180
	6210	0.25*	3745.43377765	0.000385	0.361479		0.4483	50.0	49.7	180
	4037	0.55*	3745.46354936	0.001120	0.357536		0.4462	100.0	97.5	180
	3062	0.05	3745.48063056	0.000593	0.359309		0.4470	64.1	76.6	180
	4430	0.20*	3745.48989730	0.002360	0.352056		0.4424	100.0	97.4	178
	18325	0.20	3745.50315713	0.001691	0.359301		0.4414	82.6	88.6	178
	3312	0.10*	3745.50321893	0.001051	0.350216		0.4475	97.8	96.9	180
	3344	0.10*	3745.51089154	0.002534	0.346900		0.4460	98.9	97.6	179
	3552	0.05	3745.52379435	0.001989	0.350982		0.4456	100.0	97.6	180
	2109	0.05	3745.57536192	0.002598	0.339922		0.4488	50.0	49.9	180
93	3182	44.65*	3829.84433842	0.000213	0.362167	0.375872	0.4477	59.1	70.7	182
	6639	15.50	3829.85868994	0.000164	0.360397		0.4435	60.2	69.1	180
	2508	4.00	3829.90619684	0.000523	0.363138		0.4431	32.3	26.6	182
	8282	8.65*	3829.91210881	0.000825	0.353932		0.4468	98.9	97.1	181
	2572	5.10*	3829.91995003	0.001253	0.359324		0.4432	98.9	97.4	182
	6742	1.50*	3829.92076446	0	0.362784		0.4463	17.2	29.4	182
	2225	3.80*	3829.93282075	0.001393	0.364055		0.4450	49.5	54.3	182
	4030	4.40*	3829.93683327	0.001717	0.356058		0.4443	98.9	97.0	180
	2890	2.80*	3829.93726481	0.001055	0.352693		0.4446	96.8	97.2	182
	6625	1.40	3829.94200079	0.001630	0.356002		0.4422	63.4	70.5	180
	2733	1.05*	3829.94230874	0.001116	0.351249		0.4452	97.8	97.0	182
	2617	1.05*	3829.94773193	0.001301	0.357394		0.4432	98.9	97.5	182
	10082	0.60*	3829.96290203	0.000183	0.356474		0.4458	86.0	91.2	180
	10392	0.65*	3829.96620757	0.001237	0.358821		0.4401	94.6	95.0	180
	2971	0.95*	3829.97421741	0.000776	0.356428		0.4452	98.9	97.4	182
	7000	0.70*	3829.97815077	0.002412	0.351322		0.4397	97.8	96.8	182
	2336	0.40*	3829.98564216	0.000300	0.360589		0.4460	50.5	65.7	182
	4924	0.20*	3829.98611334	0.001385	0.361367		0.4440	97.8	96.9	182
	3938	1.40*	3829.99329087	0.001490	0.347258		0.4447	98.9	96.8	182
	5630	0.10	3830.00626820	0.001435	0.353843		0.4460	97.8	97.0	181
	5166	0.05	3830.02249121	0.001789	0.355793		0.4441	50.5	49.8	182
	5158	0.10	3830.02481672	0.001418	0.344687		0.4453	96.8	97.3	182
	2722	0.05	3830.06290088	0.001280	0.354053		0.4415	100.0	97.0	182
	7179	0.05	3830.07937624	0.001795	0.351081		0.4444	97.8	97.5	181
	6637	0.10	3830.12098837	0.000302	0.359076		0.4490	53.8	47.4	182
94	4917	43.50*	3915.30926962	0	0.365679	0.373440	0.4471	24.5	29.4	184
	3249	9.90	3915.33763030	0.000260	0.364033		0.4425	66.0	77.0	184

N	Average iterations	Frequency %	Coulomb energy	Dipole moment	Coulomb angle	Tammes angle	Hole angle	% Energy diversity	% Angular diversity	Faces N_f
	1878	9.10*	3915.35216101	0.000505	0.361205		0.4448	34.0	39.6	184
	2290	5.20*	3915.41514225	0.000467	0.357315		0.4413	48.9	50.4	184
	4017	8.70*	3915.42460992	0.000958	0.359197		0.4413	97.9	97.3	184
	2373	4.15*	3915.42890409	0.000798	0.354464		0.4409	98.9	97.2	184
	5381	7.05*	3915.43908332	0.000703	0.350277		0.4422	98.9	96.8	184
	7796	2.05*	3915.44315884	0.001099	0.360016		0.4426	57.4	74.6	182
	4799	1.25*	3915.44481487	0.001392	0.355902		0.4447	97.9	97.3	184
	4409	1.10*	3915.45027523	0.000835	0.351244		0.4400	98.9	97.1	183
	5114	0.70	3915.45159808	0.002106	0.355880		0.4335	56.4	61.0	184
	5434	0.60	3915.45281248	0.000827	0.358784		0.4403	62.8	71.7	184
	2856	1.10*	3915.45967717	0.000052	0.360993		0.4452	50.0	70.6	184
	10741	0.30	3915.46280175	0.000456	0.355575		0.4437	98.9	97.2	182
	5489	0.10	3915.47416587	0.001327	0.354867		0.4423	95.7	95.3	184
	2324	0.05	3915.47460951	0.000953	0.358904		0.4439	48.9	64.3	184
	4134	0.95*	3915.47657801	0.001302	0.353930		0.4432	100.0	97.3	184
	1632	0.05	3915.47973753	0.000431	0.361005		0.4449	33.0	44.8	184
	4300	0.50*	3915.49216438	0.001251	0.351729		0.4397	97.9	97.0	184
	2955	0.20*	3915.49266383	0.002485	0.354183		0.4424	98.9	97.3	184
	3738	0.25	3915.49293708	0.001363	0.353588		0.4434	97.9	97.1	184
	2233	0.70*	3915.49372578	0.002351	0.354794		0.4394	97.9	97.2	184
	14961	0.40*	3915.49662960	0.000960	0.356566		0.4405	91.5	93.3	184
	3617	0.25	3915.49763862	0.000298	0.355783		0.4390	58.5	78.3	184
	9377	0.10*	3915.49815180	0.001574	0.351081		0.4420	96.8	97.5	184
	2446	0.25*	3915.50141193	0.001366	0.352030		0.4415	100.0	97.3	184
	5043	0.15	3915.50394770	0.001829	0.348852		0.4372	76.6	82.1	184
	3588	0.10	3915.50617610	0.001480	0.356503		0.4420	48.9	49.8	184
	7130	0.15	3915.51252701	0.001202	0.356538		0.4405	100.0	97.3	184
	4173	0.05	3915.51407010	0.000501	0.353108		0.4423	98.9	97.4	184
	3005	0.40*	3915.52008036	0.002364	0.351132		0.4370	96.8	96.8	184
	2754	0.10*	3915.52356293	0.002761	0.352597		0.4446	50.0	61.5	184
	6624	0.05	3915.52886015	0	0.358211		0.4464	20.2	46.2	180
	7251	0.10*	3915.54319693	0.002329	0.351277		0.4371	96.8	97.4	184
	3839	0.10	3915.54720228	0.002455	0.344401		0.4399	100.0	97.1	184
95	3146	56.95*	4001.77167557	0.000117	0.361479	0.369935	0.4400	53.7	65.9	186
	2965	23.90*	4001.80663427	0.000408	0.358976		0.4408	51.6	63.2	186
	4554	7.75*	4001.81894117	0.000682	0.358154		0.4405	64.2	81.5	184
	8736	3.70	4001.84343013	0.000106	0.357665		0.4396	80.0	86.6	186
	4092	0.55*	4001.87348103	0	0.362345		0.4438	18.9	40.7	186
	8716	3.85*	4001.88717904	0.002060	0.349877		0.4386	96.8	96.8	185
	5071	0.60*	4001.90696584	0.000871	0.356407		0.4393	97.9	96.6	186
	3155	0.25	4001.92060379	0.000499	0.355199		0.4404	49.5	49.8	186
	5270	0.30*	4001.92245595	0.001013	0.351863		0.4419	66.3	84.4	186
	5163	0.30*	4001.93659630	0.000770	0.356533		0.4394	100.0	96.8	184
	4763	0.65*	4001.94231614	0.001961	0.348660		0.4423	34.7	54.7	186
	3161	0.15*	4001.95525848	0.000518	0.350565		0.4428	49.5	49.7	186
	2788	0.20*	4001.96789955	0.001285	0.348385		0.4398	50.5	49.6	186
	10409	0.10	4001.96821304	0.002227	0.354032		0.4420	50.5	49.9	186
	15400	0.15*	4001.96821587	0.002195	0.352959		0.4417	49.5	49.8	185
	5496	0.15	4001.97185179	0.000973	0.354439		0.4399	71.6	79.4	184
	2724	0.15	4001.97930328	0.000284	0.354455		0.4389	49.5	59.6	186
	3067	0.05	4002.00545579	0.000861	0.355418		0.4399	100.0	96.9	186
	3528	0.05	4002.00636613	0.000831	0.356324		0.4411	100.0	95.4	186
	2763	0.10*	4002.00958028	0.001681	0.348189		0.4399	97.9	96.5	186
	5173	0.05	4002.01386735	0.002842	0.340982		0.4366	82.1	86.1	185
	10444	0.05	4002.01893501	0.000079	0.347362		0.4417	49.5	49.7	186
96	10339	56.20*	4089.15401006	0.000036	0.361049	0.368544	0.4377	49.0	49.5	186
	7508	1.90*	4089.15425120	0.000060	0.360714		0.4377	84.4	91.0	184
	15016	1.15*	4089.18961607	0.000003	0.363750		0.4378	24.0	25.4	188
	4043	6.45*	4089.19508088	0	0.359195		0.4404	17.7	37.4	188
	2621	9.15*	4089.22051843	0.000236	0.355515		0.4376	53.1	66.1	188
	7348	8.10*	4089.25754163	0.000513	0.357001		0.4368	95.8	96.7	187
	2015	0.55*	4089.25810401	0	0.357872		0.4385	8.3	9.7	188
	20000	0.95*	4089.27994849	0.000625	0.349075		0.4331	100.0	96.6	188
	3156	1.60*	4089.29813692	0.001006	0.346557		0.4395	60.4	76.4	186
	3560	1.65*	4089.31409559	0.000818	0.351814		0.4376	100.0	96.9	188
	4514	0.25	4089.32601764	0.002184	0.345804		0.4369	71.9	82.0	188
	4944	0.40*	4089.32884800	0.000975	0.349171		0.4378	99.0	96.8	188
	3423	0.90*	4089.32914181	0.000298	0.351588		0.4371	99.0	96.7	188
	3059	0.90*	4089.32934173	0.000128	0.355321		0.4382	52.1	73.5	188
	3245	0.70*	4089.32937644	0.002078	0.343830		0.4334	97.9	96.4	188
	10229	0.45*	4089.33178663	0.001262	0.355442		0.4363	100.0	97.5	187
	4143	0.20*	4089.36465058	0.000271	0.354412		0.4385	65.6	80.1	188
	7069	0.05	4089.39134612	0.000601	0.347028		0.4384	99.0	97.1	188

N	Average iterations	Frequency %	Coulomb energy	Dipole moment	Coulomb angle	Tammes angle	Hole angle	% Energy diversity	% Angular diversity	Faces N_f
	2039	0.05	4089.39260339	0.000238	0.353831		0.4388	49.0	53.4	188
	12704	0.05	4089.41039115	0.001791	0.354552		0.4381	50.0	47.5	188
	2010	0.05	4089.41837532	0.002204	0.347503		0.4313	100.0	97.1	188
	10089	0.30*	4089.41857907	0.000560	0.349882		0.4403	77.1	89.9	188
	5646	0.05	4089.42100567	0.001137	0.349877		0.4399	67.7	79.6	188
	2419	0.05	4089.47265364	0.002235	0.343688		0.4338	100.0	97.6	188
97	10458	90.20*	4177.53359963	0.000096	0.356912	0.366315	0.4353	69.1	81.3	190
	6950	5.60*	4177.59058909	0.000319	0.354241		0.4345	96.9	96.8	188
	5341	1.95*	4177.61875516	0.000443	0.353788		0.4376	44.3	70.0	190
	2406	0.95*	4177.64356494	0.000414	0.354661		0.4338	49.5	49.8	190
	5597	0.10*	4177.66799753	0.002142	0.345708		0.4305	97.9	96.6	190
	2035	0.40*	4177.71819311	0.000072	0.352609		0.4360	49.5	49.8	190
	5244	0.15*	4177.72270181	0.001956	0.343084		0.4312	97.9	97.2	190
	4572	0.10*	4177.73376330	0.001032	0.350770		0.4323	99.0	97.0	190
	3275	0.10	4177.74816006	0.001981	0.341206		0.4315	96.9	97.2	190
	3661	0.15*	4177.75166330	0.001118	0.345083		0.4379	49.5	49.8	190
	8617	0.05	4177.77558985	0.002416	0.341406		0.4296	99.0	97.0	189
	2697	0.05	4177.83805800	0.002598	0.346954		0.4332	95.9	97.0	190
98	3420	51.95*	4266.82246416	0.000113	0.356424	0.365017	0.4355	50.0	49.7	192
	2812	10.85*	4266.82617987	0.000010	0.356512		0.4370	17.3	23.5	192
	2157	8.35*	4266.83001454	0.000005	0.355677		0.4342	25.5	32.1	192
	2514	15.45*	4266.83424531	0.000073	0.356879		0.4339	50.0	49.7	192
	16766	3.45*	4266.83546709	0.000175	0.356828		0.4333	50.0	54.8	192
	1891	0.15	4266.86496975	0.000002	0.354672		0.4349	12.2	9.2	192
	4714	5.20*	4266.88905193	0.000361	0.353096		0.4323	65.3	80.8	192
	1540	0.70	4266.90771087	0.000107	0.356083		0.4323	32.7	27.9	192
	3776	0.30*	4266.94010421	0	0.352888		0.4360	17.3	17.1	192
	5620	0.30*	4266.99141130	0.001695	0.348640		0.4346	50.0	49.5	192
	6272	1.75*	4266.99290589	0.001817	0.346274		0.4323	99.0	97.0	192
	2555	0.40*	4267.02331924	0.000211	0.352952		0.4336	52.0	73.0	192
	3884	0.20*	4267.03957642	0.001741	0.340284		0.4304	99.0	96.6	192
	3170	0.05	4267.04219229	0.002046	0.341199		0.4311	100.0	97.3	192
	3763	0.20*	4267.04360487	0.001124	0.346337		0.4335	100.0	96.5	191
	7524	0.10	4267.05612322	0.002518	0.344810		0.4295	98.0	96.5	192
	3776	0.15*	4267.05691148	0.001886	0.340080		0.4321	100.0	97.2	192
	2887	0.05	4267.07313307	0.003289	0.346711		0.4294	50.0	49.4	192
	3007	0.20*	4267.09421053	0.000376	0.347308		0.4317	99.0	97.0	192
	3245	0.10*	4267.11281169	0.001422	0.341775		0.4319	100.0	96.6	191
	6130	0.05	4267.11376752	0.001001	0.347395		0.4337	87.8	92.4	192
	6586	0.05	4267.13819960	0.001122	0.341793		0.4346	99.0	97.2	192
99	14180	81.95*	4357.13916314	0.000157	0.354032	0.363478	0.4333	49.5	49.6	194
	8978	8.30*	4357.17268162	0.000332	0.352303		0.4324	97.0	97.1	194
	5779	3.30	4357.18495891	0.000852	0.351978		0.4312	58.6	63.6	194
	2252	1.05*	4357.20285542	0.000387	0.353588		0.4313	33.3	42.5	194
	3721	0.20	4357.25433676	0.001464	0.346708		0.4319	54.5	50.5	194
	4163	1.75	4357.25694427	0.000799	0.350033		0.4292	57.6	57.0	190
	5514	0.20	4357.26204992	0.000926	0.344357		0.4317	75.8	83.8	194
	5939	1.65	4357.26865095	0.000480	0.343308		0.4317	57.6	70.7	192
	3646	0.45*	4357.27634050	0.000940	0.344401		0.4300	98.0	96.7	194
	4815	0.25	4357.32511953	0.001487	0.347475		0.4319	47.5	43.6	194
	3889	0.25*	4357.32893422	0.002696	0.345178		0.4286	97.0	96.8	193
	3882	0.20	4357.33023200	0.001586	0.348309		0.4324	56.6	50.4	192
	2741	0.05	4357.35477108	0.002329	0.342488		0.4284	100.0	96.6	194
	4303	0.10*	4357.35789854	0.001819	0.342169		0.4291	99.0	96.9	191
	4149	0.15*	4357.37036331	0.001641	0.340640		0.4285	99.0	96.8	194
	11928	0.05	4357.37577617	0.002043	0.344761		0.4226	92.9	93.6	192
	2776	0.10	4357.46779855	0.000954	0.343514		0.4281	100.0	96.9	194
100	6632	43.75*	4448.35063434	0	0.354240	0.361806	0.4329	15.0	19.6	196
	4451	22.35	4448.41042065	0.000548	0.351242		0.4308	63.0	71.9	196
	1985	1.95*	4448.42088460	0	0.356163		0.4333	9.0	10.4	196
	2461	1.80*	4448.43456411	0.000232	0.351233		0.4302	49.0	50.7	196
	2746	1.10*	4448.43664953	0.000797	0.348810		0.4293	34.0	33.0	196
	12634	6.80*	4448.44720777	0.000610	0.346536		0.4332	50.0	49.6	194
	7183	2.00*	4448.44834304	0.000115	0.350778		0.4294	95.0	94.8	196
	2729	3.05*	4448.46648310	0.000681	0.346444		0.4282	100.0	96.7	196
	3908	1.75*	4448.46871243	0	0.349249		0.4302	25.0	40.8	196
	3536	4.15*	4448.47370541	0.000100	0.346810		0.4289	50.0	62.4	196
	1910	1.30*	4448.47440810	0.000596	0.349473		0.4293	50.0	49.6	196
	7079	4.75*	4448.47538457	0.000627	0.346445		0.4283	98.0	96.5	196
	4940	0.25	4448.47902256	0.001645	0.348765		0.4280	29.0	37.5	196
	3579	0.55*	4448.48018390	0.000054	0.346106		0.4303	50.0	68.9	196
	5121	0.85*	4448.48730379	0.000677	0.348757		0.4296	49.0	54.3	196
	5750	0.75*	4448.48960197	0.000466	0.349570		0.4292	49.0	59.6	196

N	Average iterations	Frequency %	Coulomb energy	Dipole moment	Coulomb angle	Tammes angle	Hole angle	% Energy diversity	% Angular diversity	Faces N_f
	3614	1.05*	4448.49667946	0.000878	0.343913		0.4281	100.0	96.8	196
	3366	0.45*	4448.50686302	0.000312	0.346927		0.4302	50.0	49.8	196
	3438	0.10	4448.54040487	0.000940	0.342441		0.4260	62.0	74.0	196
	5421	0.05	4448.56301774	0.001107	0.339114		0.4288	99.0	96.0	196
	12096	0.20*	4448.57164151	0.001349	0.339049		0.4285	97.0	96.9	195
	2441	0.05	4448.57479340	0.002504	0.338709		0.4298	63.0	73.5	196
	3806	0.05	4448.57642589	0.001049	0.340203		0.4290	66.0	81.2	196
	3372	0.05	4448.59743687	0.002589	0.341857		0.4276	75.0	86.6	196
	3653	0.15	4448.61021879	0.001183	0.342874		0.4253	99.0	96.7	195
	10105	0.10	4448.62161144	0.002121	0.332642		0.4260	98.0	96.5	195
	7394	0.05	4448.62525087	0.001769	0.338185		0.4251	97.0	96.8	196
	3762	0.15*	4448.62928026	0.001209	0.334653		0.4252	98.0	97.1	196
	3665	0.05	4448.63317178	0.001823	0.339986		0.4263	96.0	97.2	196
	5249	0.10	4448.66828993	0.000779	0.342168		0.4260	99.0	96.9	195
	3530	0.05	4448.66909039	0.001739	0.336776		0.4265	100.0	96.9	196
	9861	0.05	4448.67654431	0.001400	0.339756		0.4267	99.0	96.6	196
	2745	0.05	4448.70899783	0.001896	0.335485		0.4258	99.0	96.8	195
	2709	0.05	4448.78255856	0.003722	0.334545		0.4228	99.0	97.1	196
101	3628	40.75*	4540.59005170	0	0.349259		0.4287	17.8	36.2	198
	4832	13.30*	4540.65878548	0.000762	0.346173		0.4284	96.0	96.5	198
	3452	4.10*	4540.67532223	0.000754	0.345065		0.4279	99.0	96.8	197
	4611	2.00*	4540.67666960	0.000736	0.343724		0.4260	99.0	97.6	197
	4588	0.70	4540.67798465	0.000728	0.348626		0.4288	41.6	44.1	198
	14862	5.00*	4540.68233258	0.001700	0.344000		0.4264	90.1	90.9	198
	7956	4.25*	4540.68572575	0.001179	0.343152		0.4262	98.0	96.8	198
	8304	1.90*	4540.68669238	0.001057	0.343349		0.4262	97.0	96.5	196
	5241	2.50*	4540.69461564	0.001797	0.340756		0.4262	98.0	96.3	196
	6561	1.85*	4540.69602516	0.001118	0.343969		0.4280	56.4	74.8	198
	2065	0.70*	4540.70249096	0.000820	0.346209		0.4289	50.5	59.2	198
	7108	1.35*	4540.70405116	0.001311	0.341813		0.4280	96.0	96.5	198
	3798	2.20*	4540.70410867	0.001225	0.341380		0.4286	100.0	97.0	197
	12931	2.35*	4540.70507628	0.001346	0.338717		0.4265	99.0	96.5	198
	4280	1.55*	4540.70634842	0.001777	0.343050		0.4252	96.0	96.8	198
	8735	3.30*	4540.70663798	0.000750	0.342249		0.4278	100.0	97.0	197
	2487	1.50	4540.70701619	0.001192	0.339750		0.4290	56.4	50.2	198
	9679	0.90*	4540.70780726	0.001562	0.340204		0.4269	97.0	96.5	198
	10634	1.60	4540.71126420	0.000589	0.343480		0.4293	57.4	57.8	198
	4236	0.65*	4540.71328571	0.000828	0.341285		0.4269	97.0	96.6	198
	4249	0.55*	4540.71537082	0.000576	0.344120		0.4274	94.1	97.4	198
	6848	0.10	4540.71609656	0.001220	0.344720		0.4291	97.0	95.0	195
	5481	0.85*	4540.72616655	0.002221	0.342467		0.4291	98.0	96.3	198
	15245	0.65*	4540.73175426	0.001360	0.338741		0.4262	100.0	96.6	198
	2186	0.45*	4540.73643501	0.001409	0.337389		0.4262	98.0	96.6	198
	5746	0.30*	4540.74219207	0.001395	0.344564		0.4259	98.0	96.4	198
	7194	0.20*	4540.74368177	0.001127	0.344476		0.4265	99.0	97.0	198
	18839	0.95*	4540.74470982	0.000265	0.344598		0.4248	99.0	96.8	197
	4328	0.40*	4540.75252547	0.001231	0.341404		0.4268	99.0	96.9	198
	4120	0.75*	4540.75307454	0.001371	0.341351		0.4261	97.0	96.8	198
	2570	0.10	4540.75459130	0.001067	0.345703		0.4309	33.7	43.1	198
	6314	0.05	4540.76551282	0.001480	0.340515		0.4267	97.0	96.9	198
	3930	0.10	4540.76683798	0.001361	0.339038		0.4270	99.0	97.0	198
	3814	0.30*	4540.76853869	0.002324	0.338765		0.4258	98.0	96.9	198
	2860	0.25*	4540.77391959	0.000312	0.339712		0.4250	100.0	96.8	198
	3322	0.25*	4540.77601345	0.000804	0.344874		0.4302	63.4	81.5	198
	6089	0.10*	4540.78271386	0.001149	0.342709		0.4232	100.0	96.8	198
	7166	0.05	4540.78294548	0.001212	0.342083		0.4271	99.0	97.0	198
	5832	0.20*	4540.78977525	0.001613	0.338516		0.4284	98.0	96.6	198
	2420	0.05	4540.79799071	0.000830	0.345848		0.4295	50.5	70.9	198
	8432	0.05	4540.79800707	0.001583	0.339397		0.4284	96.0	96.8	198
	2620	0.15*	4540.79856369	0.002600	0.335211		0.4210	98.0	96.5	198
	3291	0.25*	4540.82275811	0.001659	0.333337		0.4228	98.0	96.5	198
	7546	0.05	4540.82951697	0.001935	0.341129		0.4245	50.5	49.6	198
	2910	0.05	4540.84548695	0.001689	0.340170		0.4242	99.0	97.0	198
	4638	0.05	4540.85872567	0.002410	0.332157		0.4220	72.3	80.7	197
	3721	0.10*	4540.86780715	0.002192	0.339999		0.4241	100.0	97.0	197
	5498	0.05	4540.92415697	0.002169	0.336749		0.4216	100.0	96.8	198
102	5562	44.85*	4633.73656590	0	0.349762		0.4283	16.7	35.7	200
	3487	0.05	4633.74993810	0	0.349998		0.4274	27.5	34.7	200
	3007	11.35*	4633.83689270	0.000860	0.340877		0.4238	96.1	96.4	200
	15595	1.00	4633.83812704	0.000007	0.345146		0.4229	50.0	47.3	200
	3245	0.25*	4633.83829706	0	0.345712		0.4233	43.1	45.4	196
	3073	2.00*	4633.85199367	0.001859	0.339422		0.4222	97.1	96.7	199
	7064	4.60*	4633.85207449	0.001664	0.338472		0.4227	96.1	96.8	200

N	Average iterations	Frequency %	Coulomb energy	Dipole moment	Coulomb angle	Tammes angle	Hole angle	% Energy diversity	% Angular diversity	Faces N_f
	8993	6.95*	4633.85227866	0.001764	0.338007		0.4233	98.0	97.1	200
	6035	2.60*	4633.85754458	0.000667	0.342413		0.4233	98.0	96.6	200
	3015	0.65*	4633.85931485	0	0.349061		0.4287	24.5	35.9	200
	4434	1.85*	4633.86290383	0.001930	0.337926		0.4228	97.1	96.8	200
	2642	1.75*	4633.86313546	0.000083	0.346016		0.4283	49.0	68.6	200
	3879	2.20*	4633.86358398	0.000677	0.341600		0.4243	98.0	97.3	199
	6259	1.60*	4633.86605294	0.000947	0.343398		0.4259	50.0	49.6	200
	4070	0.05	4633.86666295	0.002084	0.341072		0.4241	98.0	96.4	200
	4424	1.45*	4633.86951464	0.001037	0.337419		0.4256	99.0	96.9	200
	3587	1.85*	4633.87171213	0.001306	0.337476		0.4235	96.1	96.9	199
	5480	0.25*	4633.87266256	0.000809	0.341949		0.4253	70.6	83.9	200
	3411	0.20	4633.87295600	0.001868	0.340708		0.4241	58.8	65.9	199
	7853	0.85*	4633.88106601	0.001077	0.343487		0.4232	98.0	96.7	199
	3133	1.25*	4633.88152617	0.001448	0.341558		0.4256	97.1	96.8	200
	8247	0.20*	4633.88475300	0.000811	0.342239		0.4259	90.2	94.1	200
	5877	0.95*	4633.88698437	0.002330	0.338992		0.4177	97.1	97.0	200
	4837	0.55*	4633.88887689	0.002066	0.342432		0.4252	100.0	97.0	199
	7660	0.05	4633.88888748	0.001135	0.341990		0.4234	89.2	90.1	200
	11195	1.25*	4633.89082450	0.001926	0.345677		0.4258	82.4	91.8	200
	3824	1.60*	4633.89636032	0.000616	0.340606		0.4269	97.1	96.6	200
	3019	0.15*	4633.89906101	0.000999	0.339183		0.4262	99.0	96.3	200
	6732	0.55*	4633.90529547	0.001556	0.339756		0.4265	98.0	96.8	199
	11486	0.20*	4633.91542780	0.000970	0.339636		0.4251	95.1	96.8	199
	20000	0.20*	4633.91548667	0.000818	0.340036		0.4267	96.1	96.7	199
	4593	0.05	4633.92151679	0.001515	0.344350		0.4266	73.5	82.7	200
	1868	0.20*	4633.92154073	0.000656	0.339689		0.4276	49.0	63.4	200
	6057	0.50*	4633.92219304	0.000503	0.339727		0.4216	98.0	97.0	199
	2862	0.05	4633.92448524	0.001445	0.344620		0.4267	50.0	49.9	200
	5120	0.25*	4633.92642546	0.000502	0.340915		0.4245	73.5	82.8	200
	2953	0.05	4633.92675171	0.001141	0.340939		0.4264	64.7	72.3	200
	10611	0.10	4633.92796901	0.001733	0.337318		0.4248	100.0	96.3	200
	3246	0.10*	4633.92901937	0.000508	0.339559		0.4273	49.0	66.8	200
	3379	0.50*	4633.93247439	0.002091	0.335457		0.4194	98.0	96.5	200
	5847	0.40*	4633.93302261	0.000713	0.341365		0.4248	98.0	97.2	199
	5340	0.30*	4633.93360282	0.002304	0.337316		0.4194	99.0	96.4	200
	2327	0.05	4633.94030983	0.000414	0.339619		0.4268	50.0	68.5	200
	16801	0.05	4633.94882459	0.001482	0.341347		0.4261	95.1	94.7	200
	3737	0.05	4633.95962334	0.001724	0.338635		0.4247	99.0	96.6	199
	2344	0.10	4633.97006396	0.003630	0.335170		0.4208	96.1	96.8	200
	2291	0.05	4633.97445084	0	0.340043		0.4271	16.7	26.2	200
	3492	0.20	4633.97457151	0.003064	0.340149		0.4224	99.0	97.0	200
	3758	0.10*	4633.97895241	0.001189	0.340785		0.4238	99.0	97.0	200
	5067	0.05	4633.99094034	0.001769	0.336441		0.4266	75.5	84.5	200
	2409	0.05	4634.00951995	0.000648	0.334067		0.4243	99.0	96.6	198
	8370	0.05	4634.03801133	0.001009	0.339310		0.4184	88.2	91.5	200
	7070	0.05	4634.05539599	0.000962	0.336984		0.4266	99.0	96.8	199
103	4758	57.60*	4727.83661684	0.000201	0.347443		0.4248	50.5	49.4	202
	5130	30.65*	4727.87233500	0.000171	0.347829		0.4240	37.9	57.0	202
	4393	1.65*	4727.96451737	0.000794	0.344944		0.4225	50.5	49.7	202
	2460	1.05*	4727.97788313	0.001201	0.342853		0.4250	50.5	58.2	202
	19089	1.50*	4727.97860150	0.001467	0.344326		0.4216	97.1	96.9	200
	3267	0.05	4727.97861093	0.001488	0.344607		0.4215	96.1	96.2	198
	4423	0.55*	4727.98878377	0.000450	0.342837		0.4228	50.5	49.8	202
	6067	1.20*	4728.00679250	0.000358	0.341955		0.4187	34.0	33.1	202
	20000	0.05	4728.01191498	0.001942	0.337083		0.4239	96.1	96.1	201
	2721	0.95*	4728.01375563	0.000245	0.342511		0.4203	61.2	78.7	202
	3746	0.05	4728.02087435	0.000696	0.337122		0.4223	99.0	96.6	202
	4778	0.80*	4728.02169914	0.000188	0.341271		0.4224	67.0	81.2	202
	12345	1.00*	4728.02343366	0.000763	0.338137		0.4206	99.0	96.5	199
	4557	0.30*	4728.03114014	0.001001	0.340910		0.4218	99.0	96.4	201
	7863	0.15	4728.03201156	0.001489	0.339532		0.4229	74.8	88.5	202
	8450	0.25	4728.04710707	0.000571	0.339761		0.4244	99.0	96.5	200
	2126	0.20*	4728.04851625	0.000489	0.338829		0.4239	50.5	49.7	202
	4988	0.05	4728.05487686	0.001705	0.336514		0.4206	98.1	96.8	202
	10123	0.25*	4728.05733810	0.001016	0.334814		0.4243	100.0	96.7	201
	3005	0.35	4728.05869705	0.000466	0.338715		0.4210	98.1	96.3	202
	4538	0.10	4728.06415117	0.000165	0.340939		0.4237	99.0	96.1	201
	5276	0.15*	4728.06466480	0.001595	0.340494		0.4201	97.1	96.4	201
	3991	0.35*	4728.06784859	0.000830	0.342047		0.4236	98.1	96.6	202
	2580	0.10*	4728.07516653	0.001187	0.334958		0.4208	99.0	96.1	202
	20000	0.05	4728.08206930	0.000490	0.333983		0.4233	98.1	96.3	202
	3408	0.05	4728.09569659	0.001283	0.339427		0.4199	98.1	96.7	202
	3675	0.10*	4728.09795720	0.001141	0.341058		0.4216	99.0	96.6	200
	9033	0.05	4728.10261840	0.000583	0.340430		0.4231	99.0	96.8	201

N	Average iterations	Frequency %	Coulomb energy	Dipole moment	Coulomb angle	Tammes angle	Hole angle	% Energy diversity	% Angular diversity	Faces N_f
	2406	0.10*	4728.11348291	0.001322	0.333478		0.4201	100.0	97.0	202
	5666	0.05	4728.12048167	0.002155	0.333740		0.4231	98.1	97.2	202
	6609	0.05	4728.12107616	0.000920	0.334107		0.4208	100.0	96.6	202
	8637	0.05	4728.12232759	0.000282	0.333524		0.4224	99.0	96.7	201
	2781	0.05	4728.13299914	0.000778	0.335127		0.4228	99.0	96.4	201
	8292	0.05	4728.13599495	0.001045	0.336212		0.4248	79.6	91.7	200
104	4969	41.95*	4822.87652275	0	0.348307		0.4218	10.6	20.8	204
	7229	14.55*	4822.88031733	0	0.346364		0.4209	44.2	46.7	204
	2758	25.80*	4822.92698786	0	0.347422		0.4203	25.0	35.4	204
	3828	3.85	4822.92747363	0	0.347076		0.4237	22.1	22.3	204
	3636	2.60*	4823.01967103	0.000018	0.342357		0.4208	50.0	49.7	204
	6692	6.15*	4823.04488010	0.000611	0.337480		0.4206	97.1	96.2	204
	20000	0.05	4823.05579007	0.001039	0.338858		0.4203	98.1	96.2	202
	3056	0.35*	4823.06318322	0	0.342268		0.4232	26.0	25.4	204
	2087	0.05	4823.07366060	0	0.341980		0.4232	17.3	20.7	204
	5029	0.60*	4823.09919587	0.000697	0.335411		0.4212	98.1	96.6	204
	5319	0.35*	4823.10629624	0.002171	0.329398		0.4182	98.1	96.3	204
	4304	0.55*	4823.11156855	0.002170	0.329781		0.4172	100.0	96.3	204
	3026	0.10*	4823.12721353	0.000192	0.338367		0.4197	50.0	49.5	204
	4532	0.15	4823.12827998	0.000772	0.336981		0.4227	51.9	60.9	202
	4767	0.40*	4823.12955754	0.001213	0.333409		0.4184	98.1	97.0	203
	9419	0.10*	4823.13066751	0.000540	0.328185		0.4221	87.5	88.5	204
	3901	0.10*	4823.13066844	0.001652	0.338055		0.4190	97.1	96.5	204
	11709	0.60*	4823.13238924	0.001000	0.337818		0.4224	100.0	96.6	203
	6272	0.05	4823.13350534	0.001217	0.337101		0.4208	89.4	92.1	202
	4061	0.05	4823.13488062	0.001539	0.333034		0.4188	99.0	96.7	204
	3012	0.20*	4823.13507703	0.000475	0.333717		0.4176	99.0	96.7	204
	3064	0.05	4823.13617395	0.001688	0.334602		0.4170	97.1	96.8	204
	3466	0.15*	4823.13730803	0.001596	0.338416		0.4203	98.1	96.5	204
	7260	0.20	4823.14146505	0.001785	0.333094		0.4154	97.1	96.8	203
	13077	0.15*	4823.14729381	0.000635	0.337112		0.4211	97.1	96.7	204
	6746	0.20*	4823.15027704	0.001212	0.334667		0.4164	95.2	96.3	204
	7936	0.05	4823.15115646	0.000135	0.339055		0.4232	90.4	91.4	200
	4215	0.05	4823.15217494	0.001290	0.336176		0.4195	98.1	96.5	204
	5927	0.05	4823.17391107	0.002039	0.336342		0.4224	99.0	96.8	204
	3175	0.05	4823.17760089	0.001383	0.334108		0.4192	96.2	96.6	203
	5523	0.05	4823.18486438	0.001766	0.336363		0.4188	99.0	96.5	204
	6462	0.05	4823.18812069	0.000634	0.335494		0.4214	98.1	96.7	204
	9175	0.05	4823.18900353	0.001468	0.330288		0.4167	99.0	96.7	204
	3692	0.05	4823.19463495	0.001094	0.334986		0.4207	99.0	96.9	204
	12115	0.05	4823.20788707	0.002344	0.335637		0.4190	98.1	96.8	204
	2228	0.05	4823.21788086	0.002422	0.330432		0.4159	98.1	96.5	204
	17153	0.05	4823.23730313	0.003195	0.332397		0.4162	97.1	95.1	202
	4526	0.05	4823.24022881	0.001672	0.333170		0.4193	97.1	96.8	203
105	2104	2.55*	4919.00063762	0	0.346306		0.4185	17.1	17.0	206
	2463	2.15*	4919.01224999	0	0.346599		0.4215	17.1	27.9	206
	5422	26.50*	4919.01355167	0.000471	0.336634		0.4184	98.1	96.3	205
	9992	14.65*	4919.01702056	0.000106	0.339367		0.4180	90.5	91.8	206
	2745	9.05*	4919.01858666	0.000507	0.338347		0.4196	99.0	96.4	206
	3874	10.30*	4919.02415335	0.000756	0.338330		0.4187	97.1	96.5	205
	3280	12.35*	4919.02530716	0.000470	0.339674		0.4164	97.1	96.4	206
	4750	7.60*	4919.03708362	0.000829	0.337467		0.4196	100.0	96.5	206
	4402	2.45*	4919.03754388	0.001051	0.338603		0.4168	98.1	96.4	206
	2216	1.95*	4919.03831509	0.000450	0.339523		0.4192	50.5	49.8	206
	4698	2.95*	4919.05619732	0.001023	0.339728		0.4168	98.1	96.8	205
	4239	1.80*	4919.05909379	0.000654	0.337724		0.4173	99.0	96.2	206
	16383	0.05	4919.07988863	0.000255	0.337926		0.4191	97.1	94.2	206
	2718	0.55*	4919.09887396	0.001257	0.341413		0.4208	50.5	54.8	206
	4044	0.95*	4919.10387341	0.000342	0.338604		0.4169	97.1	96.6	205
	2956	0.05	4919.10445765	0.000456	0.338484		0.4163	99.0	96.6	206
	8912	0.20*	4919.12311186	0.001457	0.336513		0.4166	100.0	96.1	205
	4259	0.15	4919.12706371	0.001050	0.330145		0.4192	50.5	49.5	204
	5006	0.05	4919.14620223	0.000880	0.338121		0.4191	93.3	93.8	206
	9658	0.75*	4919.14879307	0.001846	0.332323		0.4152	98.1	96.3	205
	6642	0.60*	4919.15663690	0.000601	0.337815		0.4213	98.1	96.6	204
	3839	0.20*	4919.16085510	0.001798	0.330379		0.4138	99.0	96.2	206
	3024	0.25*	4919.16162258	0.000287	0.335135		0.4198	100.0	96.5	206
	2632	0.10*	4919.16264803	0.002048	0.326137		0.4157	97.1	96.4	206
	4901	0.05	4919.16797734	0.000320	0.333943		0.4189	97.1	96.4	206
	2529	0.10*	4919.17541968	0.000905	0.336405		0.4199	49.5	63.1	206
	3677	0.10*	4919.18685060	0.001853	0.328175		0.4172	98.1	96.6	206
	4095	0.15*	4919.18927498	0.001499	0.331345		0.4155	100.0	96.5	205
	1962	0.20*	4919.19282572	0.001262	0.333217		0.4162	99.0	96.2	206

N	Average iterations	Frequency %	Coulomb energy	Dipole moment	Coulomb angle	Tammes angle	Hole angle	% Energy diversity	% Angular diversity	Faces N_f
	3521	0.20*	4919.19429654	0.001220	0.332252		0.4186	98.1	96.4	206
	2124	0.15*	4919.19715296	0.001917	0.333341		0.4156	97.1	96.0	206
	4491	0.05	4919.19777251	0.001666	0.330154		0.4150	100.0	96.8	206
	2833	0.05	4919.19869612	0.001254	0.336963		0.4152	96.2	96.9	206
	3281	0.05	4919.20125556	0.001417	0.332326		0.4192	49.5	49.5	206
	4004	0.25*	4919.20167685	0.000890	0.335103		0.4188	98.1	96.6	206
	6984	0.10*	4919.20325721	0.001997	0.337011		0.4161	99.0	96.4	206
	3840	0.05	4919.20670267	0.000698	0.335856		0.4222	41.0	49.2	206
	2901	0.05	4919.22001554	0.001541	0.327261		0.4166	99.0	96.5	206
	3749	0.05	4919.22297231	0.000699	0.333374		0.4180	97.1	96.6	206
	12141	0.05	4919.22499337	0.000292	0.334094		0.4196	88.6	92.0	206
	5105	0.05	4919.22789000	0.001635	0.334827		0.4179	100.0	96.7	205
	6839	0.05	4919.24138309	0.001518	0.331023		0.4169	98.1	96.2	206
106	2997	32.40*	5015.98459571	0.000022	0.343101		0.4175	24.5	35.6	208
	2627	5.45*	5016.02907073	0.000263	0.333412		0.4164	96.2	96.2	208
	10952	24.95*	5016.03188558	0.000193	0.337740		0.4143	98.1	96.4	207
	3372	2.25*	5016.03997847	0	0.339986		0.4194	25.5	39.1	208
	2599	4.55*	5016.04404567	0.000528	0.333778		0.4160	100.0	96.4	208
	3209	0.45	5016.05148374	0.000313	0.339617		0.4158	55.7	51.2	207
	4968	5.45*	5016.05372399	0.000585	0.336943		0.4148	100.0	96.7	208
	4851	4.00*	5016.05739622	0.000488	0.336990		0.4176	60.4	79.8	208
	2628	1.20*	5016.06003956	0.000349	0.337665		0.4195	49.1	54.1	208
	6312	1.45*	5016.07238095	0.000674	0.332479		0.4161	50.0	49.7	208
	3470	0.45*	5016.07555956	0.000299	0.331744		0.4153	65.1	71.6	208
	4485	1.95*	5016.07687796	0.000420	0.331698		0.4173	98.1	96.4	207
	3885	2.50*	5016.08222957	0.001289	0.334367		0.4145	99.1	96.0	208
	6255	0.85*	5016.08328859	0.000991	0.339068		0.4150	73.6	83.1	208
	3981	0.25*	5016.08683971	0.000392	0.336611		0.4177	48.1	55.6	208
	7247	1.05*	5016.09129480	0.001014	0.335959		0.4166	100.0	96.2	207
	6096	1.90*	5016.09595341	0.000249	0.332510		0.4151	96.2	96.7	208
	3895	0.80*	5016.09732472	0.000868	0.335870		0.4170	97.2	96.1	208
	7804	0.50*	5016.09771716	0.001325	0.339396		0.4169	99.1	95.7	208
	3442	0.15*	5016.09812109	0.001338	0.338685		0.4171	98.1	96.4	208
	5184	2.35*	5016.09948825	0.001462	0.339661		0.4151	99.1	95.9	207
	2951	0.15	5016.09996656	0.000397	0.333024		0.4159	56.6	72.6	208
	5305	0.25*	5016.10952568	0.001362	0.332964		0.4167	97.2	97.1	208
	4110	0.25*	5016.11020446	0.001487	0.328548		0.4166	96.2	96.4	207
	4882	0.05	5016.11122491	0.001140	0.336392		0.4157	97.2	96.8	208
	5701	0.20*	5016.11256548	0.001232	0.331912		0.4150	98.1	96.7	208
	4422	0.95*	5016.11293661	0.000681	0.335466		0.4135	98.1	96.4	208
	2977	0.25*	5016.11667164	0.000996	0.332268		0.4145	99.1	96.1	208
	2387	0.10*	5016.12312979	0.000379	0.335243		0.4181	49.1	63.0	208
	2086	0.05	5016.12511371	0.000471	0.332627		0.4175	50.9	65.4	208
	4720	0.25*	5016.12937726	0.001574	0.330080		0.4153	98.1	96.0	208
	4646	0.10	5016.13428403	0.000382	0.333062		0.4171	84.9	84.4	208
	3083	0.25*	5016.14095562	0.002017	0.332506		0.4101	98.1	96.5	208
	3184	0.60*	5016.14460498	0.002464	0.328331		0.4112	99.1	96.4	208
	2980	0.05	5016.14845404	0.000150	0.337118		0.4170	49.1	49.8	208
	11392	0.05	5016.16609934	0.001934	0.334814		0.4126	97.2	96.4	208
	3611	0.10	5016.16730770	0.002037	0.332123		0.4085	98.1	96.4	208
	4686	0.05	5016.16837348	0.000332	0.332373		0.4152	99.1	96.4	208
	8827	0.05	5016.18438729	0.002968	0.329205		0.4135	99.1	96.4	207
	4004	0.10*	5016.18719575	0.002143	0.328745		0.4159	97.2	96.4	208
	14167	0.05	5016.19056300	0.001870	0.328538		0.4137	98.1	96.8	207
	3686	0.05	5016.19208897	0.000690	0.331646		0.4176	99.1	97.0	207
	4299	0.10*	5016.19602441	0.001489	0.330527		0.4126	98.1	96.4	207
	6259	0.05	5016.19721054	0.001927	0.329449		0.4141	95.3	97.0	208
	14737	0.05	5016.19746973	0.001256	0.334776		0.4130	91.5	94.7	206
	7877	0.05	5016.19825750	0.001862	0.329210		0.4135	97.2	96.0	207
	2427	0.05	5016.20760384	0.000499	0.331291		0.4183	49.1	49.9	208
	4805	0.05	5016.20994256	0.001107	0.329374		0.4128	99.1	96.4	208
	3669	0.05	5016.21724073	0.001073	0.331695		0.4125	98.1	96.8	208
	4699	0.05	5016.21800419	0.001003	0.333949		0.4136	98.1	96.4	208
	11792	0.05	5016.21929950	0.001644	0.327098		0.4140	100.0	96.4	208
	3374	0.05	5016.22112056	0.001616	0.329402		0.4126	96.2	96.4	207
	4237	0.05	5016.22124328	0.002021	0.327434		0.4137	98.1	95.8	208
	9289	0.05	5016.22278968	0.001946	0.328857		0.4142	98.1	96.1	208
	11011	0.05	5016.22618835	0.002488	0.332864		0.4141	80.2	89.7	206
	5031	0.10*	5016.22778255	0.002422	0.326437		0.4144	98.1	96.2	206
	6423	0.05	5016.22820174	0.000565	0.329783		0.4132	49.1	49.7	208
	3497	0.05	5016.23013185	0.000363	0.330685		0.4195	49.1	49.7	208
	4103	0.05	5016.24242732	0.000668	0.331721		0.4187	99.1	96.5	208
	4817	0.05	5016.30307750	0.001566	0.328122		0.4130	98.1	96.8	208
	8157	0.05	5016.32705914	0.001171	0.332073		0.4163	99.1	96.5	208

N	Average iterations	Frequency %	Coulomb energy	Dipole moment	Coulomb angle	Tammes angle	Hole angle	% Energy diversity	% Angular diversity	Faces N_f
107	3645	12.95*	5113.95354772	0.000064	0.337317		0.4155	50.5	49.5	210
	4563	8.80*	5113.97385010	0.000213	0.338380		0.4129	64.5	78.4	210
	5804	18.35*	5113.98085775	0.000220	0.337460		0.4154	49.5	49.6	210
	3397	1.15*	5113.98698336	0.000341	0.332633		0.4136	49.5	51.9	210
	4519	7.50*	5113.99261825	0.000811	0.333919		0.4144	99.1	96.2	210
	7598	16.40*	5114.00057902	0.000104	0.337051		0.4125	99.1	95.9	209
	3945	1.40*	5114.00134457	0.000326	0.335514		0.4121	50.5	64.3	210
	3065	3.10*	5114.00268858	0.001195	0.332411		0.4159	50.5	53.5	210
	5265	2.90*	5114.01281908	0.001369	0.333985		0.4137	95.3	96.5	209
	3716	2.00*	5114.01951688	0.001297	0.332430		0.4121	99.1	96.0	210
	6380	6.85*	5114.02098442	0.000817	0.333393		0.4164	99.1	96.2	209
	4322	2.85*	5114.02380411	0.001380	0.336739		0.4144	99.1	96.0	209
	2474	0.60*	5114.02683190	0.000267	0.331019		0.4136	50.5	49.6	210
	4003	1.55*	5114.02775097	0.001630	0.332551		0.4135	100.0	96.2	209
	8022	3.10*	5114.02844932	0.001632	0.329639		0.4125	94.4	96.0	208
	3271	0.15*	5114.03333531	0.001155	0.333825		0.4143	56.1	68.4	210
	16455	0.05	5114.03350687	0.000649	0.334338		0.4155	100.0	96.5	209
	4797	1.65*	5114.03406517	0.000540	0.334241		0.4122	99.1	96.1	209
	2125	0.90*	5114.03792376	0.000572	0.327212		0.4158	48.6	53.4	210
	4015	2.45*	5114.04005697	0.001811	0.330313		0.4130	100.0	96.0	210
	4512	0.70*	5114.04345820	0.001234	0.331829		0.4144	100.0	96.3	208
	3875	0.50*	5114.05197947	0.001333	0.336017		0.4145	98.1	96.5	210
	3902	0.25*	5114.05831959	0.002016	0.330082		0.4110	100.0	96.0	210
	4397	0.05	5114.06301739	0.002210	0.332700		0.4110	98.1	95.9	210
	4209	0.25*	5114.06764051	0.001190	0.334763		0.4152	96.3	96.0	209
	3623	0.15	5114.06999407	0.001784	0.334388		0.4143	98.1	96.4	210
	3348	0.45*	5114.07068401	0.000548	0.335563		0.4154	98.1	96.1	210
	5775	0.20*	5114.08279997	0.000553	0.333070		0.4147	98.1	96.3	210
	2395	0.25*	5114.08602239	0.000416	0.335598		0.4156	50.5	67.1	210
	2902	0.05	5114.09328058	0.000535	0.330003		0.4154	61.7	83.4	210
	6678	0.10	5114.09357220	0.001560	0.329440		0.4111	98.1	96.1	210
	2179	0.25*	5114.09869247	0.000228	0.332794		0.4136	99.1	96.1	210
	2757	0.15	5114.10110776	0.001261	0.334056		0.4151	49.5	49.7	210
	3281	0.10	5114.11514557	0.000317	0.330099		0.4152	99.1	96.6	210
	4771	0.10*	5114.11571613	0.000618	0.331224		0.4135	99.1	96.0	208
	5861	0.25*	5114.11577237	0.001645	0.334536		0.4138	98.1	96.8	210
	7484	0.05	5114.11647970	0.001003	0.331746		0.4154	99.1	96.8	210
	2645	0.25*	5114.11703802	0.000855	0.329999		0.4132	98.1	96.5	210
	2111	0.10*	5114.11962949	0.000313	0.331565		0.4175	34.6	48.7	210
	3530	0.15	5114.12171504	0.001247	0.330743		0.4136	57.0	69.2	209
	3606	0.05	5114.12234959	0.001297	0.332845		0.4149	64.5	82.8	210
	3462	0.20*	5114.12269861	0.000495	0.332245		0.4168	96.3	96.8	210
	3989	0.05	5114.14155186	0.001916	0.328905		0.4120	99.1	96.8	210
	5100	0.05	5114.14320671	0.001803	0.323100		0.4111	97.2	96.4	210
	8618	0.10*	5114.14567219	0.000800	0.330746		0.4154	98.1	96.5	208
	13181	0.05	5114.14676496	0.000923	0.328624		0.4092	56.1	50.0	209
	6087	0.10*	5114.15773096	0.000635	0.332440		0.4150	99.1	96.8	210
	5350	0.10	5114.16353781	0.000816	0.329894		0.4161	100.0	96.4	208
	4990	0.05	5114.18531290	0.000503	0.329894		0.4149	98.1	96.3	210
	4146	0.10	5114.21543765	0.001346	0.329707		0.4127	72.0	79.2	210
	4711	0.05	5114.25760386	0.002341	0.327919		0.4091	98.1	96.5	210
	3608	0.05	5114.33023734	0.001604	0.323896		0.4128	100.0	96.2	210
108	3661	30.40*	5212.81350783	0.000432	0.337313		0.4129	50.0	49.7	212
	6951	41.20*	5212.81758312	0.000436	0.336759		0.4121	98.1	95.6	212
	2481	0.10	5212.81762475	0.000486	0.337182		0.4121	97.2	95.9	211
	3439	0.75*	5212.81890852	0	0.340819		0.4147	16.7	39.4	212
	3702	5.85*	5212.82103064	0	0.340402		0.4123	40.7	42.2	212
	3386	8.55*	5212.87259090	0.000230	0.336660		0.4113	50.0	51.2	212
	1979	0.40*	5212.94775343	0	0.335144		0.4160	17.6	26.3	212
	2350	0.70*	5212.95468499	0.000352	0.336837		0.4118	32.4	38.5	212
	4050	2.60*	5212.96203966	0.000396	0.326349		0.4137	98.1	96.7	212
	3572	0.75*	5212.96252713	0.000113	0.334889		0.4144	50.0	70.0	212
	6248	0.65*	5212.96595200	0.001095	0.334867		0.4148	48.1	55.2	212
	3190	0.25*	5212.97031079	0.000543	0.335739		0.4149	49.1	64.7	212
	4952	0.65*	5212.97252200	0.001043	0.335022		0.4114	98.1	96.1	212
	8333	0.45*	5212.97645040	0.000748	0.329659		0.4111	97.2	96.5	211
	4485	1.00*	5212.97811922	0.000938	0.328288		0.4129	97.2	96.1	212
	5110	0.25*	5212.97878645	0.001098	0.336460		0.4116	50.0	66.8	212
	3052	0.75*	5212.98362560	0.000278	0.333295		0.4154	50.9	49.7	212
	9097	0.40*	5212.98609793	0.001111	0.334672		0.4114	98.1	96.4	209
	6320	0.30*	5212.98695079	0.000827	0.327804		0.4117	99.1	96.2	212
	6920	0.70*	5212.98857439	0.001051	0.330021		0.4123	99.1	95.9	212
	8180	0.45*	5212.99775092	0.001462	0.328015		0.4142	100.0	96.2	212

N	Average iterations	Frequency %	Coulomb energy	Dipole moment	Coulomb angle	Tammes angle	Hole angle	% Energy diversity	% Angular diversity	Faces N_f
	5471	0.20*	5213.00379554	0.000874	0.333383		0.4109	97.2	96.1	212
	3178	0.10	5213.00591463	0.000798	0.332016		0.4121	99.1	96.2	212
	5375	0.10	5213.00739612	0.001465	0.331220		0.4139	56.5	60.3	212
	5622	0.10	5213.01171880	0.001636	0.326744		0.4088	99.1	96.5	212
	3429	0.10	5213.01501059	0.001314	0.334884		0.4149	52.8	73.6	212
	4443	0.10*	5213.01541423	0.000158	0.325609		0.4121	59.3	75.0	212
	6962	0.55*	5213.01951579	0.001878	0.323555		0.4092	98.1	96.6	212
	4338	0.05	5213.01993758	0.002125	0.327208		0.4106	99.1	95.7	212
	7898	0.05	5213.02597286	0.001409	0.328084		0.4065	99.1	96.2	212
	2604	0.25*	5213.02687860	0.000706	0.328136		0.4127	100.0	96.3	212
	2856	0.05	5213.03439974	0.000551	0.331577		0.4135	63.9	82.6	212
	5244	0.10	5213.03628821	0.002347	0.326050		0.4062	99.1	96.0	212
	3240	0.15*	5213.04548392	0.002385	0.327668		0.4107	96.3	96.0	212
	3861	0.10*	5213.05063949	0.000983	0.327036		0.4137	97.2	95.7	210
	4009	0.10	5213.05096591	0.000159	0.325736		0.4120	50.0	49.7	212
	9144	0.05	5213.05122718	0.001912	0.332580		0.4138	50.0	54.2	212
	4683	0.20*	5213.05637717	0.002119	0.327328		0.4099	99.1	96.5	211
	3254	0.05	5213.06426316	0.001990	0.329165		0.4106	100.0	95.9	211
	4030	0.05	5213.06735088	0.001686	0.328932		0.4110	98.1	96.3	211
	6307	0.10*	5213.07431452	0	0.335165		0.4152	41.7	44.2	208
	4634	0.05	5213.07692279	0.000617	0.331603		0.4108	60.2	81.0	212
	8018	0.05	5213.07915908	0.001605	0.324787		0.4124	98.1	96.1	211
	5727	0.05	5213.08168306	0.001294	0.326452		0.4114	97.2	96.4	211
	6338	0.05	5213.08363709	0.001622	0.324108		0.4067	100.0	96.1	212
	4314	0.05	5213.12705126	0.001661	0.326574		0.4126	100.0	96.4	211
	3189	0.05	5213.15265756	0.001140	0.324681		0.4102	100.0	96.1	212
109	4800	45.50*	5312.73507994	0.000647	0.333401		0.4112	49.5	49.4	212
	2272	3.20*	5312.75464830	0.000247	0.337508		0.4127	50.5	61.2	214
	4050	3.60*	5312.77396021	0.000484	0.331108		0.4107	99.1	96.1	212
	5262	7.40*	5312.77508749	0.000056	0.334593		0.4095	57.8	65.4	214
	5075	1.30*	5312.77632903	0.000524	0.333564		0.4115	99.1	96.1	214
	2893	6.00*	5312.77865178	0.000524	0.331816		0.4119	95.4	96.1	213
	5852	3.20*	5312.79249977	0.001129	0.330098		0.4107	99.1	96.0	214
	4419	1.60*	5312.79715528	0.000062	0.330997		0.4117	99.1	96.1	214
	4662	1.40*	5312.79856954	0.001076	0.330162		0.4115	98.2	96.4	214
	4416	3.20*	5312.79985513	0.000895	0.331708		0.4107	99.1	96.5	214
	3451	3.80*	5312.80010079	0.000412	0.329964		0.4111	100.0	96.2	214
	13361	0.80	5312.80175514	0.000394	0.332414		0.4110	50.5	49.8	214
	4147	0.40	5312.80437836	0.000397	0.334958		0.4112	50.5	61.0	214
	3161	2.40*	5312.80648273	0.000629	0.329112		0.4112	99.1	96.7	214
	6775	0.30	5312.80971877	0.000106	0.331442		0.4093	70.6	83.4	214
	4992	0.20	5312.82165401	0.000167	0.330655		0.4117	50.5	49.4	214
	3811	1.90*	5312.82350767	0.000628	0.330873		0.4102	99.1	96.3	214
	4087	0.30	5312.82575643	0.000988	0.328546		0.4109	100.0	96.6	213
	2564	0.30*	5312.82582086	0.000885	0.336168		0.4131	33.9	43.9	214
	6412	0.20*	5312.82608204	0.001235	0.333333		0.4099	61.5	80.6	214
	8362	0.60*	5312.82835406	0.000833	0.333385		0.4109	83.5	88.6	214
	5370	0.40*	5312.82948191	0.000293	0.330721		0.4099	89.0	90.9	214
	3202	1.00*	5312.83631357	0.000486	0.331409		0.4103	98.2	96.0	214
	2929	0.40*	5312.83766190	0.000776	0.329988		0.4103	100.0	96.0	213
	3995	1.00*	5312.84056515	0.000108	0.332912		0.4126	50.5	72.2	214
	20000	0.30*	5312.84203408	0.001080	0.332610		0.4107	98.2	94.7	212
	5967	0.10	5312.84330444	0.000879	0.327770		0.4096	99.1	96.7	214
	4305	0.50*	5312.84536551	0.000439	0.333114		0.4109	100.0	96.0	214
	9002	0.70*	5312.84841327	0.000767	0.331461		0.4120	99.1	96.0	213
	4892	0.20	5312.85353630	0.000640	0.327640		0.4107	98.2	95.8	213
	6414	0.50*	5312.85358451	0.001019	0.325733		0.4093	100.0	96.7	214
	10183	0.10	5312.86062859	0.000288	0.328071		0.4114	98.2	96.3	214
	5292	0.80*	5312.86551212	0.000846	0.324200		0.4103	100.0	96.0	214
	5083	0.50*	5312.86634833	0.002036	0.325374		0.4060	99.1	96.0	214
	2869	0.10	5312.87443286	0.001662	0.321002		0.4113	99.1	96.3	214
	7426	0.20	5312.87619264	0.000242	0.328733		0.4072	100.0	96.4	214
	6910	0.80*	5312.88224787	0.000651	0.331100		0.4119	98.2	95.9	213
	3911	0.50*	5312.89066290	0.001968	0.326534		0.4082	99.1	96.5	214
	11181	0.20*	5312.89655576	0.001539	0.325941		0.4040	100.0	96.1	213
	12194	0.40	5312.90655106	0.001695	0.325138		0.4096	100.0	96.2	214
	9720	0.20*	5312.90689816	0.002307	0.320748		0.4044	99.1	96.0	214
	5266	0.20	5312.91325624	0.001631	0.322474		0.4083	97.2	96.1	213
	3468	0.10	5312.92460605	0.001494	0.324379		0.4076	97.2	96.3	214
	5906	0.10	5312.93676853	0.002367	0.325234		0.4076	50.5	49.5	214
	3479	0.10	5312.93983337	0.001353	0.324586		0.4098	100.0	96.4	214
	4062	0.20*	5312.94003492	0.001370	0.324357		0.4096	98.2	96.8	213
	4772	0.10	5312.94198517	0.001991	0.324873		0.4069	50.5	49.6	214
	3281	0.20	5312.94221283	0.001501	0.323345		0.4058	99.1	96.0	214

N	Average iterations	Frequency %	Coulomb energy	Dipole moment	Coulomb angle	Tammes angle	Hole angle	% Energy diversity	% Angular diversity	Faces N_f
	6146	0.10	5312.94365738	0.001400	0.327313		0.4047	49.5	49.3	214
	4195	0.10	5312.95862195	0.000633	0.325645		0.4105	98.2	96.7	214
	6815	0.10	5312.95956019	0.001653	0.326406		0.4058	99.1	95.8	214
	6813	0.10	5312.96329655	0.001730	0.329108		0.4091	99.1	96.4	212
	6107	0.10	5312.99107321	0.001512	0.326766		0.4095	99.1	96.5	212
	5307	0.10	5312.99439478	0.001535	0.325601		0.4037	100.0	96.4	214
	2998	0.10	5313.00685905	0.002025	0.323621		0.4076	99.1	96.2	214
110	3883	16.70*	5413.54929420	0.000012	0.339912		0.4106	9.1	14.6	216
	2794	17.20*	5413.56758230	0.000659	0.334684		0.4115	49.1	53.0	216
	3903	7.70*	5413.59868690	0.000112	0.333575		0.4104	50.9	72.1	216
	2368	7.10*	5413.61155043	0.000547	0.329299		0.4088	100.0	96.3	216
	2322	0.70*	5413.61560102	0	0.333605		0.4104	25.5	25.8	216
	7304	2.40*	5413.62179208	0.000783	0.329568		0.4083	97.3	96.0	216
	3392	3.80*	5413.62905287	0.000740	0.327782		0.4093	98.2	96.2	216
	3596	3.30*	5413.63183228	0.000145	0.328092		0.4092	49.1	65.7	216
	4016	6.30*	5413.63712239	0.001885	0.324388		0.4045	97.3	96.1	216
	2889	0.30*	5413.63881652	0.000152	0.331131		0.4093	54.5	71.0	216
	7111	3.70*	5413.63946560	0.000402	0.326498		0.4093	100.0	96.3	216
	6406	1.20*	5413.64231129	0.000347	0.331186		0.4089	95.5	96.2	215
	6329	3.20*	5413.64881901	0.000336	0.329843		0.4085	100.0	96.2	216
	5969	1.10*	5413.64907064	0.000397	0.328765		0.4110	50.0	49.6	216
	2700	0.40*	5413.64996374	0.000367	0.329199		0.4078	98.2	96.5	216
	4849	1.40*	5413.65048130	0.000540	0.328199		0.4088	99.1	96.5	215
	2900	2.60*	5413.65157268	0.000674	0.325866		0.4080	98.2	96.1	216
	5428	0.90*	5413.65238277	0.000368	0.327661		0.4075	97.3	96.5	216
	4014	0.80*	5413.65499335	0.000042	0.332282		0.4072	50.0	49.4	216
	4447	0.50*	5413.65724954	0.000376	0.328621		0.4065	100.0	95.7	216
	4247	0.40*	5413.65903088	0.000419	0.327953		0.4067	100.0	95.9	214
	6327	1.00*	5413.66012127	0.000435	0.327757		0.4085	100.0	95.9	214
	5988	2.10*	5413.66137962	0.000866	0.328801		0.4096	99.1	96.3	216
	2714	1.10*	5413.66159998	0.000272	0.330180		0.4086	98.2	95.9	216
	3682	0.50*	5413.66242354	0.000131	0.330004		0.4100	99.1	96.1	215
	5346	2.10*	5413.66350044	0.000474	0.329736		0.4082	99.1	96.2	215
	3986	3.20*	5413.66453234	0.001187	0.325963		0.4088	100.0	96.3	216
	4726	0.20	5413.66747167	0.000468	0.327746		0.4060	99.1	95.7	215
	4974	0.10	5413.66800668	0.000928	0.329748		0.4082	95.5	93.9	216
	3853	0.10	5413.66804358	0.000972	0.328783		0.4084	99.1	96.1	216
	14320	0.20	5413.66821468	0.000555	0.329686		0.4089	100.0	96.5	214
	6487	0.20	5413.67106097	0.000515	0.329227		0.4054	98.2	96.5	215
	9344	0.20*	5413.67225890	0.000741	0.327790		0.4082	96.4	96.6	215
	2919	0.50*	5413.67945550	0.000293	0.328632		0.4065	100.0	96.1	216
	7672	0.30	5413.68392561	0.000467	0.329572		0.4077	99.1	96.3	215
	4081	1.20*	5413.68395005	0.000991	0.331016		0.4085	99.1	96.1	216
	2916	0.30	5413.68431490	0.000542	0.327983		0.4089	98.2	95.7	216
	7199	0.70*	5413.68677176	0.000919	0.329573		0.4104	82.7	89.6	214
	11354	0.10	5413.68934422	0.000044	0.327158		0.4085	93.6	92.8	214
	5280	0.30	5413.69424335	0.000713	0.330287		0.4085	97.3	96.1	216
	13110	0.10	5413.70114673	0.000750	0.326517		0.4074	97.3	96.0	215
	5351	0.20	5413.70292809	0	0.332070		0.4096	25.5	25.4	216
	2422	0.20*	5413.70491131	0.000461	0.325462		0.4099	98.2	96.1	216
	3462	0.50*	5413.71547656	0.001773	0.322695		0.4044	97.3	96.3	216
	4859	0.10	5413.71762705	0.000510	0.327216		0.4078	57.3	73.7	216
	4486	0.10	5413.71919780	0.000259	0.327419		0.4076	79.1	85.0	214
	4136	0.90*	5413.72313200	0.000563	0.328159		0.4097	98.2	96.6	214
	2530	0.10	5413.72818239	0.002019	0.328043		0.4100	100.0	96.0	216
	3532	0.10	5413.73561358	0.002328	0.326255		0.4080	100.0	95.7	216
	6384	0.10	5413.73788035	0.000295	0.326627		0.4092	98.2	96.1	215
	12108	0.10	5413.74943853	0.000635	0.328731		0.4094	98.2	96.4	216
	9027	0.20	5413.74947669	0.001175	0.322815		0.4032	100.0	95.7	216
	3283	0.30*	5413.75213359	0.001228	0.323427		0.4100	100.0	96.6	216
	3914	0.10	5413.75692110	0.001260	0.319915		0.4059	97.3	96.7	216
	5163	0.10	5413.76229840	0.002057	0.324118		0.4016	97.3	96.0	215
	8233	0.10	5413.76322607	0.001136	0.326166		0.4040	95.5	96.2	216
	3977	0.10	5413.77236829	0.001364	0.324254		0.4097	98.2	96.2	216
	5643	0.10	5413.78197893	0.001673	0.323928		0.4041	99.1	96.3	216
111	5788	47.95*	5515.29321459	0	0.336066		0.4107	16.2	17.3	218
	5081	14.10*	5515.37822022	0.000378	0.332049		0.4088	50.5	54.6	218
	2979	0.90*	5515.39964901	0.000998	0.329809		0.4097	50.5	49.5	218
	2964	2.35*	5515.40973823	0.000628	0.331042		0.4082	98.2	96.0	218
	2523	0.10	5515.42133925	0	0.332921		0.4085	18.0	23.5	215
	4886	5.20*	5515.42556838	0.000645	0.325343		0.4065	96.4	96.1	218
	6086	3.35*	5515.42695246	0.000606	0.329950		0.4076	99.1	96.2	218
	7732	2.10*	5515.42750020	0.000248	0.330319		0.4074	59.5	77.8	218

N	Average iterations	Frequency %	Coulomb energy	Dipole moment	Coulomb angle	Tammes angle	Hole angle	% Energy diversity	% Angular diversity	Faces N_f
	2205	1.00*	5515.43691472	0.000666	0.329852		0.4070	95.5	95.5	218
	3585	2.45*	5515.43714361	0.001040	0.330017		0.4059	99.1	96.1	217
	6490	1.45*	5515.43879234	0.002212	0.327013		0.4043	94.6	95.8	218
	2729	0.25*	5515.43969989	0	0.331704		0.4101	16.2	27.0	218
	6357	1.30*	5515.44354698	0.001224	0.327275		0.4080	98.2	96.0	218
	4072	0.90*	5515.44744430	0.000347	0.329144		0.4077	53.2	74.4	218
	6392	1.10*	5515.45213408	0.000776	0.327113		0.4068	97.3	96.3	218
	7213	0.50*	5515.45333861	0.000317	0.328230		0.4059	99.1	96.0	215
	18992	2.70*	5515.45408736	0.000481	0.329046		0.4062	97.3	96.1	217
	3953	0.70*	5515.45472014	0.000870	0.330363		0.4067	99.1	96.0	217
	3313	0.15*	5515.45608011	0.000192	0.331467		0.4088	54.1	72.9	218
	5892	1.10*	5515.45771562	0.000024	0.332937		0.4112	80.2	89.9	215
	5502	0.10	5515.45884084	0.000437	0.330178		0.4073	61.3	76.9	218
	6263	0.95*	5515.46471350	0.000517	0.330129		0.4077	99.1	95.8	217
	4885	0.20*	5515.46721864	0.000055	0.330393		0.4058	50.5	49.4	218
	6650	0.30*	5515.46995593	0.000213	0.333295		0.4103	50.5	52.0	218
	4239	0.15*	5515.47277914	0.000122	0.332090		0.4057	58.6	73.2	218
	3971	0.25*	5515.47650805	0.000206	0.324838		0.4074	97.3	96.1	217
	4346	0.90*	5515.47784442	0.000331	0.325787		0.4092	98.2	96.1	217
	4325	0.85	5515.47803364	0.000367	0.326291		0.4080	56.8	50.3	218
	7784	0.45*	5515.47806647	0.000742	0.326214		0.4071	97.3	96.1	218
	4993	0.15*	5515.47920645	0.000596	0.327959		0.4062	98.2	96.1	218
	4101	0.75*	5515.47931863	0.001835	0.323489		0.4034	93.7	95.5	218
	3342	0.35*	5515.48021626	0.000125	0.326311		0.4079	50.5	65.1	218
	8738	0.30*	5515.48051908	0.000541	0.325241		0.4058	99.1	96.0	218
	5358	0.65*	5515.48439202	0.000529	0.325913		0.4069	99.1	96.8	218
	4124	0.05	5515.49412689	0.001576	0.323115		0.4011	98.2	96.3	218
	7601	0.05	5515.49885869	0.000344	0.329428		0.4079	99.1	96.6	218
	5253	0.70*	5515.50969953	0.001109	0.323321		0.4080	99.1	96.2	216
	3604	0.20*	5515.51281749	0.000073	0.329731		0.4067	50.5	49.6	218
	4363	0.15	5515.51619137	0.000191	0.325759		0.4059	97.3	96.3	217
	6225	0.25*	5515.52023040	0.001617	0.324555		0.4016	98.2	96.2	218
	3995	0.10	5515.52288453	0.000771	0.326751		0.4068	99.1	96.2	218
	4127	0.05	5515.53088257	0.001108	0.325726		0.4046	99.1	96.0	218
	3678	0.10	5515.53848192	0.000444	0.322840		0.4058	100.0	95.8	218
	7577	0.10	5515.54254505	0.000663	0.325932		0.4090	97.3	96.4	218
	7690	0.15	5515.54940105	0.001348	0.329487		0.4085	50.5	49.5	218
	5260	0.15*	5515.55299866	0.000515	0.322224		0.4064	100.0	96.2	217
	6676	0.35*	5515.55307500	0.000762	0.328647		0.4080	97.3	96.1	218
	4062	0.10	5515.56968339	0.001502	0.318141		0.4069	100.0	95.7	218
	4482	0.10*	5515.57176579	0.000889	0.325678		0.4070	100.0	96.2	217
	4643	0.05	5515.59452162	0.001952	0.318722		0.3999	99.1	95.9	217
	4238	0.05	5515.65828199	0.002024	0.320332		0.4046	98.2	96.7	217
112	3352	43.60*	5618.04488233	0	0.337747		0.4078	10.7	15.3	220
	4197	18.40*	5618.05824444	0	0.335550		0.4095	8.9	12.8	220
	6522	1.70	5618.16281873	0.001122	0.327323		0.4038	56.3	51.3	218
	8122	0.40*	5618.17022822	0.000033	0.325734		0.4037	76.8	87.5	220
	5483	6.20*	5618.17975389	0.001003	0.328821		0.4039	96.4	96.1	220
	2741	1.00*	5618.18139715	0.000508	0.319826		0.4080	49.1	49.7	220
	3771	2.40*	5618.18692576	0.000391	0.328264		0.4046	97.3	96.0	220
	3849	3.40*	5618.19123408	0.000376	0.324163		0.4056	99.1	96.0	219
	3606	1.50*	5618.19340191	0.000331	0.327719		0.4071	97.3	96.0	220
	2737	0.50*	5618.19617462	0	0.330723		0.4089	24.1	37.0	220
	3729	0.50	5618.19669597	0.000908	0.329067		0.4058	74.1	79.7	218
	3031	1.40*	5618.19682071	0.000594	0.326403		0.4066	97.3	96.3	220
	6419	0.70*	5618.19738268	0.000257	0.326579		0.4043	98.2	96.0	219
	5227	1.40*	5618.19784373	0.000363	0.329961		0.4043	98.2	95.8	219
	6874	2.10*	5618.19876503	0.001005	0.327286		0.4084	99.1	96.0	219
	10697	0.60*	5618.19996075	0.000532	0.325018		0.4069	98.2	96.4	219
	6892	0.80*	5618.20008193	0.000528	0.324998		0.4066	99.1	96.0	219
	5447	0.40*	5618.20403595	0.000831	0.327900		0.4046	97.3	96.3	220
	5129	0.80*	5618.20575583	0.000116	0.329203		0.4054	96.4	95.7	219
	7540	0.20	5618.20591159	0.000800	0.328497		0.4044	99.1	95.9	220
	3502	1.50*	5618.20836091	0.000181	0.327292		0.4043	98.2	96.0	220
	6680	0.40*	5618.20886000	0.000667	0.323681		0.4070	98.2	96.2	220
	5141	1.00*	5618.20936383	0.000675	0.327058		0.4055	95.5	96.2	220
	4532	0.80*	5618.21058012	0.000213	0.326902		0.4055	100.0	96.1	220
	6421	0.30	5618.22022487	0.000069	0.325049		0.4086	82.1	86.3	220
	5133	1.30*	5618.23448912	0.001165	0.321334		0.4066	97.3	96.4	220
	3418	0.50*	5618.24074945	0.000495	0.322422		0.4053	99.1	96.4	220
	5871	0.10	5618.24899109	0.000678	0.324842		0.4070	97.3	96.7	220
	2495	0.50*	5618.24925481	0.000256	0.327010		0.4065	98.2	96.0	220
	4381	0.60*	5618.25368022	0.001349	0.322400		0.4040	96.4	95.9	219
	11615	0.30	5618.25621803	0.001191	0.316907		0.4049	81.3	88.1	219

N	Average iterations	Frequency %	Coulomb energy	Dipole moment	Coulomb angle	Tammes angle	Hole angle	% Energy diversity	% Angular diversity	Faces N_f
	7119	0.30*	5618.25646911	0.000242	0.324503		0.4033	99.1	96.3	220
	2887	0.30	5618.25870781	0.001925	0.324573		0.4022	98.2	96.1	220
	3491	0.10	5618.27042281	0.001689	0.320620		0.4041	97.3	96.3	220
	11459	0.20	5618.27104971	0.002336	0.322996		0.3987	98.2	95.9	220
	5254	0.10	5618.27405701	0.001196	0.325236		0.4048	99.1	96.0	219
	4306	0.10	5618.27590295	0.000480	0.322857		0.4060	98.2	96.4	220
	5897	0.10	5618.27669984	0.000342	0.324160		0.4041	96.4	95.9	220
	3449	0.40*	5618.27802049	0.000681	0.325544		0.4059	98.2	95.8	219
	5045	0.10	5618.28223927	0.000720	0.328029		0.4060	49.1	49.6	220
	5368	0.20	5618.28245930	0.001964	0.325069		0.3981	98.2	96.2	219
	8640	0.20*	5618.28263752	0.000412	0.325306		0.4072	96.4	96.0	219
	3632	0.30*	5618.28434640	0.001703	0.322639		0.4011	100.0	96.1	220
	12996	0.10	5618.28804357	0.001351	0.324640		0.4071	98.2	95.8	219
	9407	0.10	5618.29354208	0.002647	0.318589		0.4028	97.3	95.9	220
	5354	0.30	5618.29659227	0.001327	0.324433		0.4024	98.2	95.8	220
	3864	0.10	5618.30033892	0.000400	0.322764		0.4054	51.8	61.0	218
	3396	0.20	5618.30235974	0.000911	0.324960		0.4058	100.0	96.3	219
	13423	0.10	5618.30367493	0.001183	0.317356		0.4028	98.2	96.4	220
	3425	0.20*	5618.30931247	0.001975	0.323746		0.4019	97.3	95.9	220
	7187	0.10	5618.32187570	0.001985	0.319207		0.4001	100.0	96.0	220
	4210	0.10	5618.34027361	0.000826	0.321902		0.4069	97.3	95.7	220
	3095	0.10	5618.34424060	0.000384	0.323462		0.4069	50.0	63.9	220
	5022	0.10	5618.34604924	0.001145	0.322203		0.4050	98.2	96.1	220
	5121	0.10	5618.34947946	0.000791	0.319789		0.4053	97.3	96.6	219
	8154	0.10	5618.36426242	0.001736	0.314963		0.3995	99.1	96.3	220
	18663	0.20*	5618.37527701	0.000542	0.324870		0.4073	91.1	93.8	217
	4829	0.20	5618.39446210	0.001252	0.323779		0.4042	97.3	96.0	220
	4277	0.10	5618.41155067	0.002074	0.321258		0.4014	98.2	96.1	220
	5520	0.10	5618.41948131	0.002252	0.317741		0.4041	99.1	96.3	219

References

1. J.J. Thomson, Phil. Mag 44 (ser. 5) (1897), 293-316.
2. J.J. Thomson, Phil. Mag. 7 (ser. 6) (1904), 237-265.
3. J.J. Thomson, "The Electron in Chemistry," Franklin Institute, Philadelphia, 1923.
4. D.S. Bethune, R.D. Johnson, J.R. Salem, M.S. de Vries, and C.S. Yannoni, Nature 366, No. 6451 (1993), 123-128.
5. S.C. Sevov and J.D. Corbett, Science 262, No. 5135 (1993), 880-883.
6. H.D.I. Abarbanel, The Inverse r-Squared Force: An Introduction to its Symmetries, in "Studies in Mathematical Physics - Essays in Honor of Valentine Bargmann," (E.H. Lieb, B. Simon, and A.S. Wightman, Eds.), pp. 3-18, Princeton Univ. Press, Princeton, 1976.
7. N. Bohr, Zeit. f. Physik 9 (1922), 1-67.
8. W. Pauli, Zeit. f. Physik 31 (1925), 765-783.
9. H.W. Kroto, J.R. Heath, S.C. O'Brien, R.F. Curl, and R.E. Smalley, Nature 318, (1985), 162-164.
10. L. Föppl, J. Reine Angew. Math. 141 (1912), 251-302.
11. J. Leech, Math. Gazette 41 (1957), 81-90.
12. P.M.L. Tammes, Recueil des Travaux Botaniques Néerlandais 27 (1930), 1-84.
13. L. Fejes-Toth, "Regular Figures," Macmillan, New York, 1964.
14. H.S.M. Coxeter, Trans. N.Y. Acad. Sci. 24 (Series II) (1961-1962), 320-331.
15. D.E. Lazić, V. Šenk, V. Šeškar, Bull. Appl. Math. Techn. U. Budapest 479, 1986.
16. B. Bergersen, D. Boal, and P. Palffy-Muhoray, J. Physics A (in press, 1993).

17. N.W. Johnson, Can. J. Math. 18 (1966), 169-200.

18. V.A. Zalgaller, "Convex Polyhedra with Regular Faces," Seminars in Mathematics, V.A. Steklov Mathematical Institute, Lenigrad, Vol. 2, Consultants Bureau, New York, 1969.

19. N.I. Fisher, T. Lewis, and B.J.J. Embleton, "Statistical Analysis of Spherical Data," Cambridge U. Press, Cambridge, 1987.

20. G.S. Watson, "Statistics on Spheres," Wiley-Interscience, New York, 1983.

21. E. Wigner, Zeit. f. Physik 43 (1927), 624-652.

22. H. Cohn, Math. Tables and Other Aids to Comp. 10 (1956), 117-120.

23. D. Gavelek and T. Erber, J. Comput. Phys. 101 (1992), 25-50.

24. D.K. Kondepudi and G.W. Nelson, Nature 314, Nº 6010 (1985), 438-441.

25. V.A. Avetisov, V.I. Goldanskii, and V.V. Kuz'min, Phys. Today 44 (1991), 33-41.

26. T. Erber, H.G. Latal, and R.P. Olenick, J. Appl. Phys. 52 (1981) 1944-1946.

27. A. Beck, Amer. Math. Monthly 97 (1990), 289-294.

28. H.T. Croft, K.J. Falconer, and R.K. Guy, "Unsolved Problems in Geometry," Springer, New York, 1991.

29. R.M. Robinson, Math. Ann. 179 (1969), 296-318.

30. D.A. Kottwitz, Acta Cryst. A47 (1991), 158-165.

31. R.F. Brown and J.H. White, Indiana Univ. Math. J. 30 (1981), 501-512.

32. L. Föppl, "Stabile Anordnungen Von Elektronen Im Atom," Göttinger Dissertation, G. Reimer, Berlin, 1912.

33. R.W. Hasse and J.P. Schiffer, Ann. Phys. (N.Y.) 203 (1990), 419-448.

34. S.L. Gilbert, J.J. Bollinger, and D.J. Wineland, Phys. Rev. Lett. 60 (1988), 2022-2025.

35. H.S. Chan and K.A. Dill, Phys. Today 46, No. 2 (1993), 24-32.

36. J.D. Honeycutt and D. Thirumalai, Biopolymers 32 (1992), 695-709.

37. P.L. Privalov, Adv. Prot. Chem. 35 (1982), 1-104.

38. T. Erber and G.M. Hockney, Am. Math. Soc. Abstr. 6 (1985), 487.

39. T. Erber and G.M. Hockney, J. Physics A 24 (1991), L 1369-L 1377.

40. L. Glasser and A.G. Every, J. Physics A 25 (1992), 2473-2482.

41. J.R. Edmundson, Acta Cryst. A 48 (1992), 60-69.

42. J.R. Edmundson, Acta Cryst. A 49 (1993), 648-654.

43. T.A. Claxton and G.C. Benson, Can. J. Chem. 44 (1966), 157-163.

44. T.W. Melnyk, O. Knop, and W.R. Smith, Can. J. Chem. 55 (1977), 1745-1761.

45. J.H. Conway and N.J.A. Sloane, "Sphere Packings, Lattices and Groups," 2nd ed., Springer, New York, 1993.

46. G.S. Ezra and R.S. Berry, Phys. Rev. A 25 (1982), 1513-1527.

47. A. Martin, J.-M. Richard, and T.T. Wu, "Stability of Three Unit-Charge Systems," TH-6227, CERN, 1991.

48. E.H. Lieb and H.-T. Yau, Phys. Rev. Lett. 61 (1988), 1695-1697.

49. F. Pacella, Arch. Rat. Mech. Anal. 97 (1987), 59-74.

50. C.K. McCord, "Planar Central Configuration Estimates in the N-Body Problem," (preprint, 1994).

51. J. Merkel, private communication, 1994.

52. E.F. Brickell and A.M. Odlyzko, Cryptanalysis: A Survey of Recent Results, in "Contemporary Cryptology," (G.J. Simmons, Ed.), pp.501-540, IEEE Press, Piscataway, N.J., 1991.

53. T.M. Apostol, "Mathematical Analysis," Addison-Wesley, Reading, MA, 1957.

54. R. Bellman, "Introduction to Matrix Analysis," McGraw-Hill, New York, 1960.

55. P. Sjögren, Arkiv Mat. 11 (1973), 147-151.

56. J. Korevaar, "Problems of Equilibrium Points on the Sphere and Electrostatic Fields," U. Amsterdam, Report 76-03, 1975.

57. T. Erber, H.G. Latal, and B.N. Harmon, "Advances in Chemical Physics," (S.Rice and I. Prigogine, Eds.), vol. 20, pp. 71-134, J. Wiley, New York, 1971.

58. T. Erber, G.R. Marousek, and G.K. Forsberg, Acta Phys. Austriaca 30 (1969), 271-294.

59. J. Vollmer and W. Breymann, Phys. Rev. B 47, No. 18 (1993), 11767-11773.

60. W. Feller, "An Introduction to Probability Theory and Its Applications," Vol. II, Wiley, New York, 1971.

61. G. Benedek, T.P. Martin, and G. Pachioni (Eds.), "Elemental and Molecular Clusters," Springer Series in Material Sciences, vol. VI, Springer, Berlin, 1988.

62. B.G. Englert, "Semiclassical Theory of Atoms," Lecture Notes in Physics 300, Springer, Berlin, 1988.

63. H. Buchholz, "Elektrische und Magnetische Potentialfelder," Springer, Berlin, 1957.

64. D.R. Gavelek, unpublished (1984).

65. C.E. Porter, "Statistical Theories of Spectra: Fluctuations," Academic, New York, 1965.

66. P. Pearce and S. Pearce, "Polyhedra Primer," Van Nostrand Reinhold, New York, 1978.

67. R.E. Williams, "Handbook of Structure Part I: Polyhedra and Spheres," Res. Commun. 75, Douglas Advanced Research Laboratories, 1968.

68. N.W. Johnson, Private communication.

69. E.C. Catalan, J. École Impériale Polytechnique, 24 (1865), 1-71.

70. J.R. Heath, Spectroscopy 5 (1990), 36-43.

71. M. Hamermesh, "Group Theory and Its Application to Physical Problems," Addison-Wesley, Reading, MA, 1962.

72. H.S.M. Coxeter, "Introduction to Geometry," J. Wiley, New York, 1961.

73. K. Mislow, "Introduction to Stereochemistry," W.A. Benjamin, New York, 1965.

74. F.J. Almgren Jr. and E. H. Lieb, Annals of Math. 128 (1988), 483-530.

75. T. Erber and A. Sklar, Macroscopic Irreversibility as a Manifestation of Micro-Instabilities, in "Modern Developments in Thermodynamics," (B. Gal-Or, Ed.), pp. 281-301, J. Wiley, New York, and Israel Universities Press, Jerusalem, 1974.

76. K. Schütte and B.L. van der Waerden, Math. Ann. 123 (1951), 96-124.

77. "Contemporary Cryptology," (G.J. Simmons, Ed.), IEEE Press, Piscataway, N.J., 1992.

78. J. Radon, Sitz. K. Akad. Wiss. Wien, Math. - Naturw. Kl. II a, 122, No. 7 (1913), 1295 - 1438.

79. T. Tarnai [private communication, 1991].

80. K. Bezdek, R. Connelly, and G. Kertesz, On the Average Number of Neighbors in a

Spherical Packing of Congruent Circles, in "Intuitive Geometry," (K. Böröczky and G. Fejes Toth, Eds.), pp. 37-52, Colloq. Math. Soc. Janos Bolyai, 48, North Holland, Amsterdam, 1987.

81. L.J. Campbell and R. Ziff, A Catalog of Two-Dimensional Vortex Patterns, LA-7384, Los Alamos, (unpublished), 1979.

82. E. Madelung, Phys. Zeitschr. 19 (1918), 524-532.

83. C. Kittel, "Introduction to Solid State Physics," Wiley, New York, 1961.

84. R.O. Jones and O. Gunnarsson, Rev. Mod. Phys. 61 (1989), 689-746.

85. Y.Y. Ye, C.T. Chan, K.M. Ho, and B.N. Harmon, Int. Jr. Supercomputer Appl. 4 (1990), 111-121.

86. G.A. Williams and R.E. Packard, Phys. Rev. Lett. 33 (1974), 280-283.

87. A.M. Mayer, Scientific American Supplement, V, No. 129, (1878), 2045-2047.

88. C. Lanczos, "The Variational Principles of Mechanics," U. Toronto Press, Toronto, 1966.

89. K.F. Sundman, Acta Math. 36 (1913), 105-179.

90. Z. Xia, Annals of Math. 135 (1992), 411-468.

91. R.C. Howison and C.K. McCord, "Equilibria of Spherical Charge Distributions" (preprint, 1994).

92. H. Frauenfelder and P.G. Wolynes, Phys. Today 47, No. 2 (1994), 58-64.

93. R.E. Davies and P.J. Freyd, J. Chem. Education 66, No. 4 (1989), 278-281.

94. F.H. Stillinger and T.A. Weber, Science 225, No. 4666 (1984), 983-989.

95. E.A. Rakhmanov, E.B. Saff, and Y.M. Zhou, Math. Res. Lett. 1 (1994), 647-662.

96. A. Edelman and E. Kostlan, Bull. Am. Math. Soc. 32, No. 1 (1995), 1-37.

97. V. Pareto, "Manuale di Economia Politica," Societa Editrice Libraria, Milan, 1909.

98. E.L. Altschuler, T.J. Williams, E.R. Ratner, F. Dowla, and F. Wooten, Phys. Rev. Lett. 72, No. 17 (1994), 2671-2674.

99. T. Erber and G.M. Hockney, Phys. Rev. Lett. 74, No. 8 (1995), 1482.

100. E.L. Altschuler, T.J. Williams, E.R. Ratner, F. Dowla, and F. Wooten, Phys. Rev. Lett. 74, No. 8 (1995), 1483.

101. J. Milnor, "Morse Theory," Annals of Math. Studies 51, Princeton U. Press, Princeton, 1963.

102. J. Mawhin and M. Willem, "Critical Point Theory and Hamiltonian Systems," Springer, New York, 1989.

103. P. Painlevé, Compt. Rend. 138 (1904), 1555 - 1557.

104. A. Wintner, "The Analytical Foundations of Celestial Mechanics," Princeton U. Press, Princeton, 1941.

105. G.E. Forsythe, M.A. Malcolm, and C.B. Moler, "Computer Methods for Mathematical Computations," Prentice-Hall, Englewood Cliffs, N.J., 1977.

106. R.L. Burden and J.D. Fares, "Numerical Analysis," P.W.S. Kent, Boston, 1989.

Figure Captions

Fig. 1(a). Charge configuration for N = 16 (metastable state). This is a perspective view showing the charges arranged in a highly symmetric pattern of four rings with four charges in each ring. These rings are symmetrically positioned with respect to the equator at 11.342° North & South latitude, and 51.684° North & South latitude. The auxiliary lines show the associated Coulomb polyhedron: this figure has 26 faces and 40 edges.

Fig. 1(b). Charge configuration for N = 16 (metastable state). This is a plan view of the four ring structure looking down from the North pole. The squares, and open and filled circles indicate corresponding points on Fig. 1(a) and Fig. 1(b).

Fig. 1(c). Charge configuration for N = 16 (ground state). This is another perspective view similar to that shown in Fig. 1(a). The ground state is less symmetric than the metastable state. In fact, as shown in Fig. 1(d), this configuration can exist in two enantiomorphic variants.

Fig. 1(d). Charge configuration for N = 16 (ground state). The relative orientation of Fig. 1(c) and Fig. 1(d) can be inferred by comparing the positions of the filled and open circles on the two diagrams. The enantiomorphic character of this configuration can be verified by copying it on a transparency; flipping the transparency over; and checking that the obverse figure cannot be rotated into coincidence with the original diagram.

Fig. 2. Variation of the number of states with the number of particles. The $M_C(N)$ points are plots of the data given in Table I. The fitted line represents the exponential function in Eqs. (3.2b and c). $M^m(N)$ shows the corresponding data for magnetic dipole arrays, cf. (3.3) and reference [57, 58].

Fig. 3. Energies of the surface Coulomb states. The dashed $\langle E^{Ran}(N) \rangle$ curve represents the average energies of randomly chosen initial states (cf. Table II). The crosses show the minimum energies found by computer searches (cf. Table VIII). The semi-empirical formula (3.8) matches the data points more accurately than can be shown on this graph.

Fig. 4. Density of states. The histogram combines level statistics for N = 111 and 112 compiled from Table VIII. In both cases, the zero of energy is taken to be the ground state energy.

Fig. 5. Density of states weighted by the probability of occurrence. This is a semi-logarithmic plot that shows the qualitative shift in the histogram of Fig. 4 when the probabilities of occurrence are taken into account.

Fig. 6. Total and individual Coulomb energy differences. The graph shows a scatter plot of the ratio R(N) defined in Eq. (3.15) for all values of N in the range $16 \leq N \leq 112$. The only values of N for which the average energy differences *within* configurations are smaller than the average total energy differences *between* configurations are N = 32, 51, 77, *and* 78. The two smallest values of R --- R(32) = 0.26 and R(78) = 0.51 --- are highlighted by the arrows. The maximum value is R(45) = 305.

Fig. 7. Scatter plot of the energy diversity, Eq. (3.16). Large values of this ratio are correlated with irregular charge configurations. The bands in the vicinity of D_e ~ 100% *and* 50% indicate a marked statistical preference for these values.

Fig. 8. Distribution of dipole moments, Eq. (1.2a). This is a graphical summary of all the dipole moments listed in column 5 of Table VIII.

Fig. 9. Scatter plot of the angular diversity, Eq. (4.3). Large values of this ratio indicate irregular charge configurations; small values are correlated with symmetric polyhedra, cf. Table V. The bands at 50% and 95% are the result of statistical preferences analogous to those in Fig. 7.

Fig. 10. Correlation of angular diversity and energy diversity. Symmetric configurations cluster near the origin, D_e *and* $D_a < 20\%$; irregular configurations near $D_e \approx D_a \sim 100\%$. There is also a statistical cumulation around $D_e \approx D_a \sim 50\%$. The plot indicates that D_e *and* D_a always yield consistent measures of regularity.

Fig. 11. Surface Coulomb configuration for N = 19. The symmetry of this arrangement is partly illusory. The 50 edges are composed of 10 groups of 4 congruent edges and 5 groups of 2 congruent edges. The polygonal faces are too irregular to fit into the standard scheme of polyhedra [17, 18].

Fig. 12. Comparison of Coulomb and Tammes angles. $\Theta_T(N)$ is the optimum angular diameter of a spherical cap in the Tammes packing problem. $\Theta_C(N)$ is the minimum angular separation between adjacent charges in the spherical Coulomb problem. The graph shows the relative difference between the two sets of angles, Eq. (4.13).

Fig. 13. Positions of N points in a unit square arranged so that the minimum distance between any pair is as large as possible. The configurations for $N \leq 9$ are known to be optimal. This diagram is reproduced from reference [28] with permission of Springer Verlag.

Fig. 14(a) & (b). Energy landscape of a gradient system. The plan view in (a) shows three minima and a mountain range. Some of the corresponding heights are indicated in the elevation (b). Paths 1 and 2 are two possible gradient routes linking E_m *and* E_{m+1}. If $E(SP^{(1)}) < E(SP^{(2)})$, then path 1 is the 'minimax' route [102]. The valley bottom at E_m is a locally stable minimum if we omit path 4. But if path 4 is joined to E_{m-1} through a narrow exit, then E_m is numerically stable only relative to a coarse search grid. The positions of the saddle points $SP^{(1)}$, ... , $SP^{(5)}$, indicate the extent of the capture basin surrounding E_m.

Fig. 14(c).Topography of the energy surface in the vicinity of a Hessian singularity. This rippled stalagmite is a schematic representation of the cumulation of local maxima and/or minima around a non-isolated Hessian singularity.

Fig. 14(d).Topography of the energy surface in the vicinity of Hessian singularity. The fluted landscape surrounds valleys whose minima are networks of lines rather than isolated points. In higher dimensions these lines correspond to areas, i.e. 'flat' valley bottoms.

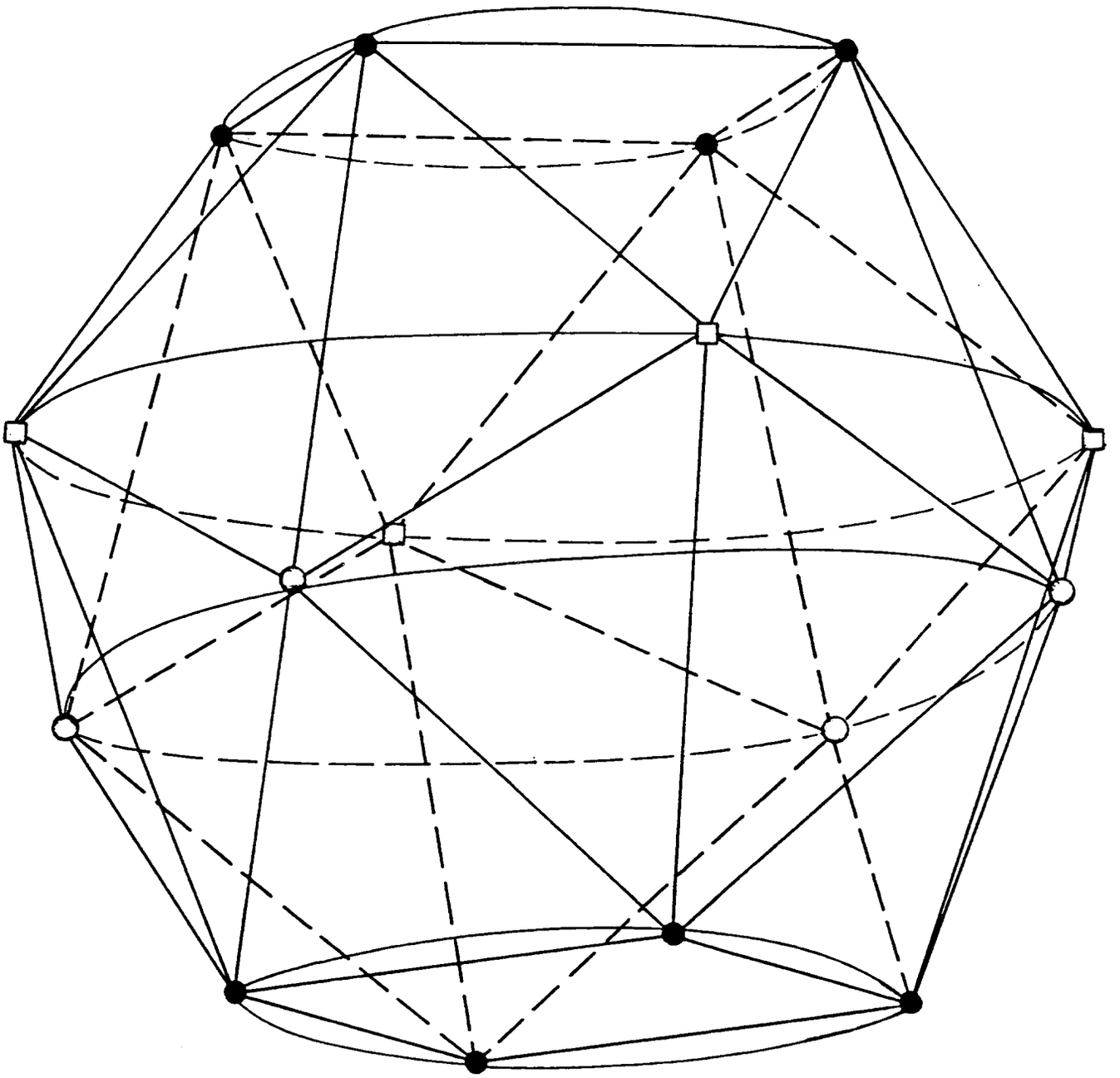

Figure 1 (a)

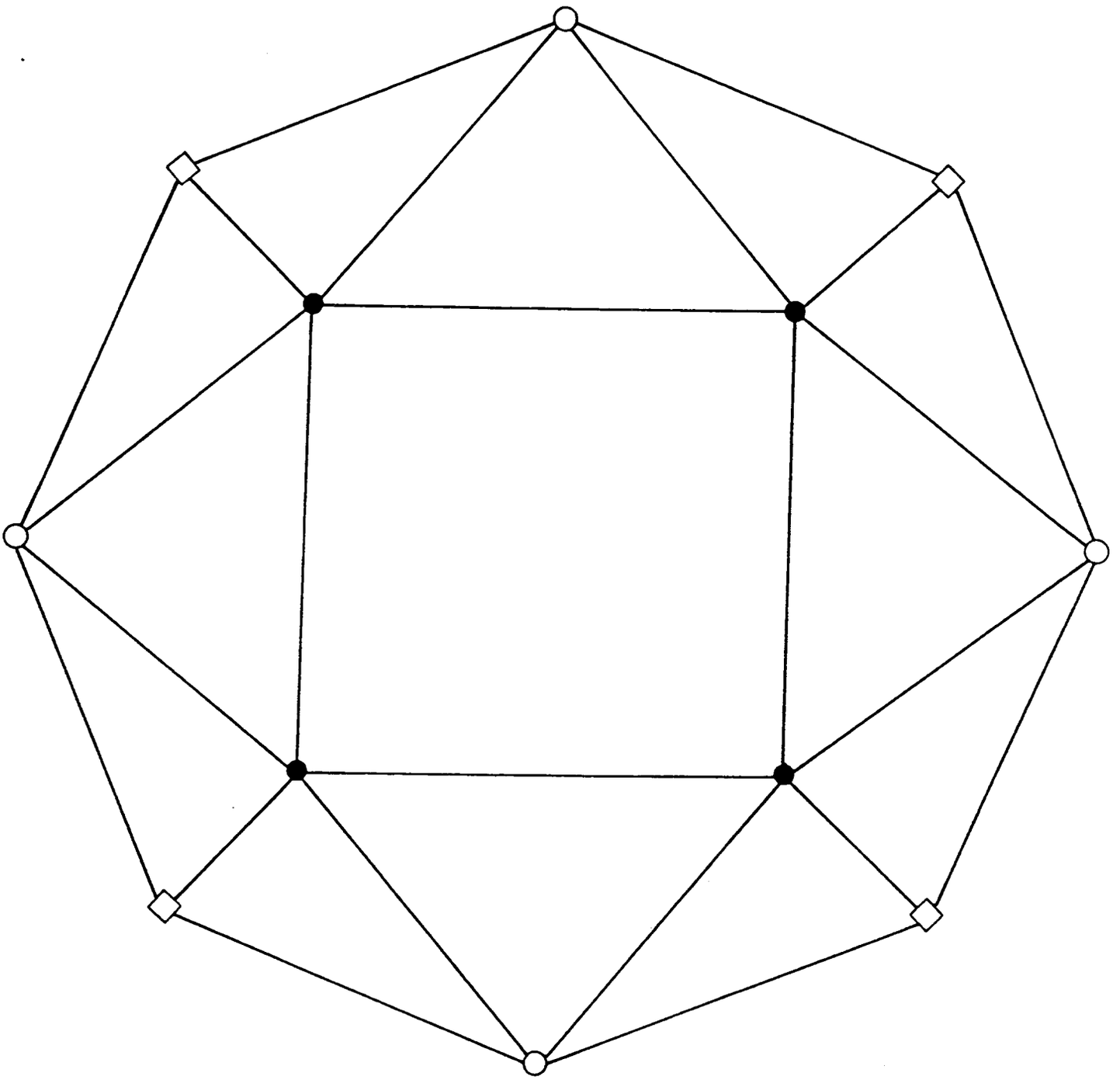

Figure 1 (b)

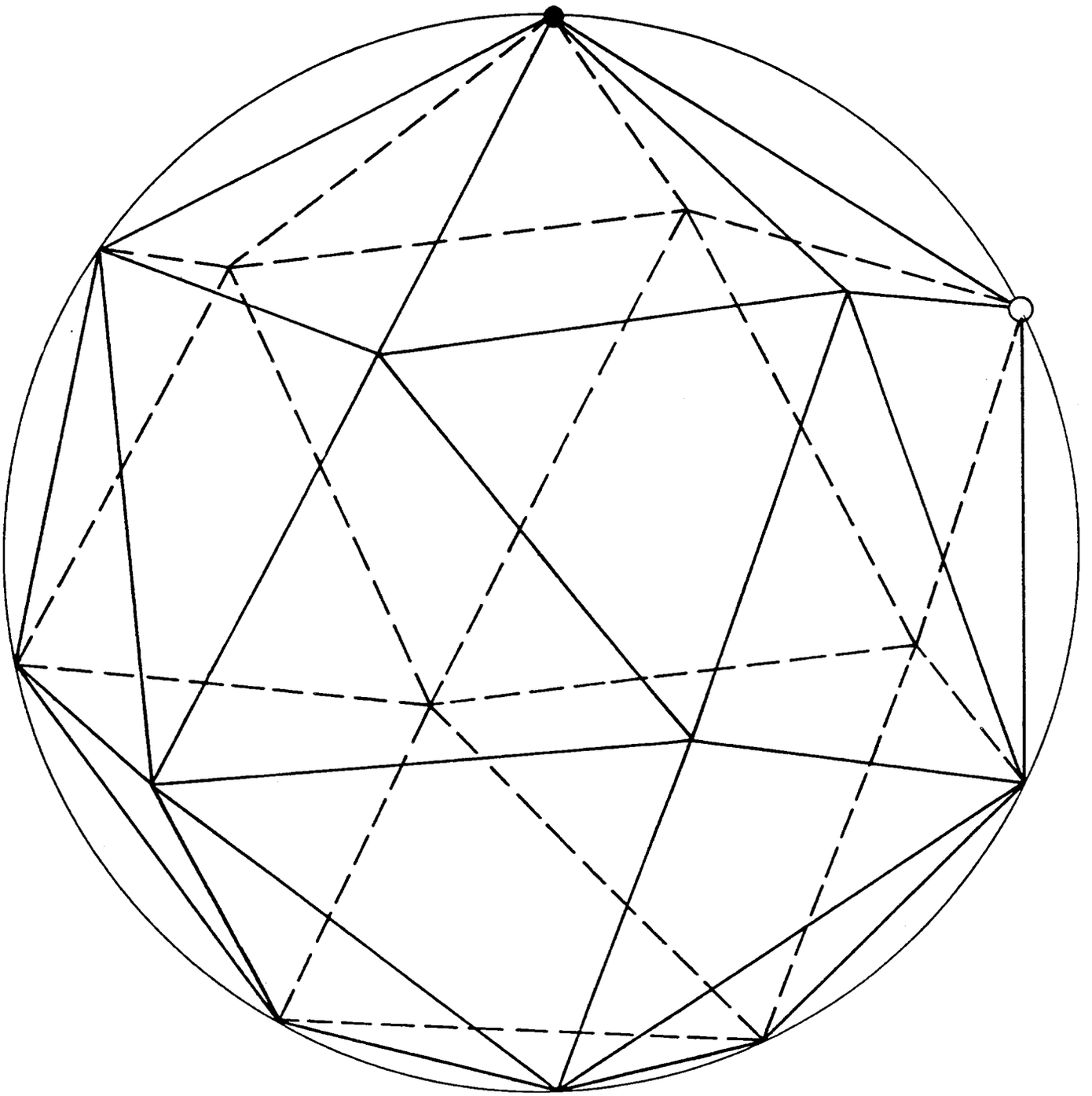

Figure 1 (c)

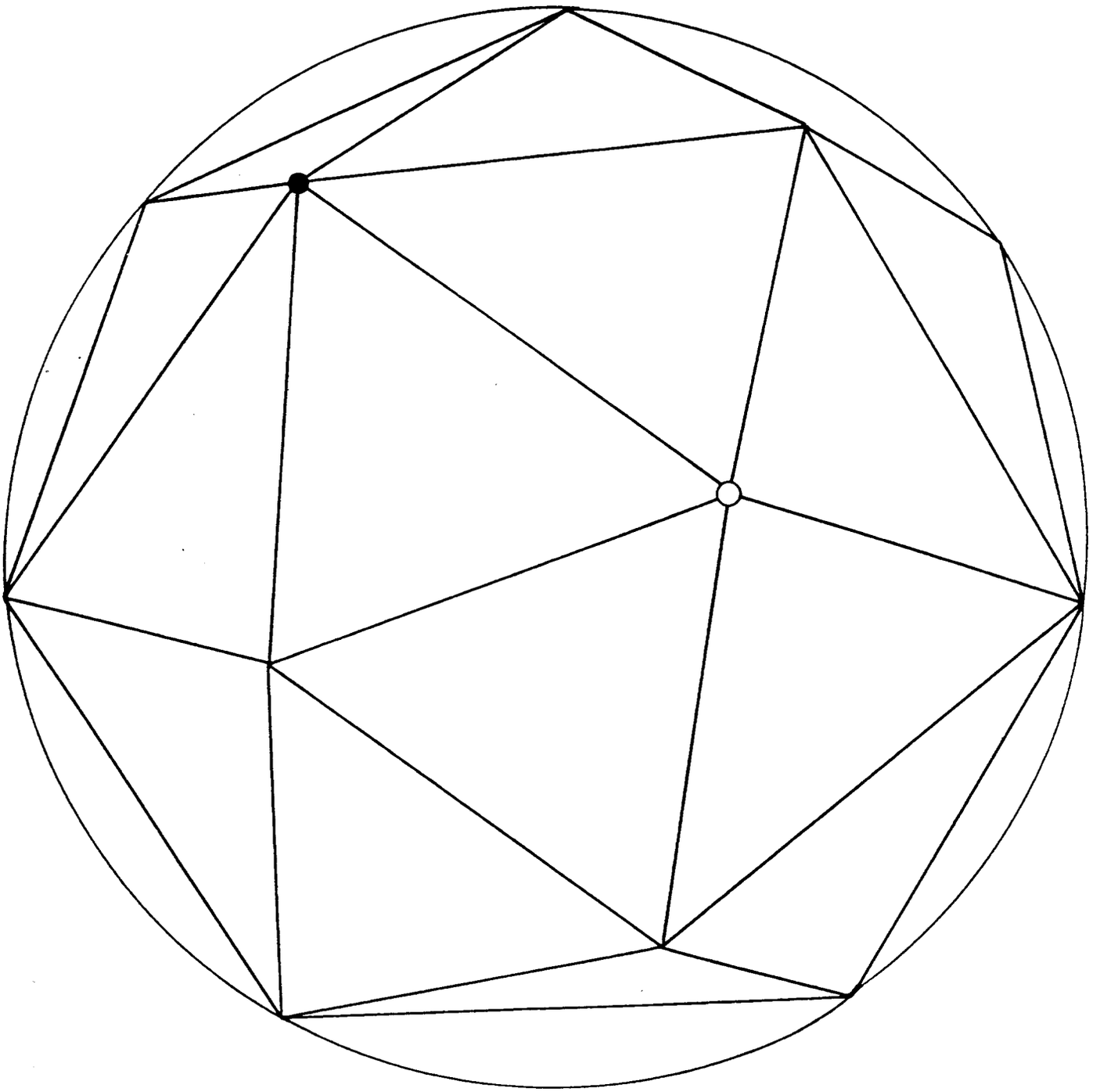

Figure 1 (d)

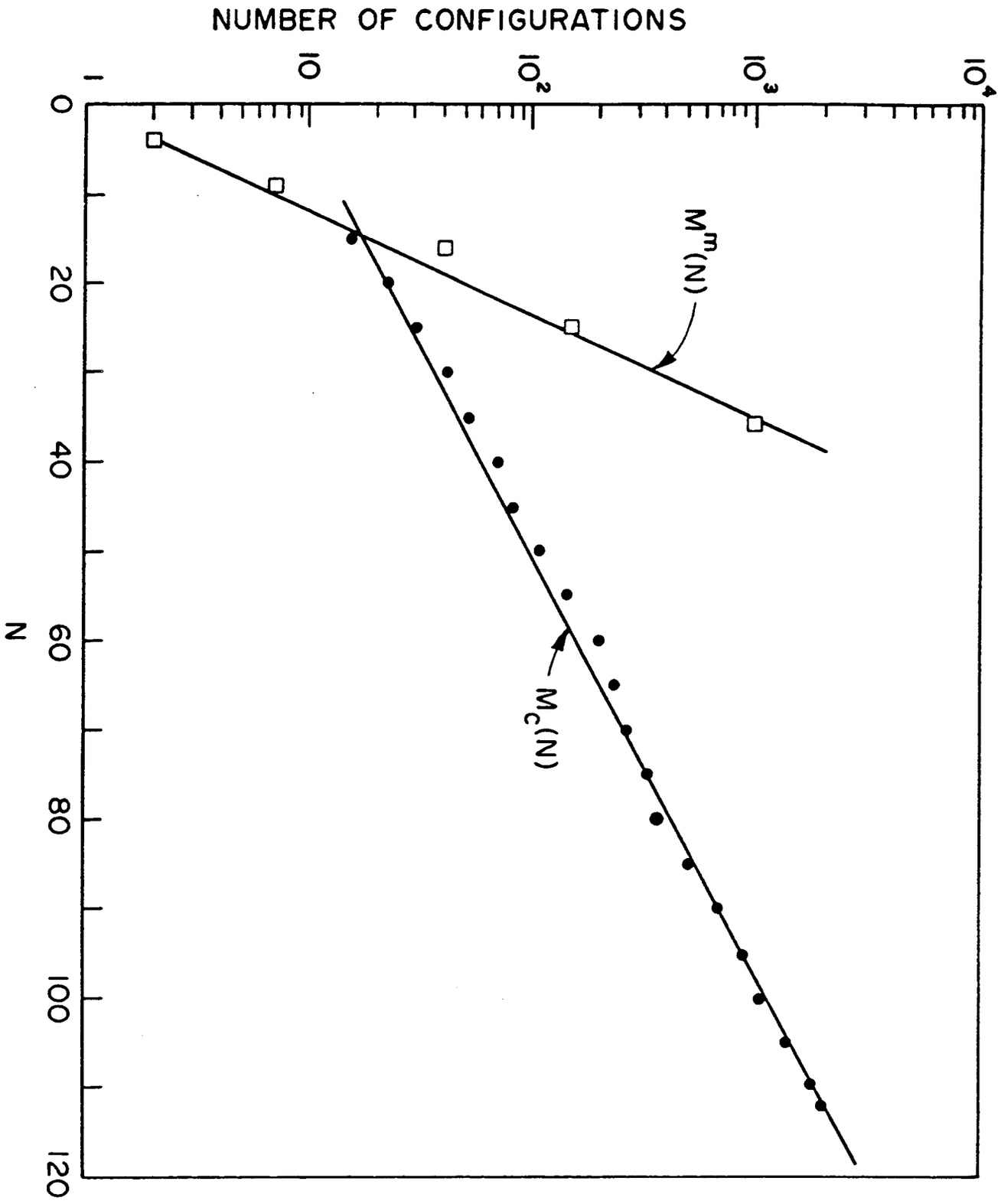
NUMBER OF CONFIGURATIONS
1
10
10²
10³
10⁴
0
20
40
60
80
100
120
N
M^m(N)
M_c(N)

Figure 2

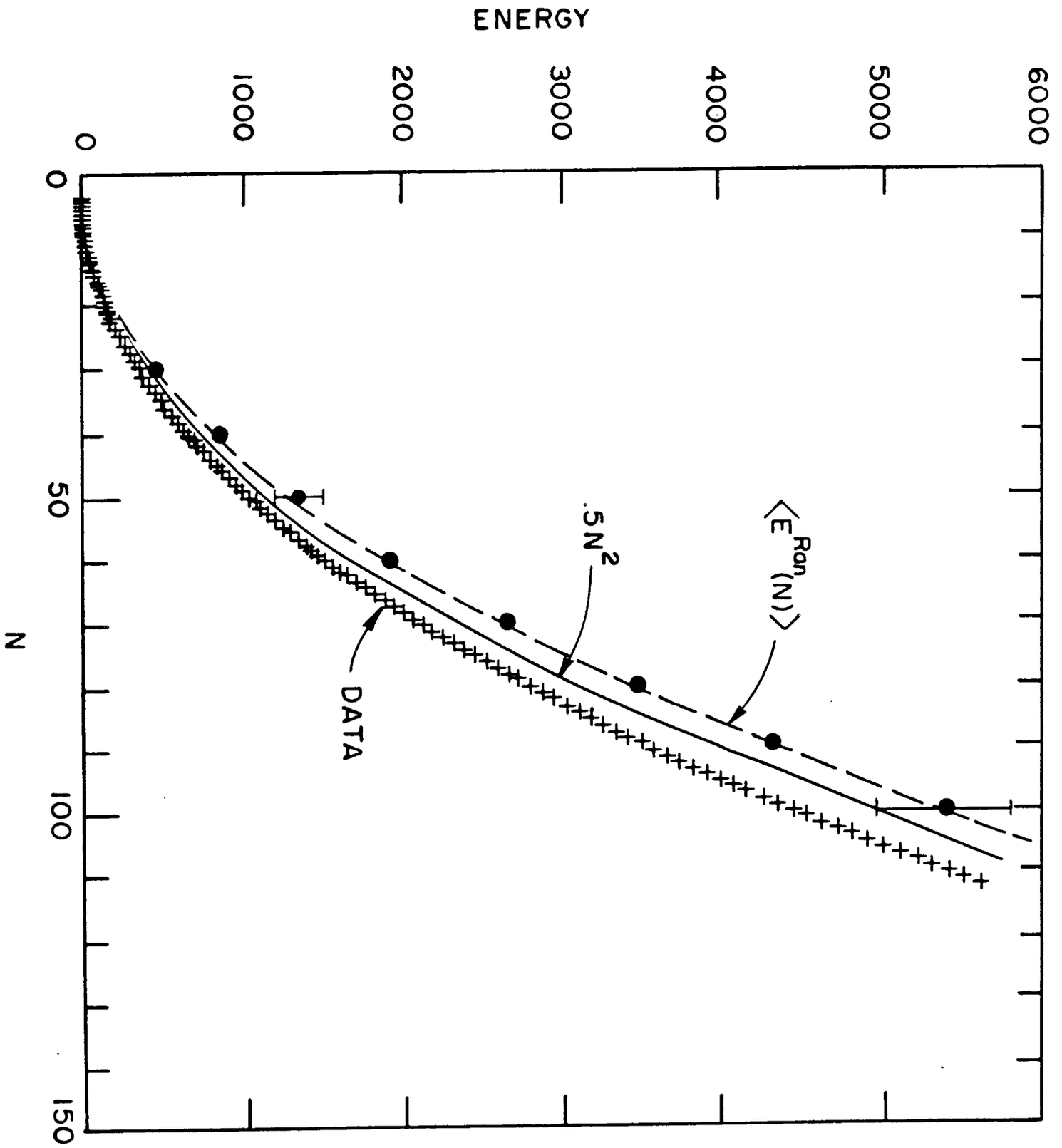
ENERGY
0
1000
2000
3000
4000
5000
6000
N
0
50
100
150
DATA
.5N²
⟨E^Ran(N)⟩

Figure 3

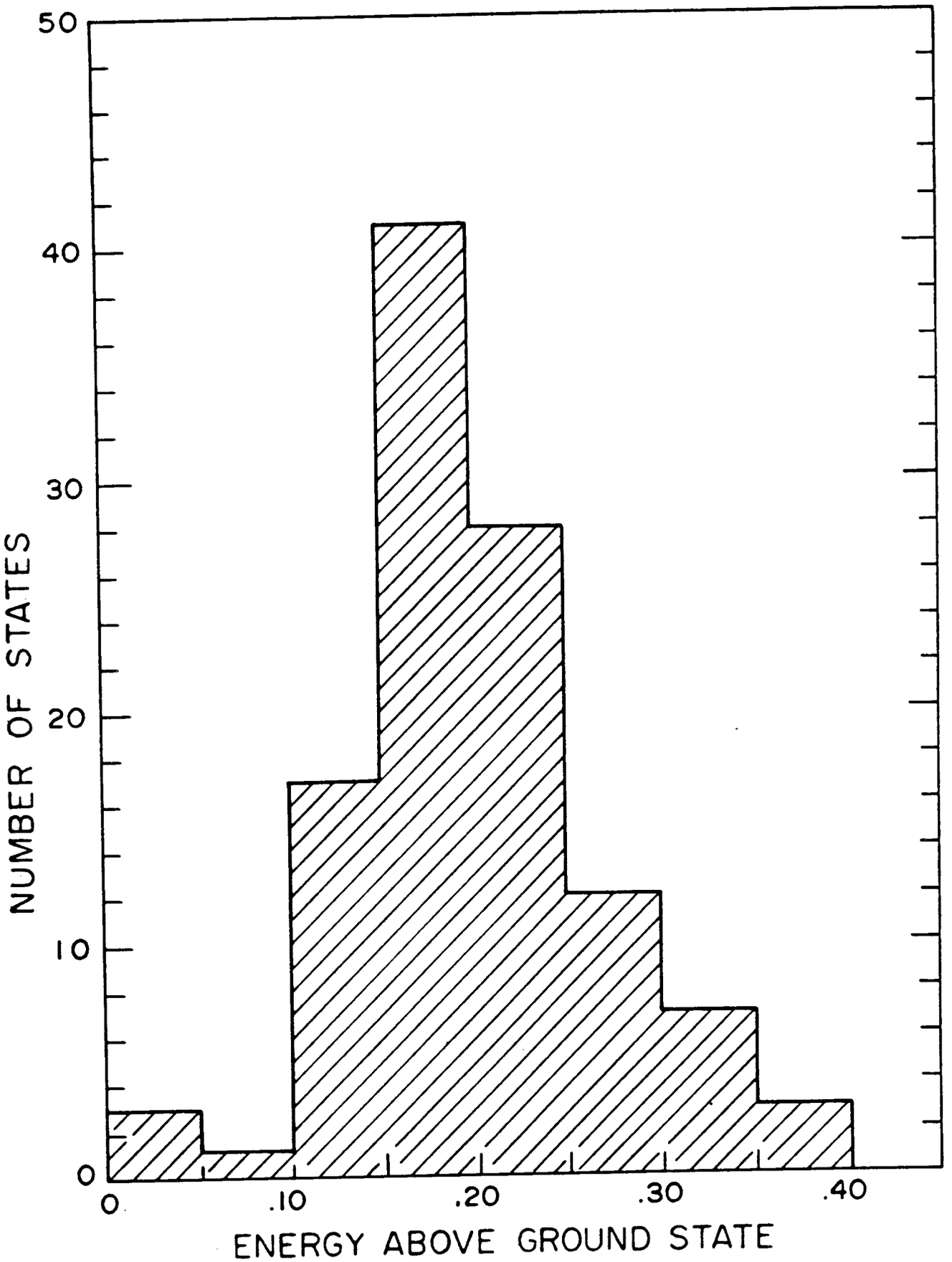
50
40
30
20
10
0
NUMBER OF STATES
0
.10
.20
.30
.40
ENERGY ABOVE GROUND STATE

Figure 4

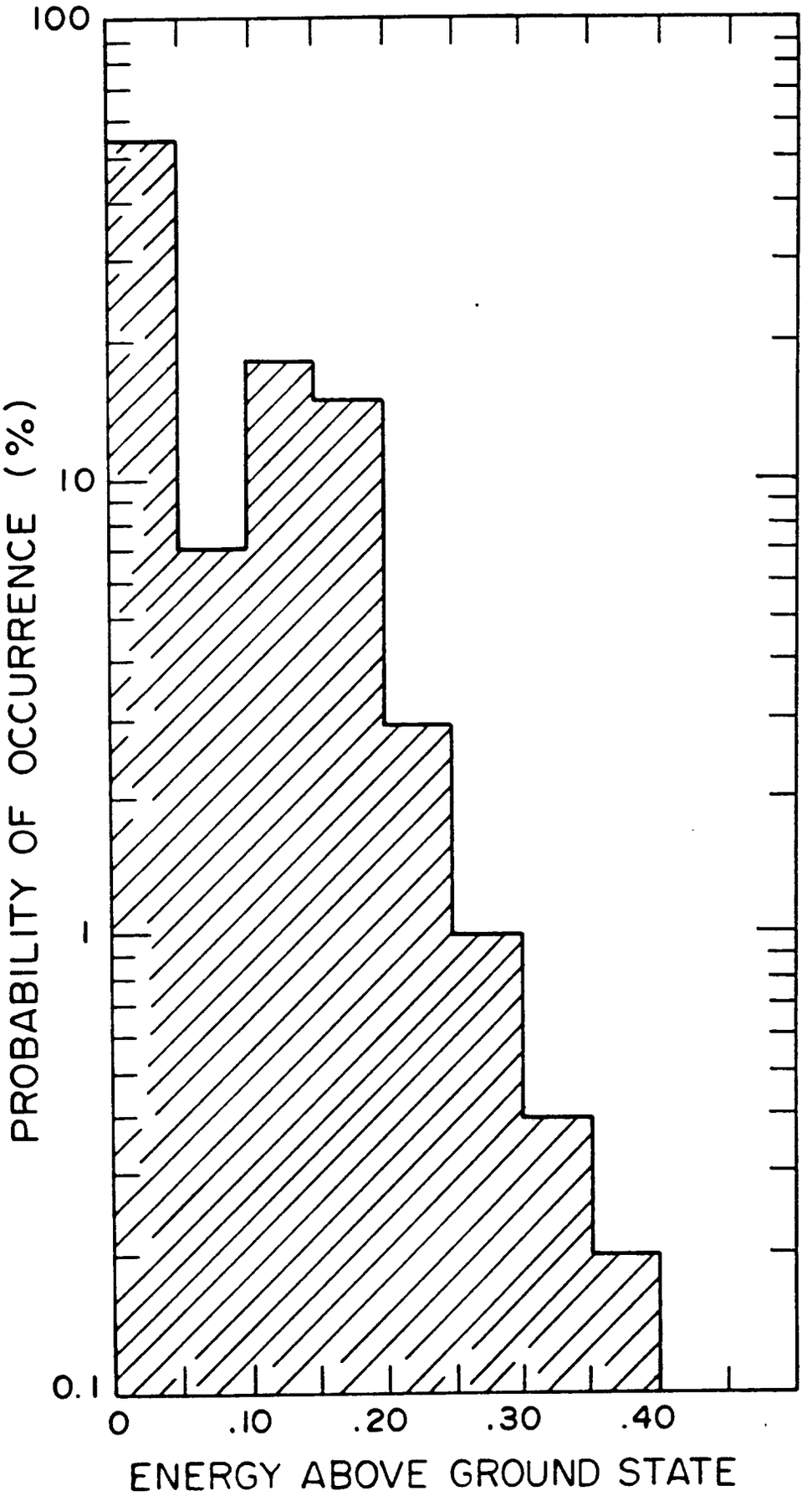
100
10
1
0.1
PROBABILITY OF OCCURRENCE (%)
0
.10
.20
.30
.40
ENERGY ABOVE GROUND STATE

Figure 5

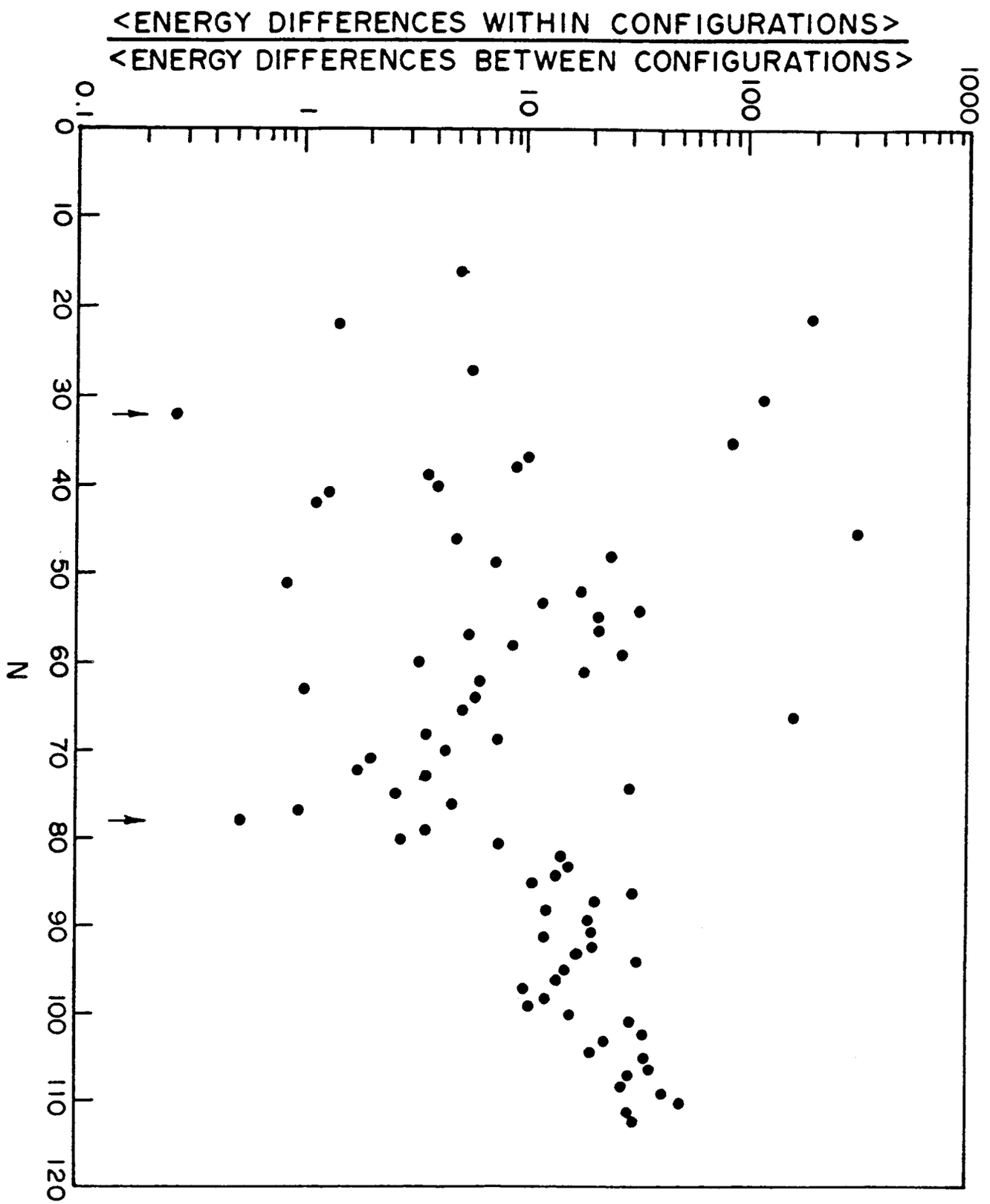
<ENERGY DIFFERENCES WITHIN CONFIGURATIONS>
<ENERGY DIFFERENCES BETWEEN CONFIGURATIONS>
0.1
1
10
100
1000
N
0
10
20
30
40
50
60
70
80
90
100
110
120

Figure

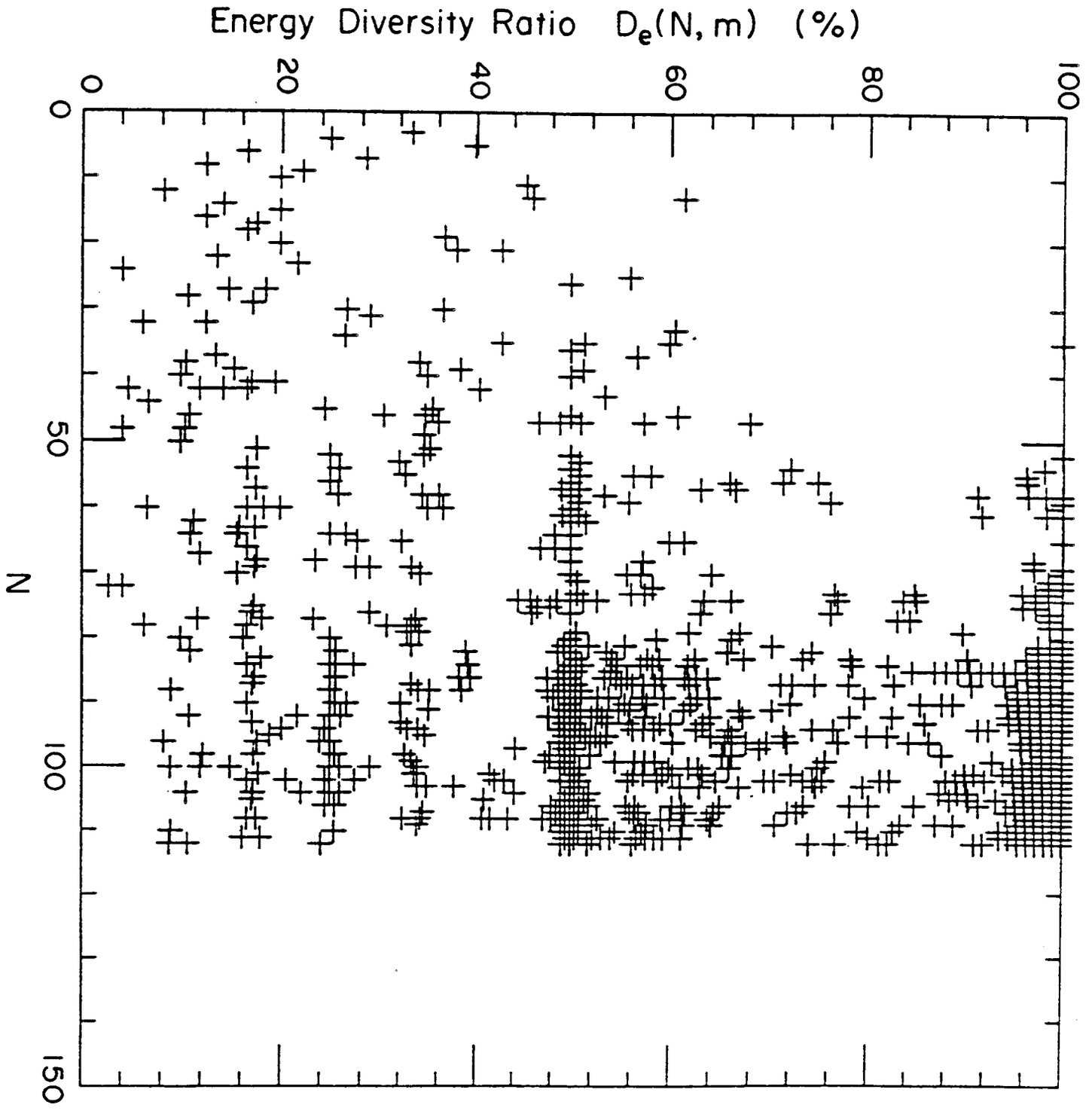

Figure

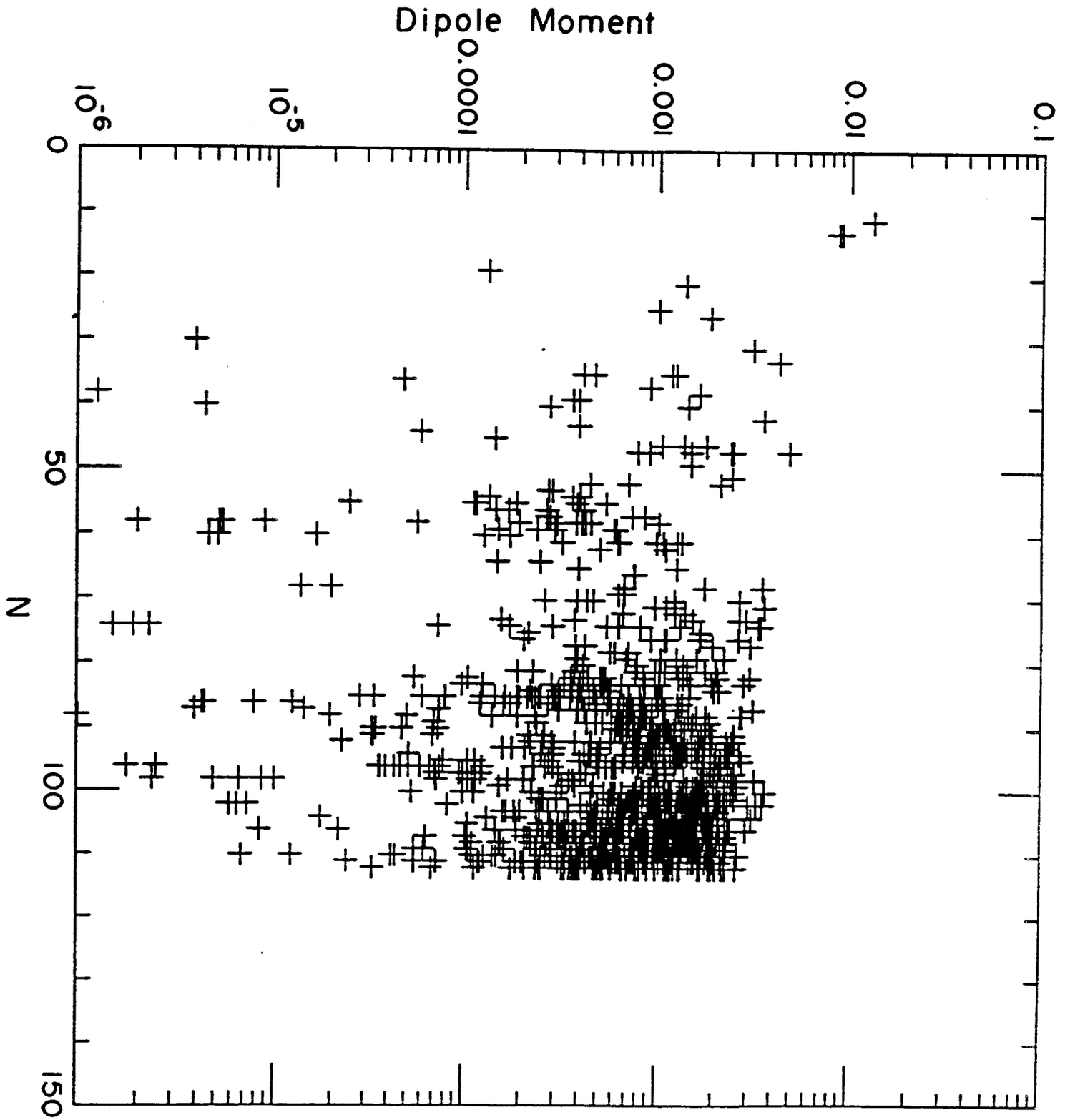

Figure

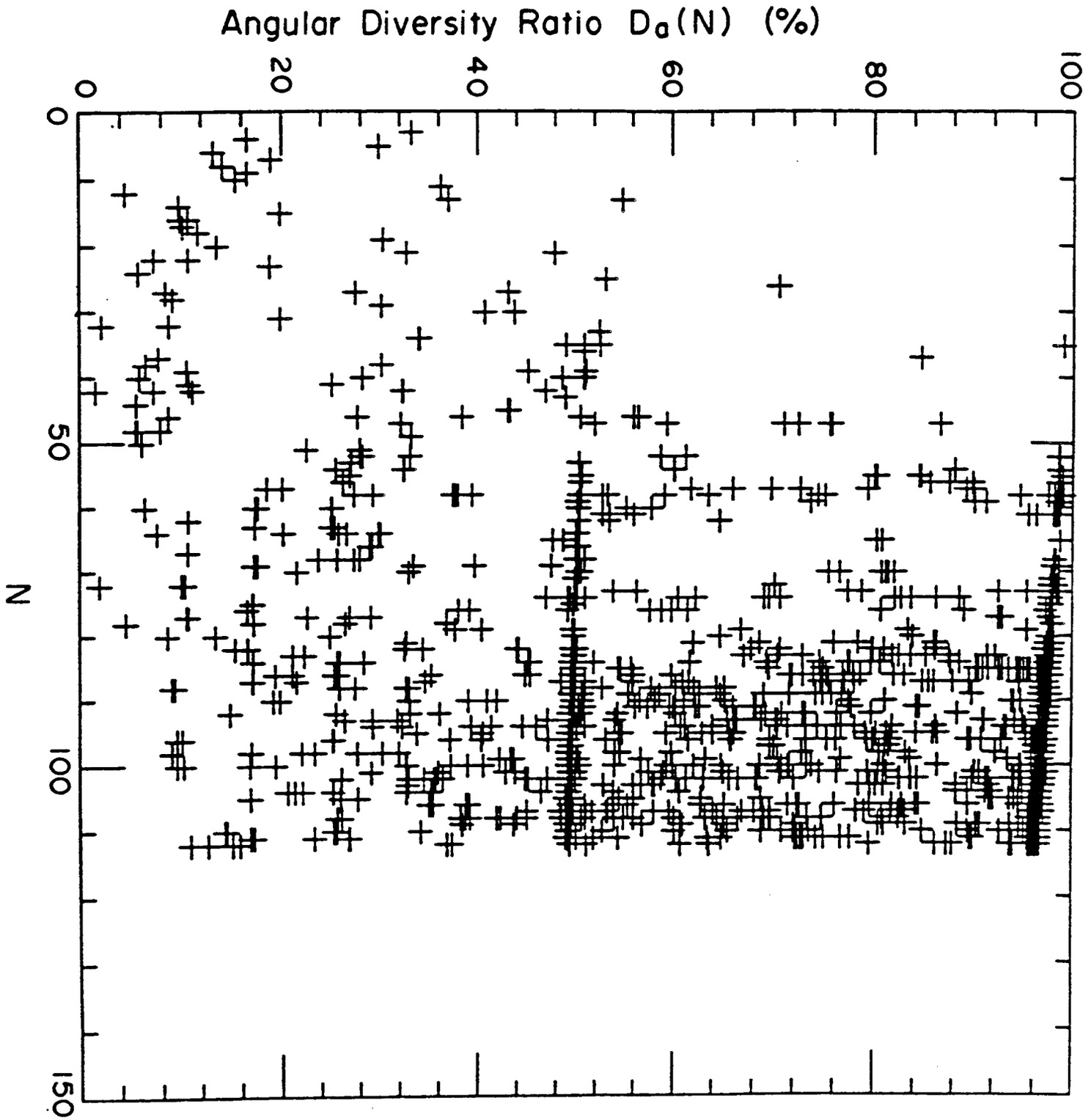

Figure

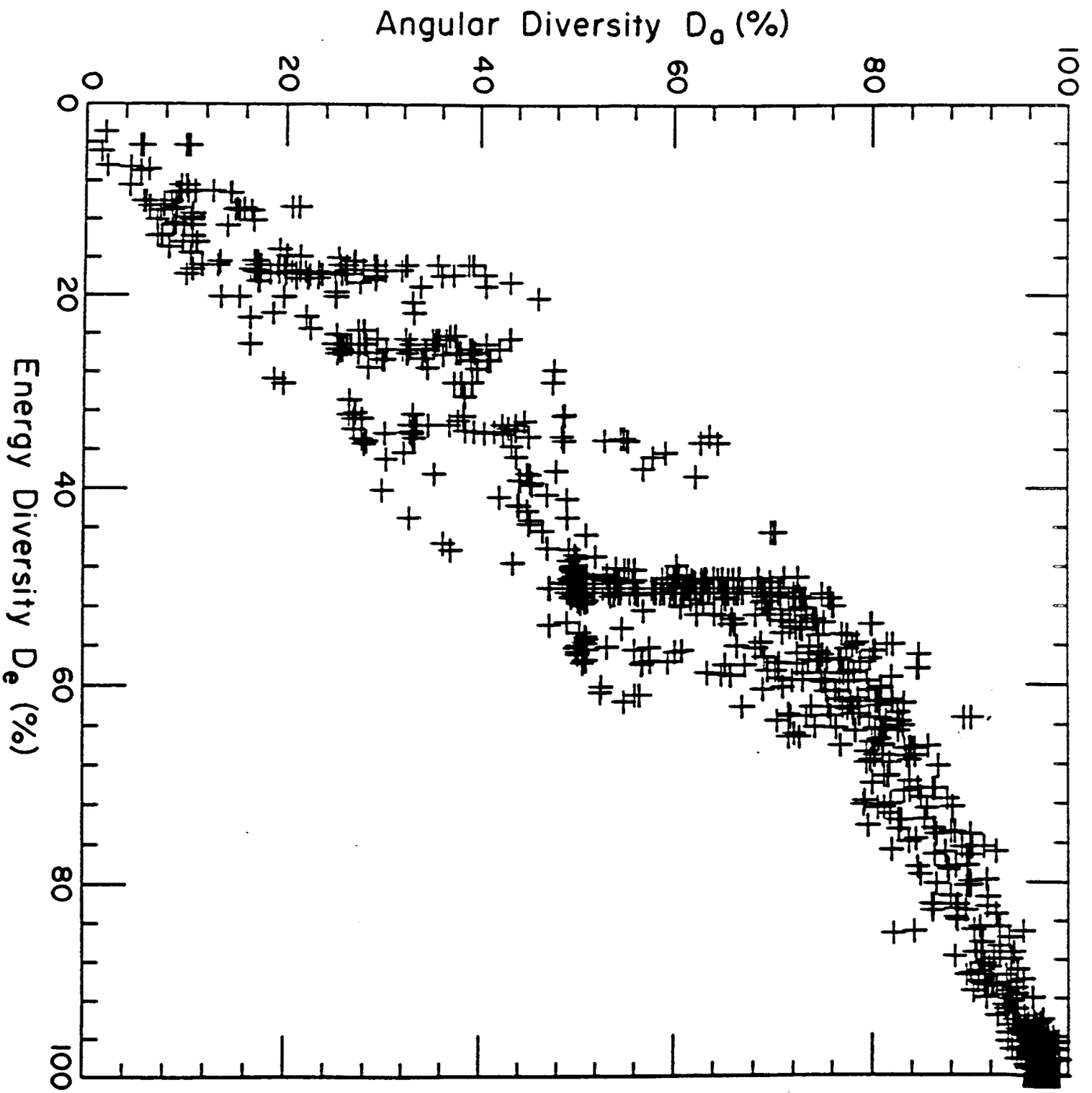
Angular Diversity D_a (%)
0
20
40
60
80
100
Energy Diversity D_e (%)
0
20
40
60
80
100

Figure 1

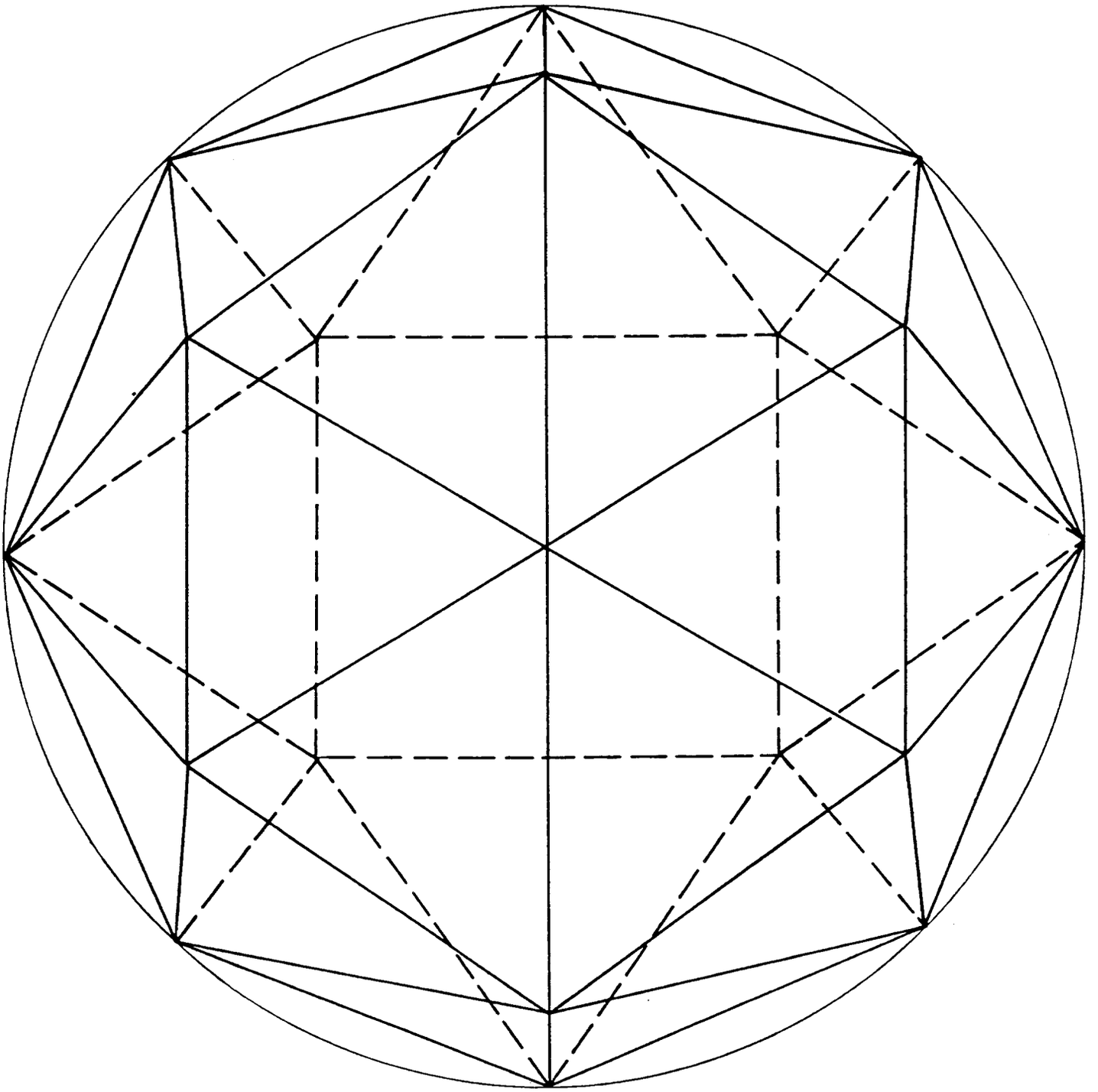

Figure

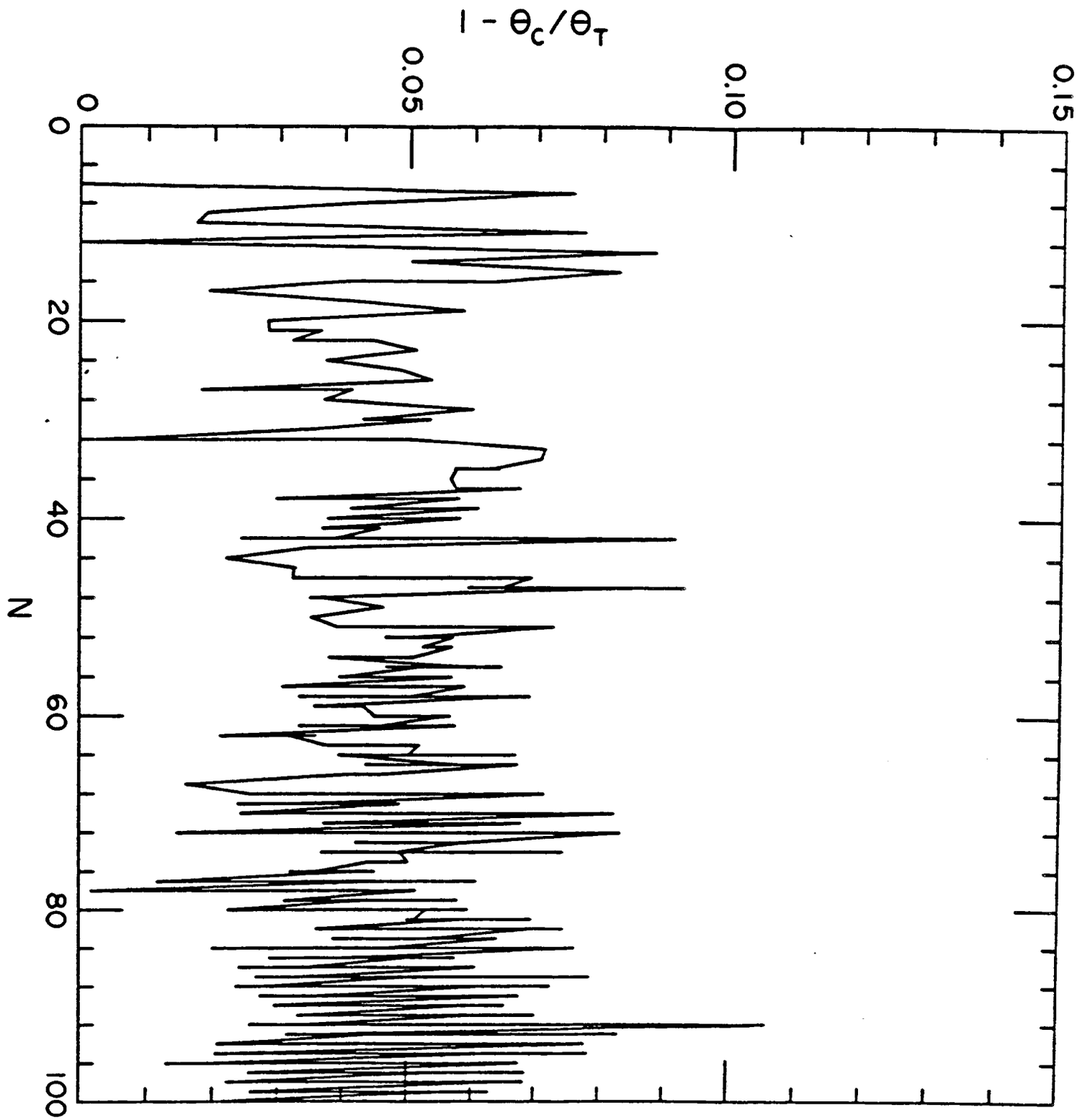

Figure 1

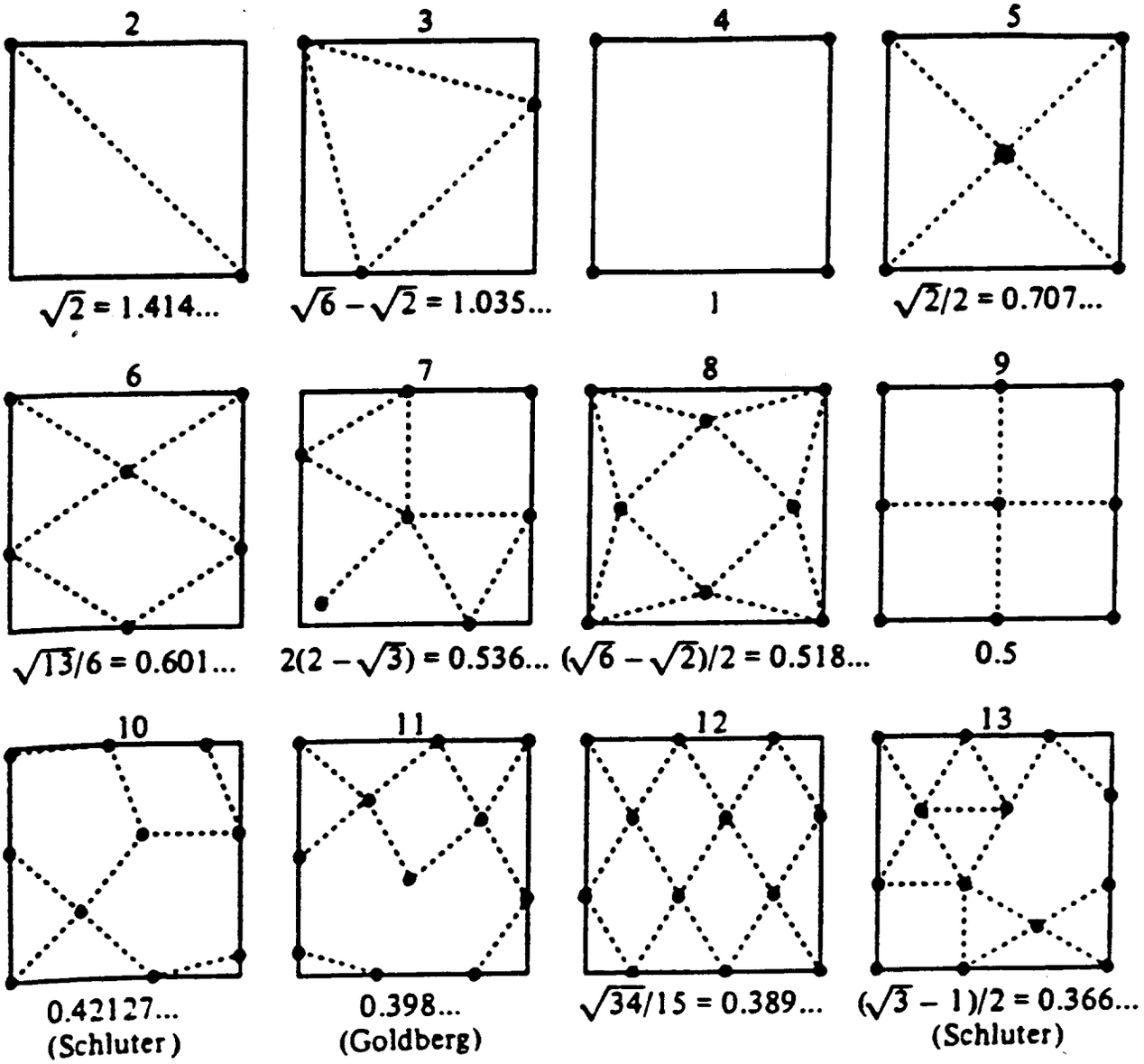
2
$\sqrt{2} = 1.414...$
3
$\sqrt{6} - \sqrt{2} = 1.035...$
4
1
5
$\sqrt{2}/2 = 0.707...$
6
$\sqrt{13}/6 = 0.601...$
7
$2(2 - \sqrt{3}) = 0.536...$
8
$(\sqrt{6} - \sqrt{2})/2 = 0.518...$
9
0.5
10
0.42127...
(Schluter)
11
0.398...
(Goldberg)
12
$\sqrt{34}/15 = 0.389...$
13
$(\sqrt{3} - 1)/2 = 0.366...$
(Schluter)

Figure 13

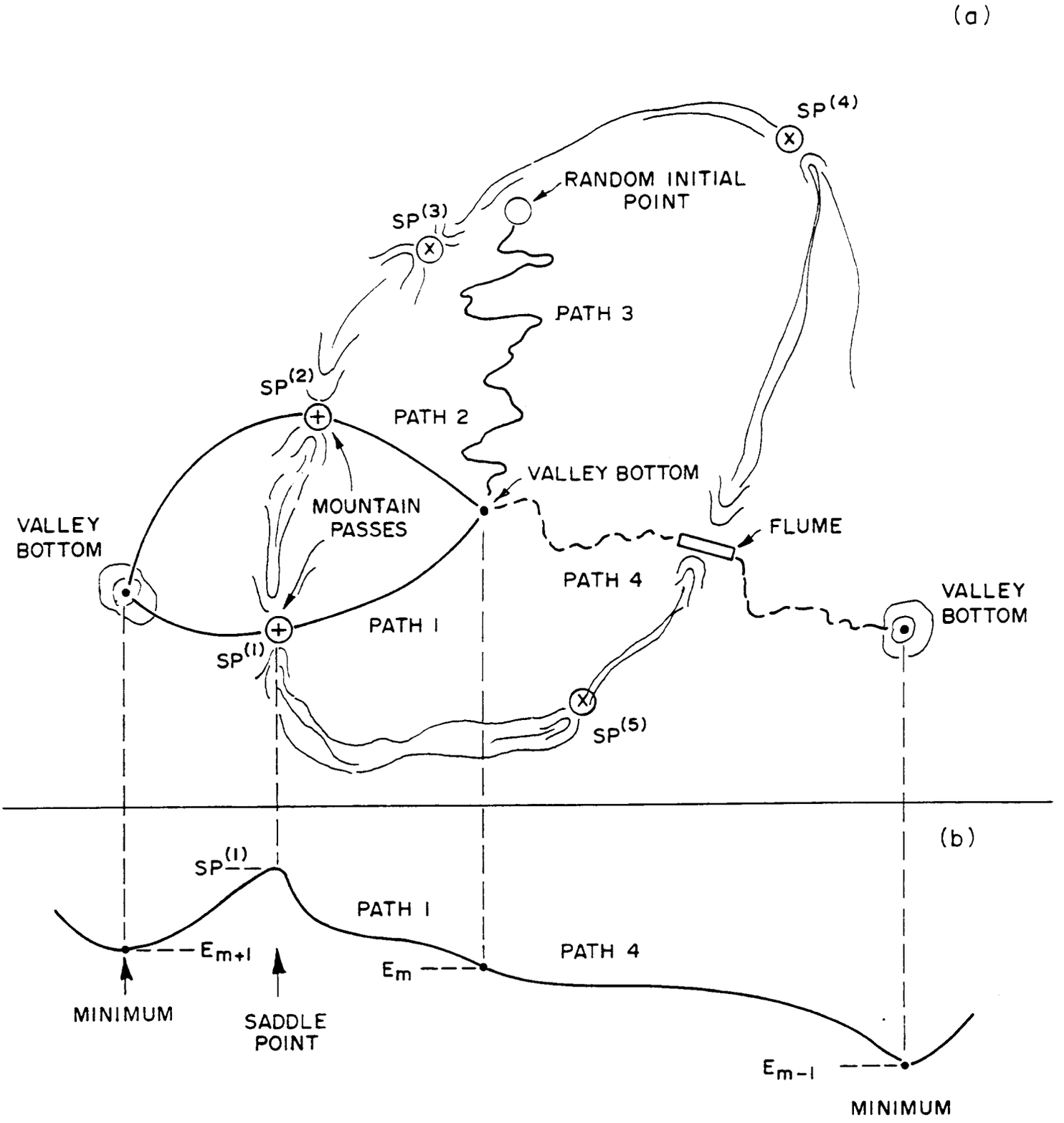
(a)
SP(4)
RANDOM INITIAL POINT
SP(3)
PATH 3
SP(2)
PATH 2
VALLEY BOTTOM
MOUNTAIN PASSES
VALLEY BOTTOM
FLUME
PATH 4
VALLEY BOTTOM
PATH 1
SP(1)
SP(5)
(b)
SP(1)
PATH 1
Em+1
PATH 4
Em
MINIMUM
SADDLE POINT
Em-1
MINIMUM

Figure 14(a) & (b)

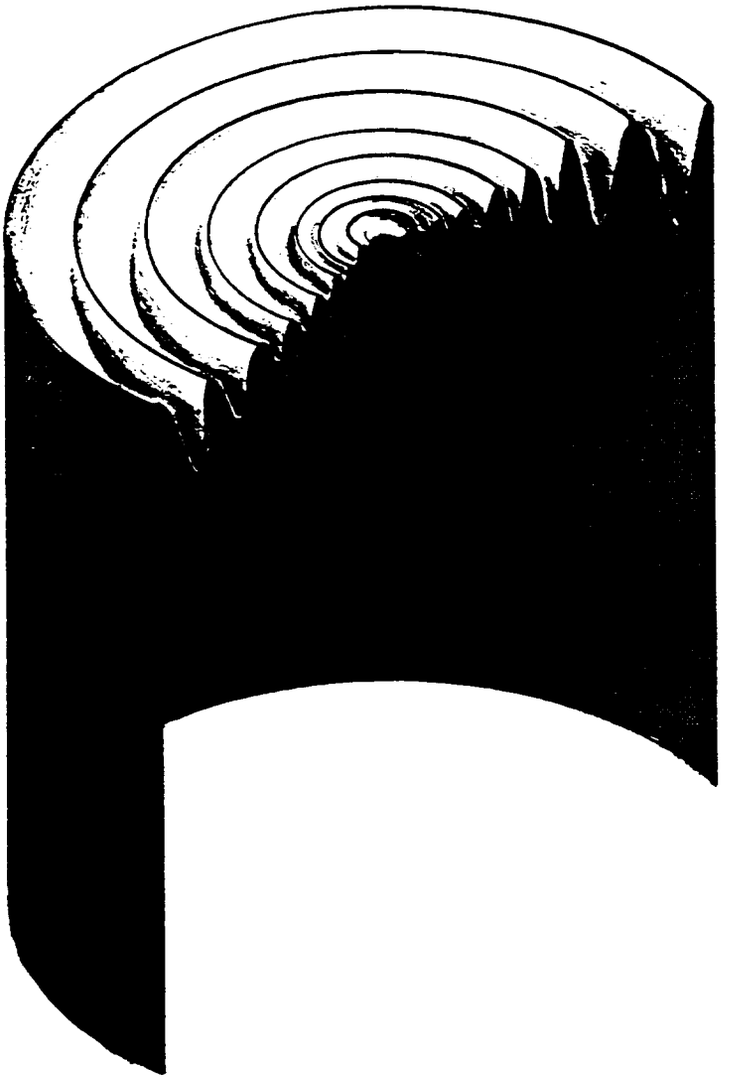

Figure 14(c)

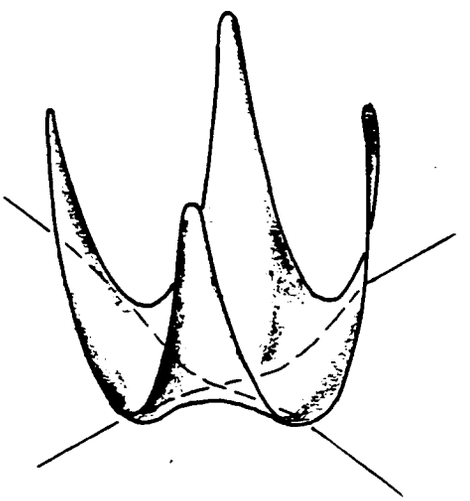

Figure 14(d)